Parameter estimation methods based on binary observations - Application to Micro-Electromechanical Systems (MEMS)

Kian Jafaridinani

N° d'ordre : 2012-11-TH

THÈSE DE DOCTORAT

DOMAINE : STIC

SPECIALITE : Electronique

Ecole Doctorale « Sciences et Technologies de l'Information des Télécommunications et des Systèmes »

Présentée par :

Kian Jafari

Sujet :

Estimation des paramètres d'un système à partir de données fortement quantifiées, application aux MEMS

Soutenue le 09 juillet 2012 devant les membres du jury :

M. Eric WALTER	LSS	Président
M. Salvatore MIR	TIMA	Rapporteur
Mme Alina VODA	GIPSA-LAB	Rapporteur
M. Yann LE GORREC,	AS2M	Examinateur
M. Morgan ROGER,	Supélec	Co-encadrant
M. Jérôme JUILLARD	Supélec	Directeur de thèse

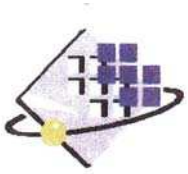

N° D'ORDRE: 2012-11-TH

Ecole Supérieure d'Electricité

Parameter estimation methods based on binary observations
Application to Micro-Electromechanical Systems (MEMS)

Kian JAFARI
09 July 2012

Department of Signal Processing & Electronic Systems
Ecole Supérieure d'Electricité
(SupElec)
France

Thesis committee :

M.	Walter	Eric	President
M.	Mir	Salvador	
Mme.	Voda	Alina	
M.	Le Gorrec	Yann	
M.	Roger	Morgan	Co-director
M.	Juillard	Jérôme	Thesis director

Submitted in partial fulfillment of the requirements
for the degree of Doctor of Philosophy.

To Roozbeh, Shahin and Bahman

Acknowledgements

This work would have not been possible without the contribution of many people. First and foremost, I feel indebted to my supervisor, Prof. Jérôme JUILLARD, for his guidance, effort and patience. I will never forget his continued presence, the way he taught me, our interesting discussions, and particularly his kindness. I am also grateful to him for reading this entire manuscript. I am deeply grateful to my second supervisor, Prof. Morgan ROGER, for his support throughout this work.

I would also like to thank Prof. Salvador MIR and Prof. Alina VODA for reviewing this work, providing insightful comments and attending my defense. I would like to thank as well Prof. Yann LE GORREC and Prof. Eric WALTER for attending my defense as examiners and for their helpful comments. I am grateful to my colleagues in IEF and ESIEE for providing me data for Chapter 5 and attending my defense.

I would also like to thank my colleagues at Supélec: Prof. Gilles Fleury, Director of Research and Industry Partnerships, Prof. Stéphane FONT, the head of the Department of Signal Processing & Electronic Systems (SSE), Ms. Karine BERNARD, Prof. Arthur TENENHAUS, Prof. Alain BONNOIT and Prof. Laurent BOURGOIS for their useful comments, Prof. Julien BECT, Prof. José PICHERAL, Prof. Elisabeth LAHALLE and Luc BATALIE.

I am very grateful to the department to support me for attending conferences. My special thank to my friends Alireza, Farhad, Armin, ALi, Mahboubeh, Sepideh, Jean-Michel, Arash, Atoosa and Amir, for all the good times we had together.

Finally, but most importantly, I wish to thank my lovely family, Shahin ABBASI, Bahman JAFARI and my brother ,ROOZEH, for all their love, support and encouragement.

Abstract. While the characteristic dimensions of electronic systems scale down to micro- or nano-world, their performance is greatly influenced. Micro-fabrication process or variations of the operating situation such as temperature, humidity or pressure are usual cause of dispersion. Therefore, it seems essential to co-integrate self-testing or self-adjustment routines for these microdevices. For this feature, most existing system parameter estimation methods are based on the implementation of high-resolution digital measurements of the system's output. Thus, long design time and large silicon areas are needed, which increases the cost of the micro-fabricated devices. The parameter estimation problems based on binary outputs can be introduced as alternative self-test identification methods, requiring only a 1-bit Analog-to-Digital Converter (ADC) and a 1-bit Digital-to-Analog Converter (DAC).
In this thesis, we propose a novel recursive identification method to the problem of system parameter estimation from binary observations. An online identification algorithm with low-storage requirements and small computational complexity is derived. We prove the asymptotic convergence of this method under some assumptions. We show by Monte Carlo simulations that these assumptions do not necessarily have to be met in practice in order to obtain an appropriate performance of the method. Furthermore, we present the first experimental application of this method dedicated to the self-test of integrated micro-electro-mechanical systems (MEMS). The proposed online Built-In Self-Test method is very amenable to integration for the self-testing of systems relying on resistive sensors and actuators, because it requires low memory storage, only a 1-bit ADC and a 1-bit DAC which can be easily implemented in a small silicon area with minimal energy consumption.

Résumé. Bien que les dimensions caractéristiques des systèmes électroniques aient été réduites aux micro- ou nano-échelles, leur performance reste très sensible à des facteurs extérieurs. Les variations lors du processus de fabrication des microsystèmes et celles dans leurs conditions de fonctionnement (température, humidité, pression) sont la cause habituelle de ces dispersions. Par conséquent, il est important de co-intégrer des routines de self-test ou d'auto-ajustement pour ces micro-dispositifs. La plupart des méthodes d'estimation des paramètres du système existantes sont fondées sur la mise en uvre de mesures numériques haute résolution de la sortie du système. Leur mise en uvre nécessite ainsi un long temps de conception et une grande surface de silicium, ce qui augmente le coût de ces micro-dispositifs. Les méthodes d'estimation de paramètres basées sur les observations binaires ont été présentées comme des méthodes d'identification alternatives, nécessitant seulement un Convertisseur Analogique-Numérique (CAN) 1-bit.
Dans cette thèse, nous proposons une nouvelle méthode d'identification récursive pour le problème d'estimation des paramètres à partir des observations binaires. Un algorithme d'identification en ligne avec de faibles besoins de stockage et une complexité algorithmique réduite est introduit. Nous prouvons la convergence asymptotique de cette méthode sous certaines hypothèses. Ensuite, nous montrons par des simulations de Monte-Carlo que ces hypothèses ne doivent pas nécessairement être respectées dans la pratique pour obtenir une bonne performance de la méthode. De plus, nous présentons la première application expérimentale de cette méthode dédiée au self-test de MEMS intégrés. La méthode de «Built-In Self-Test» en ligne proposée est très intéressante pour le self-test de capteurs, car elle nécessite des ressources faibles de stockage, un seul CAN 1-bit et un

seul CNA 1-bit qui peut être facilement mis en uvre dans une petite surface de silicium avec une consommation réduite d'énergie.

Contents

List of Figures

List of Tables

Introduction

Context of the study

"Inferring models from observations and studying their properties is really what science is about. The models may be of more or less formal character, but they have the basic feature that they attempt to link observations together into some patterns" [1]. System identification treats the problem of proposing mathematical models of dynamical systems from observed data. Since many phenomena in our surroundings can be modeled by dynamical systems, system identification approaches have a extensive range of applications [2].

Especially, in the past few years, parameter estimation methods based on binary or quantized outputs have absorbed an increasing interest in various domains ranging from automobile and aerospace to biomedical applications (i.e. switching and industrial sensors, chemical process sensors, pressure and power levels sensors, gas content sensors, etc.). In medical applications, estimation and prediction of causal effects with dichotomous outcomes are closely related to binary-valued output systems [3, 4]. In the context of microdevices,it can also be used to estimate the parameters of microsystems [5, 6]. The use of such methods is mostly motivated by the fact that low-resolution observations are usually much cheaper or easier to obtain than high-resolution ones.

In this work we restrict our attention to system parameter estimation from binary (quantized) observations aimed at the parameters measurement, test and packaging of microsystems such as Micro Electro Mechanical Systems (MEMS) and Nano Electro Mechanical Systems (NEMS). MEMS are the physical components used for sensing and actuating in System-on-Chip (SoC) applications. Typical quantities sensed by MEMS are acceleration, rotation, pressure, etc. However, several factors limit the development of the microdevices [7]. First of all, their mechanical properties are subject to strong variations. These variations may be, not only, from dispersion of their fabrication processes, but also from the changing environment (temperature, ambient pressure, humidity and so on); it is not rare that the characteristic values of a given MEMS (such as its resonance frequency, its quality factor, etc.) differ from its nominal values by more than 20% [6]. Imperfect knowledge of small-scale physical phenomena that play an important role in the MEMS functions are also a large source of uncertainty.

Objective of the dissertation

Typical sources of dispersion in microdevices are variations in the fabrication process or changes in the operating conditions (as explained before). On the one hand, because of the high sensibility of these microdevices to changes in the operating conditions, it is possible to produce various accurate microdevices (such as temperature or pressure sensors) to sense and measure these changes. On the other hand, their high sensibility to different sources of dispersion make them difficult to use in several other applications. For instance, changes in the operating temperature or pressure can affect an acceleration sensor resulting in an inaccurate measurement of the existing acceleration. Thus, it is usually impossible to guarantee a priori that a given device will function properly without robust testing methods. The tests that are run after fabrication under different operating conditions, ensure that only suitable devices are commercialized. However, these tests are very costly: It is estimated that MEMS testing and packaging costs are in the range of 30%−75% of the components total cost [8, 9].

A solution is to integrate low-cost measurement, self-test (and self-tuning) features such as parameter estimation routines, in each device, so that, it can not only measure various quantities that are so sensitive to changes in the operating conditions (such as temperature, pressure, humidity, etc.) but also can compensate the undesirable effects of these sources of dispersion, if necessary. However, most classical parameter estimation methods [1, 2] do not easily scale down to the micro or nano-world. This is because these methods rely on high-resolution digital measurements of the system output. Their integration requires the implementation of high-resolution analog-to-digital converters (ADCs) and, thus, results in longer design time, larger silicon areas and increased cost. One of our goals in this research work is to investigate the various existing identification methods based on quantized (ideally binary) observations and to study their implementation possibility and computational complexity in the context of microdevices. The main objective is then to develop new parameter estimation methods that relies on very low resolution (ideally binary) measurements, in order to keep the added cost as small as possible in the context of microdevices. Furthermore, the properties and convergence analysis of the proposed methods are studied not only in a mathematical framework but also confirmed by simulation results and experimental validation of the concepts.

Dissertation Organization

The structure of the dissertation is the following.

- Chapter 1 is divided into two parts. The first is an overview of MEMS technology and their applications. MEMS fabrication and micromachining techniques are also addressed in this chapter. In the second part, the problem of MEMS testing is discussed.

- Chapter 2 presents various existing identification methods based on binary or quantized observations. The advantages and drawbacks of the methods are also investigated with a special focus on the field of microdevices.

- In Chapter 3, an offline weighted least squares (WLS) method using binary observations is proposed. The asymptotic properties of this WLS method are also investigated. Furthermore, the estimation quality of this criterion is mathematically derived and verified by simulations. Finally, its advantages and drawbacks under different scenarios compared to an existing approach is shown by simulation results.

- In Chapter 4, we present an original online identification method which relies on Least-Mean-Square (LMS) algorithms. We show that the asymptotic convergence of the proposed method is tied to some conditions on the input signal. In particular, we prove the convergence of this method provided that the input signal satisfies a strong mixing property. Some simulation results are then given in order to illustrate the properties of this method under various scenarios.

- The experimental application of the method developed in Chapter 4, for a micromachined pressure sensor, is presented in Chapter 5, followed by general conclusions and future works given in Chapter 6.

Publications

The publications that resulted from this work are as follows:

- Kian Jafari, Jérôme Juillard, and Morgan Roger. Convergence analysis of an online approach to parameter estimation problems based on binary observations, *Automatica*, Accepted, 2012.

- Olivier Legendre, Hervé Bertin, Olivier Garel, Hervé Mathias, Souhil Megherbia, Kian Jafari, Jérôme Juillard, and Eric Colinet. A low-Cost built-in self-test method for resistive MEMS sensors, In *The* 25^{th} *EUROSENSORS Conference, Athens, Greece, September 4-7*, 2011.

- Kian Jafari, Jérôme Juillard and Eric Colinet, A recursive system identification method based on binary measurements, In *The* 49^{th} *IEEE Conference on Decision and Control (CDC2010), Atlanta, Georgia, USA, December 15-17*, 2010.

- Jérôme Juillard, Kian Jafari and Eric Colinet, Estimation quality of a weighted least-square parameter estimation method based on binary observations, In *2010 European Signal Processing Conference (EUSIPCO-2010), Aalborg, Denmark, August 23-27*, 2010.

- Jérôme Juillard, Kian Jafari and Eric Colinet, Consistency of weighted least-square estimators for parameter estimation problems based on binary measurements, In *The* 15^{th} *IFAC Symposium on System Identification (SYSID09), Saint-Malo, France, July 6-8*, 2009.

Chapter 1

Overview of MEMS technology and its applications

This chapter contains general information about MEMS, their fabrication and their applications. Several methods for MEMS testing are also studied. Furthermore, the topic of system identification for testing, calibrating and, more generally, measuring the parameters of these microdevices are addressed in this chapter.

1.1 Micro Electro Mechanical Systems (MEMS)

Micro Electromechanical Systems (MEMS) are miniature devices fabricated by using micromachining technologies and integrated circuit (IC) processes. MEMS devices have begun to materialize as commercial products since the mid-1990s [10, 11]. To qualify as a MEMS (respectively a NEMS), a device should have at least two of its characteristic dimensions smaller than one millimeter (respectively micrometer). MEMS typically consist of a micromachined structure, used as a sensor or as an actuator, together with some electronics for signal amplification. The MEMS device and its electronics are part of a System-on-Chip (SoC), which includes high-level information processing blocks. MEMS sensors are the ears and eyes of SoCs, MEMS actuators are their hands and feet.

MEMS have enabled the development of 'smart' products by providing an interface between computational power and physical world, through the perception and control capabilities of microdevices or systems (e.g. microsensors and microactuators [7]). These microdevices and systems are inherently smaller and lighter than their macroscopic counterparts, and in many cases are also more sensitive and less power-consuming. MEMS are emerging in numerous markets and are expected to have enormous opportunities in the commercial markets (Figure 1.1) due to the low-cost, high functionality, small size and weight of the devices.

MEMS are used to make pressure, temperature, chemical and vibration sensors, light reflectors and switches as well as accelerometers for airbags, vehicle control, pacemakers and games. The technology is also used to make inkjet printheads, microactuators for read/write heads and optical switches, etc.

In the next section, the fundamentals of micromachining techniques are given. Then, we take a closer look at some common applications of these devices and, through simple models, try to show how their performance can be affected by uncertainties.

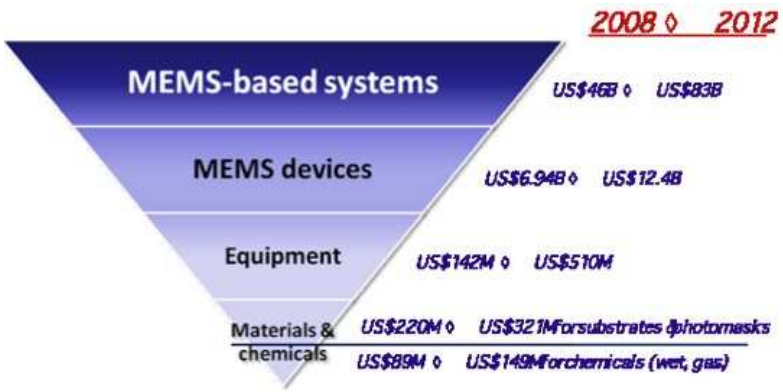

Figure 1.1: The MEMS supply chain size, 2008-2012 (Source: SEMI, Yole).

1.2 MEMS fabrication and micromachining techniques

The goal of MEMS micromachining technology is to create three-dimensional structures and devices with dimensions in micrometers from the bulk of a silicon wafer. At an industrial scale, potentially hundreds of MEMS devices can be fabricated on the same wafer: this batch fabrication process results in very low fabrication cost per unit and it is one of the key points of the development of MEMS technologies. Historically, the development and growth of micromachining technologies is anchored in the integrated circuit (IC) industry. Several devices and processes from the IC industry are nowadays applied to MEMS micromachining [12].

The major micromachining techniques are surface micromachining and bulk micromachining [13, 14, 15, 16], of which we will give a brief overview, in the next subsections. There exist a great variety of more exotic techniques, such as LIGA (lithographe, galvanoformung, abformung) [17], for example, which are not addressed in this manuscript. A typical MEMS device can be realized by using any of these processes in their most prevalent form or several variants of these processes can be used. The choice of the fabrication process is essential because it affects greatly the overall performance and cost of the micromachined part [18]. In this section, we introduce some basic micromachining techniques.

1.2.1 Bulk micromachining

One of the most popular micromachining techniques is bulk micromachining [19], in which matter is selectively chemically removed from the bulk of the silicon wafer (hence its name). Bulk micromachining [20, 12] usually relies on a combination of photolithographic masking and isotropic or anisotropic etching of single-crystalline silicon to form such micromechanical structures as membranes, trench, holes and so on from the bulk of the silicon wafer (Figure 1.2). The etchants may be liquid (so-called 'wet etchants'), such as potassium hydroxide (KOH) or tetramethylammonium hydroxide (TMAH), or not ('dry etchants'). In dry etching, the substrate is submitted to a bombardment of ions, which usually removes matter in a very directional way.

As an example, deep reactive ion etching (DRIE) is a typical bulk silicon micromachining technology. In this process, etch depths several microns deep with nearly vertical sidewalls can be reached. The basic technology relies on the so-called "Bosch process" because the original patent was registered by the Robert Bosch German company [21]. In Bosch process, two different gas compositions are alternated in the reactor. The first gas composition creates a polymer on the surface of the substrate and the second gas composition etches the substrate. The physical part of the etching sputters away the polymer immediately, but only on the horizontal surfaces and not the sidewalls. Because the polymer dissolves very slowly only in the chemical part of the etching, it is built up on the sidewalls and protects them from etching. As a consequence, etching aspect ratios of 50 to 1 may be obtained.

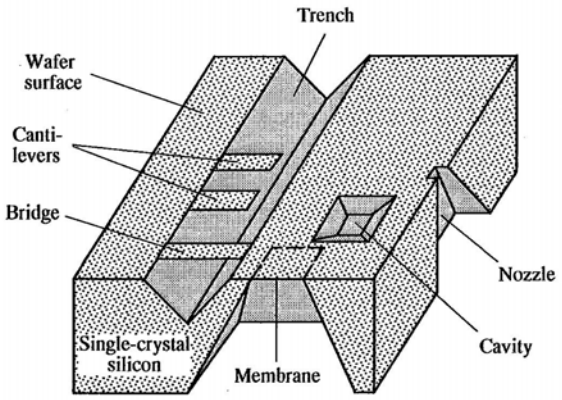

Figure 1.2: General bulk micromachining structures [22].

Although bulk micromachining is a mature technique, its outcome can be affected by even minute variations in the fabrication conditions, such as variations in temperature, pressure, etchant concentration, etching duration, etc. Consequently, no two MEMS devices are perfectly alike, even if they come from the same batch (uniform etching conditions cannot be guaranteed across the width of the silicon wafer).

1.2.2 Surface micromachining

In surface micromachining techniques, matter is not removed from the bulk silicon wafer, but thin structures are deposited on its surface, and released with a chemical step. The process typically employs films of two different materials: a structural material (commonly silicon) and a sacrificial material (oxide). They are deposited and etched in sequence. Finally the given mechanical structure is defined by removing the sacrificial layer and releasing the structure layer (Figure 1.3).

A compatible set of structural materials, sacrificial materials and chemical etchants are required in this method. These materials must be adapted to the device application. Furthermore, the structure materials should provide good mechanical properties such as high yield and fracture stress, minimal creep and fatigue as well as good wear resistance. The etchants must also capable to etch the sacrificial materials quickly without affecting the structure materials (etch selectivity).

Although potentially surface micromachining makes it possible to fabricate very complex structures, provided a sufficient number of masking/depositing/etching steps is made, it is clear that the more layers and the more complex the structure is, the more difficult is to fabricate and thus, it is more sensitive to variations in the fabrication conditions [23].

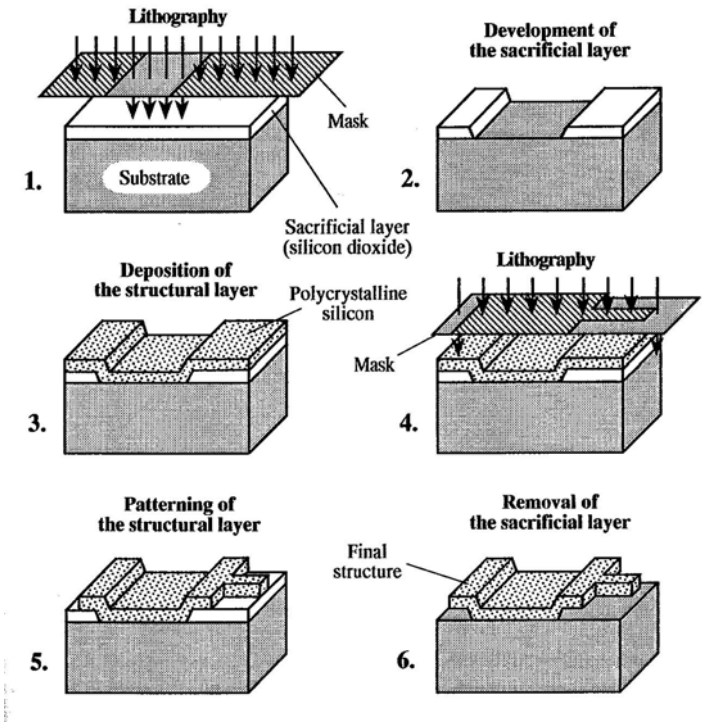

Figure 1.3: A schematic of different steps of typical surface micromachining [22].

1.3 MEMS sensors and actuators

1.3.1 MEMS sensors

In MEMS sensing applications, the electromechanical characteristics of micromachined structures are modified by external phenomena, such as changes in mass, acceleration, pressure, temperature, etc. (Figure 1.4), and translated into electrical signals. The electrical signals output by MEMS devices are then amplified, digitized and processed. Some sensors may include an electronic feedback loop in order to enhance their sensitivity and dynamic range.

Many sensing and detection principles are employed to measure phenomena associated with electrical, mechanical, chemical, biological, and optical fields [25]. In the next subsections, we will focus on three typical MEMS sensors and show how the parameters of these systems can be affected by their environment, whether it is by design or not.

Piezoresistive and capacitive pressure sensors

A material qualifies as piezoresistive when its resistance changes when a stress is applied to it. Significant development in piezoresistive sensing started in 1970 with the development by Kurt Peterson, from IBM research laboratory, of a micromachined pressure sensor

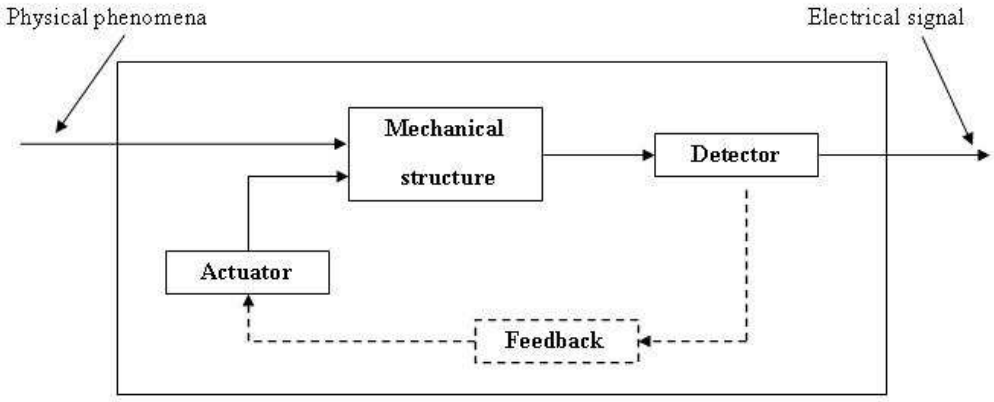

Figure 1.4: General schematic of a MEMS sensor [24]. The feedback loop (- - -) is optional.

using a silicon diaphragm. This is one of the earliest commercial successes of microsystems devices [26].

Various novelties and progresses have been achieved for silicon pressure transducers in the following years and the production volume of silicon pressure sensors has been developing gradually since then, however the basic principles are the same even today. To understand these working principles, a detailed explanation follows regarding Figure 1.5.

Four piezoresistors are formed (by boron diffusion or ion implantation) on the right-hand side of the diaphragm. The four piezoresistors are connected to form a Wheatstone bridge as shown in Figure 1.5 (right). The maximum deflection x of the diaphragm is related to the pressure differential P across the diaphragm by

$$x = \frac{PS}{k}, \tag{1.1}$$

where S is the surface of the diaphragm and k its stiffness. The stiffness is an elastic constant which depends on the actual geometry of the diaphragm, its dimensions, its material(s), and on the intrinsic stress of the membrane. The pressure-induced displacement results in a supplementary stress and in a longitudinal strain in piezoresistors 2 and 3. Thus, the resistance of these piezoresistors depends on the displacement of the diaphragm and, hence, on the pressure differential across it. On the other hand, the resistance of the other two piezoresistors is almost unaffected by the deflection of the diaphragm. Thus, when the four piezoresistors are placed in a Wheatsone bridge arrangement, as illustrated in Figure 1.5, a pressure differential results in a voltage difference, which can be considered as a first approximation proportional to the pressure differential.

Several reasons may cause such a sensor to stray from the nominal behaviour described above. For example, the output signal may be afflicted with a large offset or with temperature drift, caused by mechanical stress or thermal mismatch between the sensor chip and the packaging material. The stiffness of the membrane will likely depend on the temperature of the diaphragm. Such quantities as the intrinsic built-in stress or the thickness

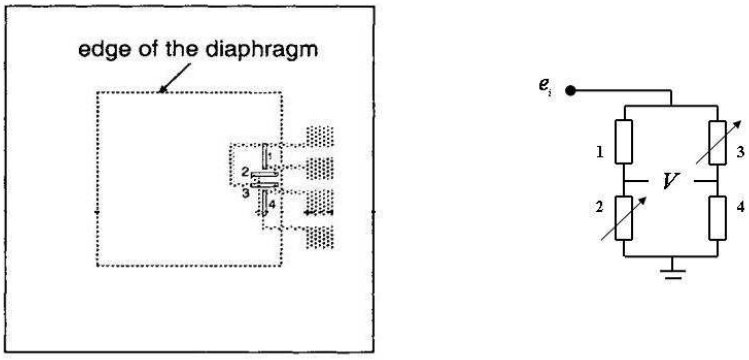

Figure 1.5: Illustrations of a typical silicon pressure sensor [27, 28]: top view (left), Wheatstone bridge (right). For clarity, the area of the diaphragm is shown by dotted lines.

of the membrane are highly fabrication-dependent and cannot be guaranteed beforehand. Consequently, for several applications, these sensors must be carefully calibrated and their defects compensated.

The use of capacitive sensing techniques is also very commonplace. Figure 1.6 represents a capacitive pressure sensor: a silicon chip with an thin diaphragm is attached to a glass plate by electrostatic bonding. A metal film connected to the glass under the cavity is one electrode of the capacitor and the silicon diaphragm used as the other electrode. The diaphragm displacement depends on the applied pressure, P. Thus, the capacitance is a function of pressure. By using a capacitive bridge arrangement, the motion of the diaphragm (and hence the pressure differential), can be measured, pretty much in the same way as for piezoresistive sensors. Although capacitive pressure sensors, like their piezoresistive counterparts, are subject to changes in their operating conditions and, consequently, require careful calibration and compensation, they are less affected by variations in their (simpler) fabrication process and are also intrinsically less noisy [26].

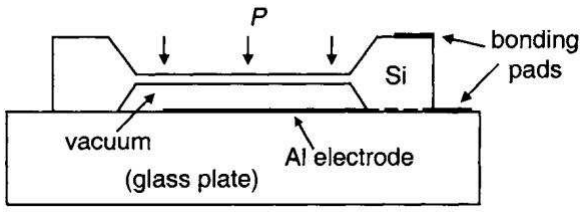

Figure 1.6: Illustration of a basic capacitive pressure sensor [29].

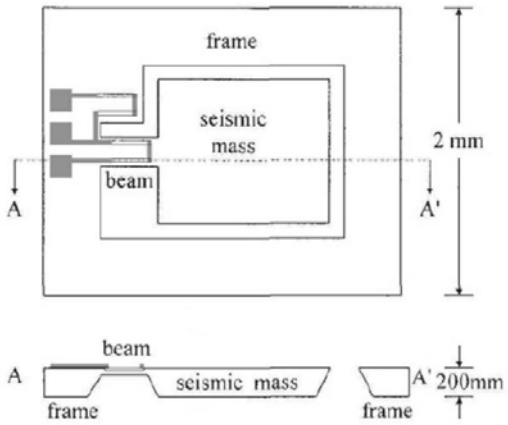

Figure 1.7: Schematic structure of the first silicon piezoresistive accelerometer [30]: top view (top) and cross-sectional view of the chip (down).

Piezoresistive and capacitive inertial sensors

In most inertial sensors, there exist some moving parts whose position is affected by occurring acceleration, deceleration or rotational movement. Historically, the success of silicon piezoresistive pressure sensors encouraged scientists towards the idea of developing a silicon piezoresistive accelerometer. The first silicon accelerometer was produced in Stanford University in 1979 [30]. The key operation principle of the sensor is somewhat simple (Figure 1.7). When the seismic mass of the device undergoes an acceleration, the beam holding the mass is forced to bend by the inertial force on the mass. This causes stress in the beam which, in turn, results in a change in the resistance of the piezoresistor(s) on the beam. Thus, the output of the half bridge formed by two piezoresistors is proportional to the acceleration. Inertial motion can be also detected and measured in other ways, for example capacitively, in which case a comb of sensing fingers is typically fabricated as shown in Figure 1.8. As the mass undergoes an acceleration, the capacitance between the moving fingers (attached to the seismic mass) and the fixed fingers changes. This change in capacitance is typically measured via a charge amplifier.

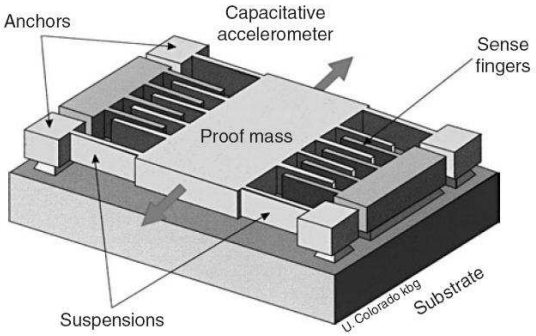

Figure 1.8: MEMS capacitative accelerometer (Source: University of Colorado).

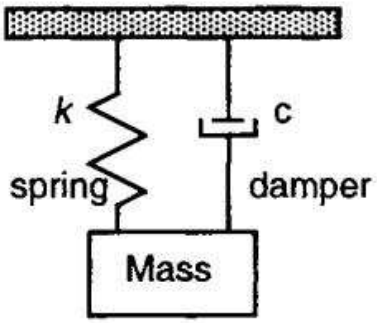

Figure 1.9: Mass-spring-damper system.

One of the most essential features of an accelerometer (e.g. for an airbag application) is its dynamic performance: an ideal accelerometer should provide a uniform sensitivity over as large a frequency bandwidth as possible. As a first approximation, the micromechanical structure may be modeled as a mass-spring-damper system (Figure 1.9). The differential equation governing the mass movement, x, can then be expressed as:

$$kx + b\dot{x} + M\ddot{x} = Ma_0, \tag{1.2}$$

where M is the mass, k is the stiffness of the spring, b is the damping coefficient and a_0 the acceleration of the inertial frame. The quantity

$$w = \sqrt{\frac{k}{M}} \tag{1.3}$$

is the natural free vibration frequency of the system and its quality factor is defined as

$$Q = \frac{\sqrt{kM}}{b}. \tag{1.4}$$

The quality factor indicates the sharpness of the resonance peak: a large Q may be desirable for some applications (such as resonant sensing), but it is detrimental to lowpass applications such as those described in this section. In order to preserve the flatness of the frequency response, the nominal value of Q is typically 0.5. However, this quantity is subject to changes in operating conditions, such as changes in temperature and pressure. The quality factor, like the natural frequency, also depends on the geometry of the device and may then differ from one device to the other, because of small changes in the fabrication process. Thus, dynamic sensors, such as inertial sensors, are even more subject to uncertainties than static ones.

The same sensing principle can be used to detect accelerations in two directions with the same structure. For example, Figure 1.10 shows a close-up of the folded flexure used as a spring in a two-axis capacitive accelerometer. In this case, the system can be modeled as two coupled mass-spring-damper systems, each with its own dispersion-dependent and operating-condition-dependent vibration frequency and quality factor, as well as coupling coefficients. More generally, the more complex a sensing system is, the more effort should be spent in its calibration and compensation.

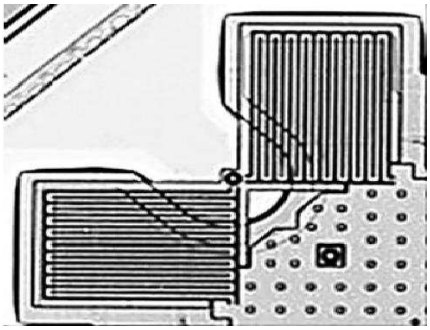

Figure 1.10: Detail of a two-axis MEMS accelerometer (Source: Analog Devices Inc).

Resonant sensors and parametric sensors

The sensitivity of the frequency response of a micromachined structure to external phenomena is not necessarily a drawback. In fact, this sensitivity can be exploited to actively sense changes in the operating conditions of the MEMS device, by monitoring changes in its frequency response. Most usually, this is achieved through a resonant sensing scheme (Figure 1.11), in which the structure is designed to have a stiffness or a mass depending on a physical quantity, such as acceleration, pressure or mass (the so-called 'artificial noses') [31]. Since the stiffness or the mass of the structure changes, so does its natural vibration frequency. Placing the structure in a self-oscillating feedback loop, it is then possible to continually monitor the changes in the external quantity of interest thanks to the sensor's intrinsically digital output. Thus, by design, the natural frequency of a resonant sensor is made sensitive to changes in its operating conditions.

Consider for example the case of resonant accelerometers [31, 32, 33, 34]. A resonant accelerometer typically consists in a large seismic mass which induces axial strain in a

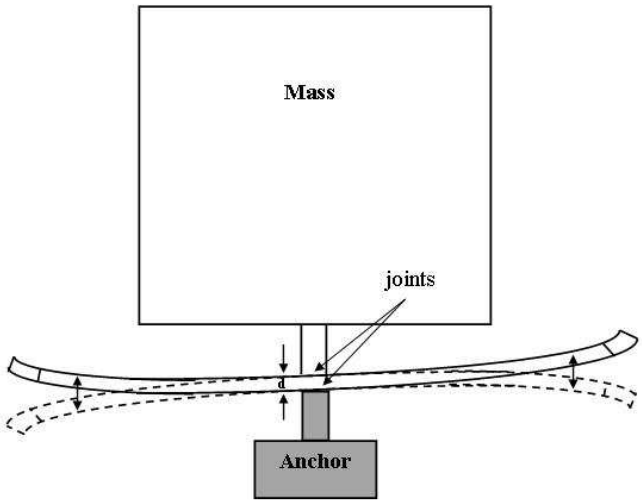

Figure 1.11: Illustration of a resonant accelerometer based on rigidity change [32].

small beam, when it is subject to acceleration. The beam can be depicted as a tiny guitar string, which is more or less stretched, depending on the acceleration acting on the seismic mass, so that its natural frequency is given by:

$$w = \sqrt{\frac{k(Ma_0)}{m}}, \tag{1.5}$$

where k is the stiffness of the beam, m its mass and Ma_0 is the inertial force acting on the seismic mass. The relation between the stiffness and the inertial force is usually nonlinear.

The concept of resonant sensing can be extended into that of 'parametric' sensing, in which a structure is designed so that its quality factor, its cutoff or resonance frequency (frequencies), its static gain, etc. are made sensitive to external changes. Parameter estimation methods can then be used not only to calibrate the system, but also to monitor its frequency response and keep track of the changes in its environment. This is for example the case of the sensor developed in the SYSRECAP project [35], to which the methods developed in this thesis will be applied as addressed in Chapter 5.

1.3.2 MEMS actuators

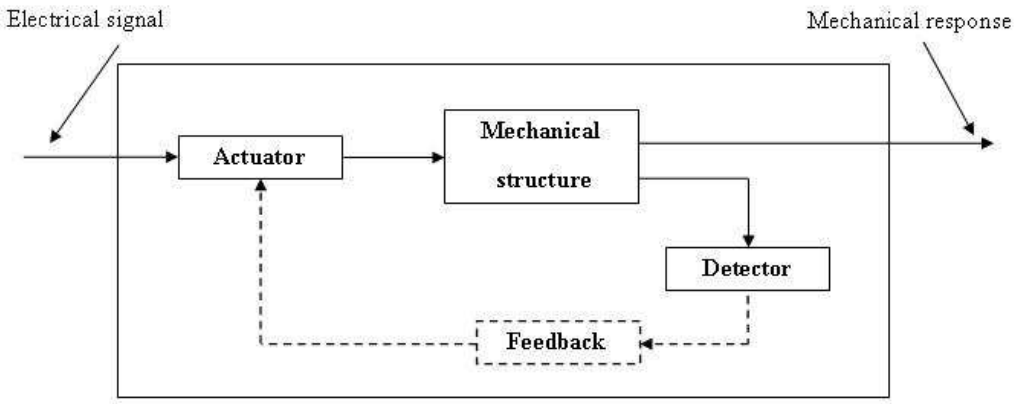

Figure 1.12: General schematic of a MEMS actuator [24]. The feedback loop (- - -) is optional.

MEMS actuators are employed to convert electrical signals into mechanical motion (Figure 1.12) in order to perform an action of deformation, positioning, vibration, pumping, etc. At the microscale, it is inefficient to use actuation principles relying on volume forces (such as magnetic forces, for example). The most prevalent microactuation principles are electrostatic force, thermal expansion and piezoelectricity [36, 37]. In this section, we give a brief overview of these actuation schemes.

Electrostatic actuation

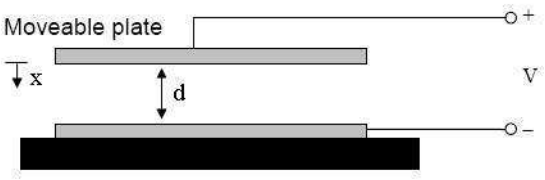

Figure 1.13: General schematic of an electrostatic microactuator [37].

By far the most common of the actuation principles used in MEMS, the electrostatic force is created by applying a voltage difference across two conducting bodies. A typical setup is the parallel-plate arrangement described in Figure 1.13. Usually the two conducting plates are separated by air. When a voltage V is applied across the capacitor, the potential energy in the system E is defined as:

$$E = -\frac{1}{2}CV^2, \tag{1.6}$$

where the capacitance C depends on the plate area A and the distance between the two plates d as:

$$C = \epsilon_0 \frac{A}{d}.$$

Thus, the resulting electrostatic force F along the x-axis is equal to:

$$F = -\frac{\partial E}{\partial d} = \frac{1}{2}\frac{\epsilon_0 A}{d^2}V^2. \tag{1.7}$$

Even though this actuation scheme is highly nonlinear (with respect to voltage and to the distance across the plates), it is the most widely-used in MEMS applications, because from the fabrication view point, it can be easy to cointegrate (i.e. to fabricate with the same process) an electrostatic microactuator with its control electronics on a SoC.

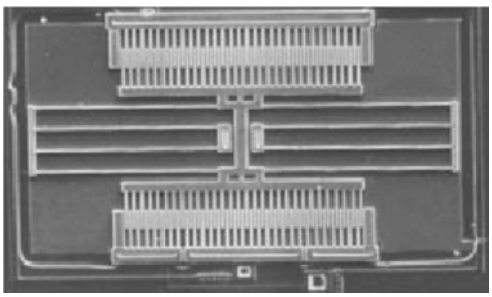

Figure 1.14: Scanning Electron Microscope (SEM) picture of a comb-drive electrostatic microactuator [38, 39].

Note that electrostatic actuation can be used for generating gap-closing forces, as described above, as well as forces parallel to the plate area, as in comb-drive microactuators (Figure 1.14) [38, 39].

Thermal actuation

Several forms of thermal actuation are used in MEMS applications, using such different principles as Shape Memory Alloys (SMA), bimetal effect, thermomechanical expansion, pneumatic actuation, etc [40, 41, 42].

For example, a thermal bimorph microactuator is made of two layers of material with different coefficients of thermal expansion (Figure 1.15). When heated (typically by driving a current through a resistive path), the difference in the thermal expansion coefficients results in a bending moment across the bimorph, which produces the deflection.

Generating a relatively large force and displacement at low actuating voltage is one of the advantages of thermal microactuators over electrostatic ones. Moreover, the dependence of the deflection on the actuating voltage is linear aver a very large range. Furthermore, it is also possible to cointegrate thermal actuators on a SoC. However, their use is practically limited by their high power consumption and low switching frequency. Moreover, the fabrication of a thermal actuator is usually a more complex process than that of an electrostatic actuator. Thus, thermal actuators are inherently more sensitive to variations in the fabrication process than their electrostatic counterparts.

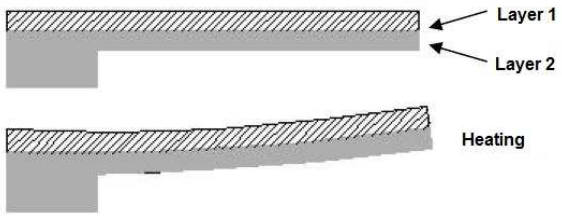

Figure 1.15: General schematic of a thermal bimorph microactuator [42].

Other actuation schemes

A great number of other actuation schemes may also be employed in MEMS applications, such as magnetic actuators and piezoelectric actuators [43, 44]. For example, the latter rely on the inverse piezoelectric effect, which is the deformation of a material subject to an electric field. In Figure 1.16, we show a typical piezoelectric microactuator, consisting of one layer of piezoelectric material sandwiched by two metallic plates. When a voltage is applied across the plates, the piezoelectric material expands in the direction of the beam axis, which results in a bending moment and a deflection [45]. Thus, piezoelectric

actuators behave similarly to thermal bimorphs. They have a number of advantages over these, such as smaller power consumption and larger switching frequencies. However, their fabrication is much more complex (at least three layers of material are necessary) and costly. Moreover, this type of actuators cannot be integrated in a standard CMOS process.

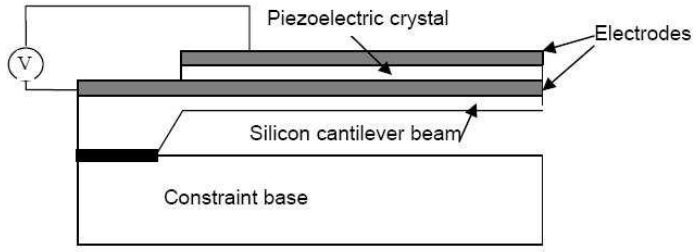

Figure 1.16: Schematic of a simple piezoelectric microactuator [45].

1.4 MEMS testing and identification

In the previous sections, we have tried to highlight in what respect MEMS sensors and actuators are sensitive to variations in their fabrication process and to their operating conditions. Although the latter may be put to use in parametric sensing applications, this sensitivity is usually a drawback with a negative impact on the reliability of MEMS devices. Another source of uncertainty, which also impacts MEMS reliability, is simple lack of precise knowledge regarding the physics of MEMS devices, most MEMS devices being designed thanks to reduced-order models based on over-simplifying assumptions [46]. Consequently, there is a need for testing, calibrating and possibly tuning MEMS devices before they are put on the market and all along their life-time [47, 48, 49]. Before they are commercialized, MEMS devices undergo a series of tests, under several operating conditions, to ensure that they meet a severe set of constraints. These tests are very expensive, the figure of 1/3 of the cost of a device being generally accepted as quite below the truth [9]. Moreover, they are very conservative, unless the MEMS device includes self-testing or self-calibrating features, so that it may adapt to changing operating conditions. One of the other issues of microsystem testing is caused by the multiple energy domains that exist in these microsystems. This particularity makes important issues against developing an inexpensive test method for high-volume complex microsystems [50]. Some of these issues are summed up in Appendix A.

The purpose of testing is to verify that the fabricated device is equivalent to the actual design and to indicate that a device can ensure all required specifications ("good" device). A typical chain of microsystem testing is shown in Figure 1.17 [51, 52]:
Test stimuli relies on the specifications of the device under test (DUT), with the goal

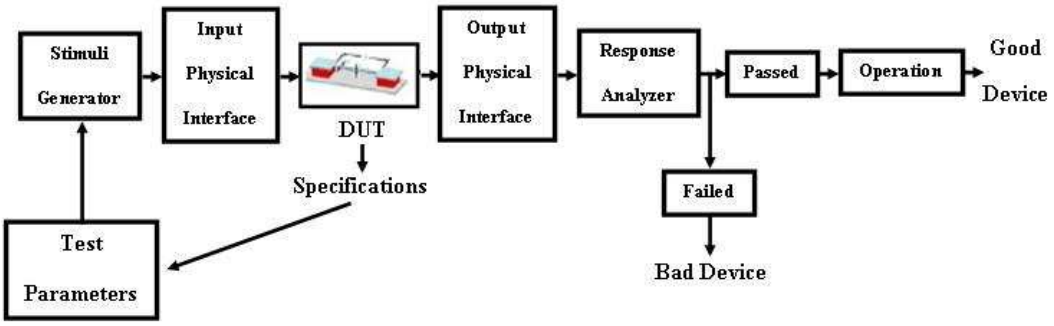

Figure 1.17: Typical chain of microsystem testing.

to achieve an appropriate test quality which can be evaluated based on test parameters (Figure 1.17). Communications between the stimuli generator and the input physical interface module is established through an electrical interface. The device (DUT) is then put to the test stimuli via the input physical interface module which can transform the electrical stimuli into an appropriate non-electrical shape, if required (i.e. when the input is non-electrical such as in sensors). Next, the output of the device under test is passed to the response analyzer via an output-physical-interface module which can transform the non-electrical test response into an electrical voltage or current (i.e. when the output is non-electrical such as in actuators). At last, the pass/fail status of the DUT is determined by the response analyzer according to specifications of the DUT.

During the last decades, different existing methods for testing and adjusting the microsystems have been developed which are briefly studied in the next subsections.

1.4.1 Related works in microsystem testing

The increasing request of MEMS in technology and industry motivates the need to develop robust testing methods as mentioned before. Recently, some significant contributions have been reported. Table 1.1 (extended from [51, 52]) summed up some previous works for different devices and objectives. Some important ones are investigated in the following.

In [53], Hartzell and Woodilla addressed a probabilistic approach to analysis the failure of the device under test. They proposed an empirically-generated model to estimate the accelerometers sensitivity while exposed to high mechanical shocks. It has been shown that as the shock level increases, the accelerometers recovery rate decreases and one can define an appropriate range for the shock test stimulus. Reliability characteristics of inertial sensors are commonly measured by vibration and shock tests [51]. Different frameworks of mechanical vibration test for commercial accelerometers and gyroscopes have been presented in [54, 55, 56].

In 1998, Kolpekwar and Kellen presented a classification method for defects in resonators. They generated 3D mesh models for the device. Finite Element Analysis (FEA)

of the resulting meshes has been then employed to define the resonant frequency that is an important parameter of the resonator [57]. They classified faults into three categories (harmless, parametric and catastrophic) according to the resonant frequency variations from the determined value. The extensions of this method have been reported in [58, 59] where the authors noted that one may not detect a defect in the capacitive sense structure of a resonator by means of mechanical resonant frequency test and it should be detected by an electrical sensitivity test. In [60], a testing method was also proposed for a magnetic field sensor based on a same fault classification. Castillejo and his co-workers also followed the similar fault classification method for different failure mechanisms that can influence CMOS-compatible MEMS [61].

Although several works on low-level analysis of MEMS misbehavior modeling like FEA have been reported in the related literature, some others presented various high-level modeling approaches (e.g., Analog Hardware Description Language (AHDL) models) to describe the behavior of MEMS [60, 62, 63, 64, 65]. For instance, Charlot and his co-workers modeled an electro thermal converter by using purely electrical models [65, 63]. They also modeled misbehavior by using extra electrical elements. In [60] and [64], the authors modeled, respectively, misbehavior of a magnetic field sensor and of an electrostatic comb-drive based on AHDL models. The parameters of comb-drive model (such as number of fingers) are modified to compensate misbehaviors (i.e., broken or missing fingers).

Recently, some methods aimed to the test of Micro-Opto-Electro-Mechanical Systems (MOEMS) have been also developed. For example, a testing method was presented in [66] where a micro-array of pixels with optical functionality is put to the test to detect individual damaged pixels. Furthermore, life duration testing is performed by exposing the pixels to deep ultra violet radiation (DUVR). Experimental results showed that over-exposure to DUVR may essentially decrease the pixels sensitivity.

Many of the previous contributions mentioned until now, suppose that test stimuli are produced by an external tester for MEMS application. However, some other methods [67, 68, 69, 70, 71, 9, 72, 73, 74] have been developed based on built-in, on-chip stimuli generation known as Built-In Self-Test (BIST) approaches which is studied in the next subsection.

Type of microdevice	T1: Pressure sensors, T2: Inertial MEMS T3: Thermal sensors, T4: Magnetic sensors T5: MOEMS
Nature of results	N1: Experimental, N2: Simulation, N3: Theoretical

Authors	Reference no.	T1	T2	T3	T4	T5	R1	R2	R3
Allen et al.	[67]		√					√	
Olbrich et al.	[68]		√						√
De Bruyker et al.	[70]	√					√		
Maudie et al.	[75, 76]	√	√						√
Castillejo et al.	[61]	√	√	√					√
Blanton et al.	[57, 58, 59]		√					√	
Kim et al.	[62]				√			√	
Beegle et al.	[54]		√				√		
Charlot et al.	[9, 63, 64, 65, 71]		√	√				√	
Hartzell et al.	[53]		√					√	√
Tanner et al.	[55, 56]		√				√		
Rosing et al.	[77]	√	√						√
Beroulle et al.	[60, 69, 72]				√			√	
Aikele et al.	[73]		√				√		
Durr et al.	[66]					√	√		
Puers et al.	[74]		√					√	
Xiong et al.	[78]		√					√	
Deb	[52]		√					√	

Table 1.1: Classification of some important related works in microsystem testing [51, 52].

1.4.2 Built-In Self-Test (BIST) methods

Built-in self-testability is becoming an essential design specification for microsystems. These techniques are very appealing for industrial applications to decrease testing cost and issues. Automatic microsystem testing and robust verification can be available thanks to BIST. These approaches are low-cost, compared with the very expensive testers used to check the microsystem after packaging. They also provide a monitoring possibility over the whole microsystem lifetime [52].

In built-in self-test approaches, it is essential to design a simple self-testable circuit with a minimum overhead, sufficient capability to satisfy the needed specifications and good accuracy in the case of parametric variations. It must also be robust against noise to provide test repeatability [52]. Hereafter, we briefly review a selection of works in this domain:

Pressure sensors

In [70], De Bruyker and his co-authors proposed a self-test method for pressure sensors based on thermal actuation of the sensor diaphragm. The schematic of the technique is shown in Figure 1.18. A resistive heater is employed to increase the air temperature in the sensor cavity under the membrane. The resulting pressure stimulates the membrane, thus, results in a diaphragm displacement that is measured by the gauge (Figure 1.18).

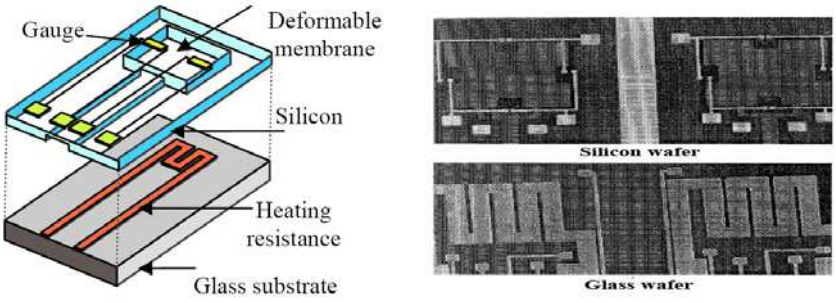

Figure 1.18: A self-test pressure sensor based on thermal actuation.

Inertial MEMS (resonator, accelerometer)

Several authors have presented self-test approaches for acceleration sensors in their works [67, 73, 74]. In 1989, Allen and his co-workers developed a basic idea of a self-test method for an accelerometer where the accelerometer is equipped with two self-test fingers [67]. An electrostatic force which is produced by applying an electrical signal, affects the seismic mass[1]. The displacement is then electrically detected by the capacitive gauges formed by the fingers and the fixed electrodes (Figure 1.19).

Alternative techniques of self-test stimuli generation for accelerometers, such as thermal and electromagnetic, have been also presented [73, 74, 79]. For instance, in [79], the authors proposed to replace the electrostatic actuation used to stimulate accelerometers by generating an electromagnetic force in the presence of magnetic field.

Recently, a BIST method aimed at capacitive MEMS accelerometers has been also proposed in [78]. The authors studied the use of different accelerometer technologies such as surface micromachined comb accelerometer, bulk micromachined capacitive accelerometer and so on.

In [68, 77], different self-test techniques and the use of temporal and spatial redundancy to increase the testing performance are investigated. The authors propose to use the spatial redundancy in an inertial sensor by selectively actuating identical sub parts of the device such as comb-drives in resonators. Nevertheless, no practical results or simulations are illustrated to confirm their claims.

[1]It is also called shuttle or proof mass of the accelerometer. While this mass is subjected to an acceleration, a resulting force displaces it.

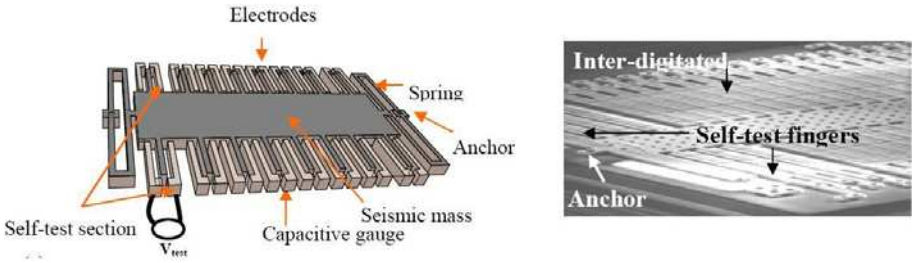

Figure 1.19: A self-test method for an accelerometer using electrostatic force.

Magnetic sensors

In [69, 72], testing methods for a magnetic field sensor are presented. In these methods, it is necessary to specify numerous parameters for each given device. Consequently, the full characterization of a given device is very expensive. The authors propose to use an oscillation-based test methodology to reduce the price of testing approaches. They use a feedback circuit to reconfigure the DUT into an oscillating device and to measure indirect parameters that are easier to observe. However, they do not provide any information about the performance and cost of the additional feedback circuitry.

Thermal sensors

A self-test method for a thermal sensor (an infrared-imager) consisting of a two-dimensional micro-array of pixels has been proposed in [71]. In this approach, thermopiles are fixed on four thin arms that suspend a membrane over the substrate and resistive heaters are used to increase the sensor temperature (Figure 1.20). The pixels are put to the test depending on the voltage signal value at the output of the thermopile. This testing method may take a long time in the case of large pixel arrays, because pixels are tested serially to reduce power consumption.

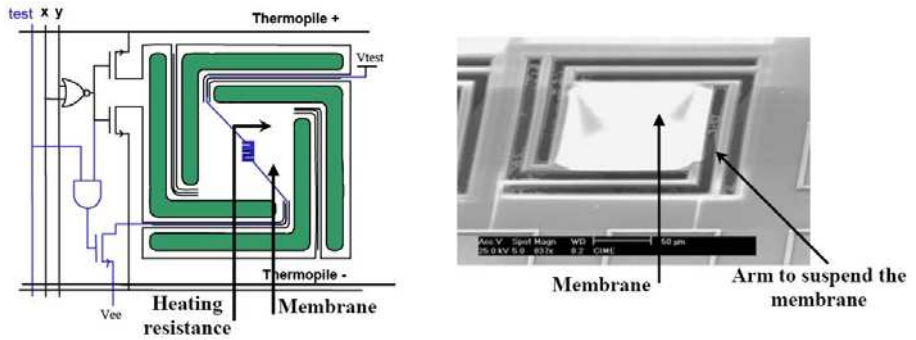

Figure 1.20: A self-test method for a thermal sensor (an infrared-imager).

1.4.3 Summary

As discussed in previous sections, several researches in recent years [50, 73, 74, 79, 78, 52, 51] have focused on proposing to include simple self-test features to MEMS devices. These may go from ad hoc solutions such as the development of particular electrical stimuli or mechanical test structures [50, 73, 74, 79] to more general application- and fabrication process-independent approaches based on parameter estimation methods [35, 51, 5]. These methods are summarized in Table 1.1. In this dissertation, we will concentrate on the latter type of methods and show how parameter estimation methods based on quantized or binary observations can be put to use in the context of MEMS testing, as well as that of parametric sensing. Quantized or binary identification methods (Figure 1.21) are good candidates for being implemented in a SoC with little added cost: in these methods, test-data acquisition requires only low-resolution (ideally 1-bit) ADCs or DACs, resulting in small silicon area and limited power consumption. Furthermore, the optimization routine used for the parameter estimation proper, based on the test-data, can be performed in the digital processing unit of the SoC. Ideally, this optimization routine should require as little data storage as possible and have a low computational complexity, so as to be easily implemented.

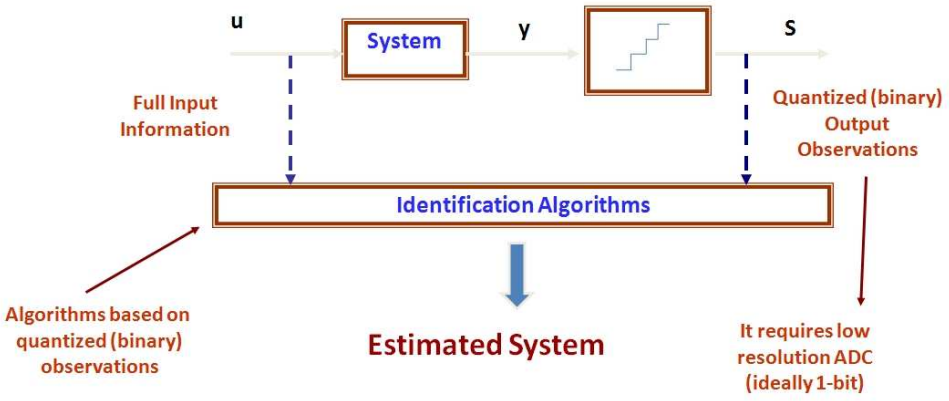

Figure 1.21: A general scheme of the identification methods based on quantized or binary observations.

1.5 Conclusion

In this chapter we have given an overview of MEMS technology and its applications, trying to highlight the many sources of uncertainty that may impact the reliability of MEMS device. These uncertainties may come from lack of knowledge, dispersions in the fabrication process and changes in their operating conditions.

In this light, the main objective of this thesis is to propose simple self-test or self-calibration methods to be integrated in a SoC, so that the constraints on the MEMS post-fabrication tests can be relaxed and the costs of these tests reduced. As explained above, the choice of parameter estimation methods relying on binary observations is made, because they are generic approaches, they imply little added cost (in terms of added silicon area or power-consumption) and they potentially have little computational complexity. Some important contributions in the field are presented in next chapter.

Chapter 2

Existing identification methods from binary or quantized observations

As concluded in the previous chapter, an alternative for expensive and complex MEMS testing methods is to integrate measurement, self-test (and self-tuning) features, such as parameter estimation approaches, in each device, in order to compensate the dispersions caused by changes in fabrication process or operation conditions for these microdevices. However, most parameter estimation methods [1, 2, 80, 81, 82, 83] do not easily scale down to the micro or nano-world. This is because these methods rely on high-resolution digital measurements of the system output. Their integration requires the implementation of high-resolution analog-to-digital converters (ADCs) and thus, results in longer design times, larger silicon areas and increased costs.

As a consequence, the methods based on quantized (ideally binary) outputs are appealing, because they require the integration of low-resolution ADCs (ideally only 1-bit) which is easy and low-cost to implement on System-on-Chip (SoC). These methods can be divided in two large categories, depending on whether they are probabilistic approaches or deterministic ones. We define probabilistic methods as methods in which the statistical properties (for example, the probability density function) of some signals are used explicitly to specify the solution of the parameter estimation problem. On the other hand, deterministic approaches do not explicitly rely on such knowledge. For example, in classical (non-quantized) parameter estimation problems, the least-mean squares (LMS) approach is deterministic. The general framework of these approaches is shown in Figure 2.1 where the unknown system is excited by an input signal u_k to produce the the system output z_k at time k ($z_k = y_k + b_k + d_k$). Let d_k be an additive dithering signal at the system output and b_k an additive noise with ${\sigma_d}^2$ and ${\sigma_b}^2$ as the second-order moment of the signals. The system output is then quantized to provide N quantized or binary observations s_k. These methods can be also divided in two subcategories, depending on whether they rely on the use of a dithering signal. A dithering signal acts as reference amplitude in the approaches relied on the use of this signal. In other words, it is not possible to identify the system's gain in these methods while ${\sigma_d}^2 = 0$ except if the quantizer

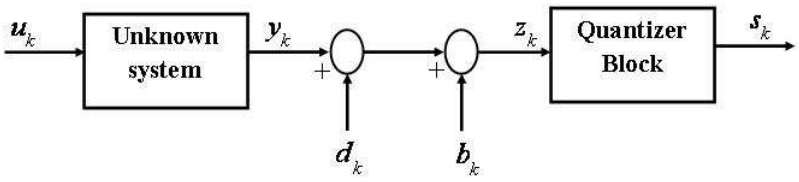

Figure 2.1: General framework of the approaches based on quantized or binary outputs.

has at least one threshold value different from zero. In this chapter, we present a selection of important approaches in this area with the same notations as introduced above. Furthermore, the advantages and limitations of these different methods are discussed in terms of computational complexity, storage requirements and ease of implementation in the context of microelectronics.

It should be mentioned that the sign regressors and sign-sign algorithms [84, 85, 86, 87] do not correspond to the context of binary or quantized outputs. Because in these cases, the output of the system z_k is available (Figure 2.2) and thus, the sign of the error is used: $sign(z_k - \hat{z}_k)$, where $\hat{z}_k$ is the estimated output ($\hat{z}_k = \hat{y}_k + d_k$). On the other hand, in our case of study, just the sign of the output $s_k = sign(z_k)$ is available. Note that the information contained in $sign(z_k - \hat{z}_k)$ is completely different from that contained in $s_k - \hat{s}_k$, where $\hat{s}_k = sign(\hat{z}_k)$: $sign(z_k - \hat{z}_k) \neq s_k - \hat{s}_k$. That is why the methods based on sign-sign errors are not investigated in this research work.

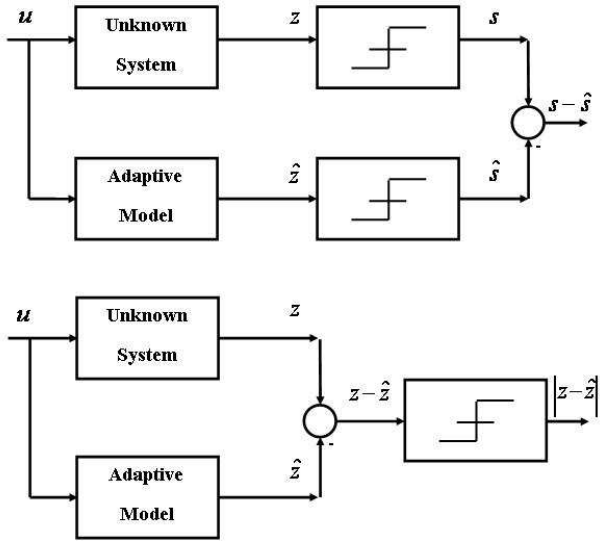

Figure 2.2: The general schematic of the algorithms based on binary outputs (top) and of the methods relied on sign-sign errors (down).

2.1 Probabilistic methods

2.1.1 Methods using a dithering signal

In 2003, Wang and his co-authors [3] have presented a method for estimating parameters from binary (or quantized) data in a stochastic framework by using a dithering signal (Figure 1.1 with $d_k \neq 0$). The threshold of the quantizer C is "randomly specified" by a partially known dithering signal d_k[1] as shown in Figure 2.3. The convergence of the algorithm is ensured provided that d_k is a sequence of independent and identically distributed (i.i.d.) zero-mean random variables with distribution function $F(d)$, which is a continuous function whose inverse F^{-1} exists and is known continuous.

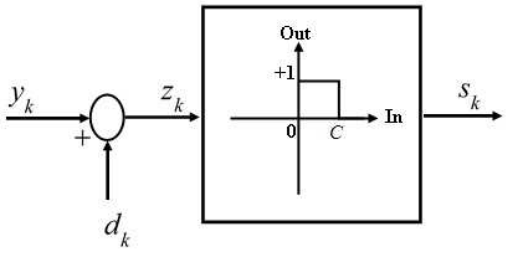

Figure 2.3: Quantizer block presented in [3]: the threshold of the quantizer C is randomly specified by a dithering signal d_k.

The proof of the convergence is first studied for a basic estimation approach where system is assumed with only one unknown parameter to be estimated. This basic approach that can be then generalized to Finite Impulse Response (FIR) models is investigated hereafter:

$$\begin{cases} z_k = \theta + d_k \\ s_k = S(z_k) \end{cases}, \tag{2.1}$$

where θ is to be estimated, z_k is the output of the system when a unit step function is used as the input signal ($u_k = 1, \quad \forall k > 0$) and s_k is binary-valued observations with threshold C. When $s_k = 1$,

$$z_k \leq C \Leftrightarrow d_k \leq C - \theta. \tag{2.2}$$

Considering equation above (2.2), it is possible to write:

$$p = E[s_k] = P(s_k = 1) = P(d_k \leq C - \theta) = F(C - \theta). \tag{2.3}$$

By assuming invertibility of $F(x)$,

$$\theta = C - F^{-1}(p). \tag{2.4}$$

[1]From the point of view of electronics, this "randomly specified" threshold can be implemented as an addition of a dithering signal at the input of the (fixed-threshold) quantizer.

If p can be estimated, then θ can also be estimated. We obtain an empirical measure of p by taking N measurement of s_k:

$$\xi_N = \frac{1}{N}\sum_{k=1}^{N} s_k. \tag{2.5}$$

Using (2.5) as an empirical measure of p and (2.4), we can deduce:

$$\hat{\theta}_N = C - F^{-1}(\xi_N). \tag{2.6}$$

It is then established that if $F(x)$ is continuously differentiable and non-zero [88]:

$$\xi_N \xrightarrow{N\to\infty, w.p.1} p \Rightarrow \hat{\theta}_N \xrightarrow{N\to\infty, w.p.1} \theta. \tag{2.7}$$

The main contribution in [3] is to extend this basic estimation problem to FIR models:

$$\begin{cases} z_k = a_0 u_k + ... + a_{n-1} u_{k-n+1} + d_k \\ s_k = S(z_k) \end{cases}, \tag{2.8}$$

where $\boldsymbol{\theta} = [a_0, ..., a_{n-1}]^\top$ is to be estimated, u_k is assumed to be n-periodic[2], d_k is i.i.d. distributed with a distribution function $F(x)$ and s_k is binary-valued observations with threshold C. When u_k is n-periodic, $w_k = a_0 u_k + ... + a_{n-1} u_{k-n+1}$ is also n-periodic. Thus,

$$\boldsymbol{w} = \boldsymbol{\Phi}\boldsymbol{\theta}, \tag{2.9}$$

where, $\boldsymbol{w} = [w_1 ... w_n]^\top$ and

$$\boldsymbol{\Phi} = \begin{pmatrix} u_1 & u_2 & ... & u_n \\ u_2 & u_3 & ... & u_1 \\ . & . & ... & . \\ u_n & u_1 & ... & u_{n-1} \end{pmatrix}. \tag{2.10}$$

Now, it is possible to derive n basic estimation problems such as:

$$\begin{cases} z_{nl} = w_1 + d_{nl}, \quad s_{nl} = S(z_{nl}), \quad l = 0, 1, ... \\ z_{nl+1} = w_2 + d_{nl+1}, \quad s_{nl+1} = S(z_{nl+1}), \quad l = 0, 1, ... \\ . \\ . \\ . \\ z_{nl+n-1} = w_n + d_{nl+n-1}, \quad s_{nl+n-1} = S(z_{nl+n-1}), \quad l = 0, 1, ... \end{cases} \tag{2.11}$$

As in the basic approach, for $i = 1, 2, ...n$, Nn measurement of s_k is then taken to achieve the empirical measure of $p_i = F(C - w_i)$:

$$\xi_N^i = \frac{1}{N}\sum_{l=1}^{N} s_{nl+i}. \tag{2.12}$$

[2] $\forall t, \quad u(t+n) = u(t)$

The estimation of w_i is then obtained as:

$$\hat{w}_N^i = C - F^{-1}(\xi_N^i). \tag{2.13}$$

By the Glivenko-Cantelli Theorem:

$$\boldsymbol{w_N} \xrightarrow{N\to\infty, w.p.1} \boldsymbol{w}, \tag{2.14}$$

where $\boldsymbol{w_N} = [w_N^1 ... w_N^n]^\top$.

When the input signal u_k is n-periodic, $\boldsymbol{\Phi}$ (2.10) is a circulant Toeplitz matrix and is full rank[3]which yields:

$$\hat{\boldsymbol{\theta}}_{\boldsymbol{N}} = \boldsymbol{\Phi}^{-1}\boldsymbol{w_N} \xrightarrow{N\to\infty, w.p.1} \boldsymbol{\Phi}^{-1}\boldsymbol{w} = \boldsymbol{\theta}. \tag{2.15}$$

Therefore, the convergence is guaranteed in this method under two conditions:

- The input signal is n-periodic and full rank.

- The distribution function $F(x)$ of dithering signal is known and invertible.

In [89], the optimality of this algorithm is also established by deriving the Cramer-Rao lower bound. Furthermore, this work has been extended to nonlinear Wiener models [90] as well as Hammerstein systems [91].

This method and its extensions are interesting for macro-applications in different domains [92, 93, 94, 95, 96, 97]. However, its major constraint in the field of microdevices is that $F(x)$ must be invertible. Although it is usually possible to generate continuous dithering signals, this constraint prevents their approach from being used with discrete-valued dithering signals, which are very easy to generate in the context of microelectronic applications. Recently, the authors relaxed the second assumption where it is proved that the cumulative distribution function of the threshold does not have to be known a priori and it can be estimated along with the system parameters [98]. However, a 2n-periodic full rank input must be employed in this method.

In [99], Rafajlowicz proposed another parameter estimation algorithm using a dithering signal. This method is based on the Von Neumann theorem [100, 101] and on the maximum likelihood (ML) principle. He considers a linear system excited by an input signal. The output of the system is measured via a quantizer whose threshold is "randomly specified". An argument based on Von Neumann's theorem is then used to estimate the Fourier transform of the quantizer's input from the quantized data and, knowing the inputs, it becomes simple to estimate the transfer function of the system. Since this method is of the same nature as the previous one but much less general in scope, we do not go into further details.

[3]The n-period input is said to be full rank if $\boldsymbol{\Phi}$ is invertible [3].

2.1.2 Methods without a dithering signal

In 2003, Negreiros [102] suggested to use a white Gaussian input to excite the unknown linear system and to estimate the power spectral density (PSD) of the binary output in order to derive the modulus of the transfer function of the unknown system (Figure 2.1 with $d_k = 0$).

Considering the system output, $y(t)$ is a normal stationary process with zero mean, the autocorrelation of the output of the quantizer (Figure 2.4), $s(t)$ is obtained as ([103], eq.10-71, p.307):

$$R_s(\tau) = \frac{2}{\pi} \arcsin \frac{R_y(\tau)}{R_y(0)}, \tag{2.16}$$

where R_y is the autocorrelation of the system output. Thus, one can estimate the power spectrum density of the system output from this autocorrelation function. The magnitude of the system transfer function is then calculated by the ratio of the power spectrum densities (PSDs) of the input, $G_u(f)$ and of the system output $G_y(f)$:

$$|H(f)|^2 = \frac{G_y(f)}{G_u(f)}. \tag{2.17}$$

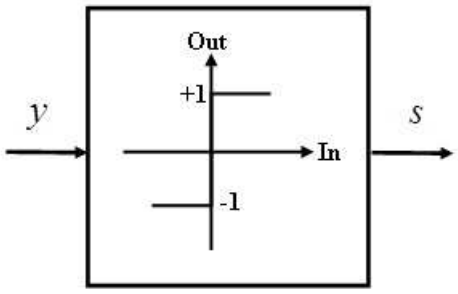

Figure 2.4: A single bit quantizer.

This simple method is appropriate for linear circuits with very low cost and the smallest possible analog overhead area. It is suitable to be implemented in the System-on-Chip (SoC) environment, as we can also reuse the resources which have been already available in the system [102].

Another method has been presented in [104] where the authors used a white Bernoulli input as an exciting signal instead of using a white Gaussian input. They calculated an estimation of the cross-covariance between u_k and s_k:

$$\hat{C}_{su}(p) = \frac{1}{N} \sum_{k=1}^{N} s_k u_{k-p}. \tag{2.18}$$

It has been then shown that the relation between the coefficients of the impulse response and the cross-covariance function is almost linear by using ([104], eq.13, p.579). Therefore, it may be approximated with sufficient accuracy with a third- or fifth-order Taylor expansion. Provided the mixing properties of the linear system are good (i.e. its impulse response does not vanish too quickly), it is then possible to identify the unknown system by using the analytical relationship between the cross-covariance function of the binary inputs and outputs and the impulse response of the unknown system. They also established the statistical properties of (2.18) in the case of binary inputs and outputs:

$$E\left(\hat{C}_{su}(p)\right) = \frac{1}{N}\sum_{k=1}^{N} E\left(s_k u_{k-p}\right) = C_{su}(p), \tag{2.19}$$

$$\mathrm{var}\left(\hat{C}_{su}\right) \approx \frac{1}{N}. \tag{2.20}$$

It is then shown by simulations that (2.20) is valid in the case of any white and centered input u_k.

Recently, Wigren and his co-workers presented a new method for linear systems with quantized outputs based on Maximum Likelihood estimation [105]. The problem is considered when noise enters not only between the linear system and the quantizer (Figure 2.1), but also after the quantizer. This makes the setup different from their previous works [106, 107] that will be studied in the next subsection. They used the Expectation Maximization (EM) algorithm with a hidden[4] variable, called

$$\boldsymbol{Z_N} := z_1, z_2, ..., z_N. \tag{2.21}$$

The idea in the EM algorithm is then to iterate by first finding an estimate of $\boldsymbol{Z_N}$, called $\hat{\boldsymbol{Z}}^i_N$ using a trial value of system parameters $\boldsymbol{\theta}$, called $\hat{\boldsymbol{\theta}}_{\boldsymbol{i}}$, and then maximizing a quantity related to:

$$P\left(\boldsymbol{S_N}, \hat{\boldsymbol{Z}}^{\boldsymbol{i}}_{\boldsymbol{N}} | \boldsymbol{\theta}\right), \tag{2.22}$$

with respect to $\boldsymbol{\theta}$. The main contribution of this work is to propose a scenario-based form of the EM algorithm in order to simplify the calculations [105].

Some other works in this domain can be also found in the literature where the authors have used different assumptions such as Gaussian random input [108, 109, 110] or an unknown invertible nonlinearity (quantizer block) [111, 112].

[4]The terminology arises from the statistics literature.

2.2 Deterministic approaches

A classical Least-Square (LS) approach for estimating the system parameters is to minimize a quadratic distance between the observed outputs (s_k) and the estimated ones ($\hat{s}_k$). In the case of quantized or binary observations, the LS criterion may be written as:

$$J_0^N = \frac{1}{4N}\sum_{k=1}^{N}(s_k - \hat{s}_k)^2. \tag{2.23}$$

It is clear that $0 \leq J_0^N \leq 1$. Moreover, since $(s_k - \hat{s}_k)^2$ takes only two values, 0 and 4, it is simple to see that J_0^N is a multiple of $\frac{1}{N}$. Thus, the classical LS criterion is not continuous which results in optimization problems, when applied to binary observations.

Another issue lies in the non-uniqueness of the minimizer of the classical LS criterion (J_0^N), when used in binary contexts. That is why some LS-based approaches [106, 107, 5] have been presented during the previous years in order to solve these issues. Figure 2.1 ($d_k = 0$) represents a general setup for this kind of approaches, however it is also possible to use a dithering signal for these methods.

In [107], one of these approaches has been proposed by Wigren to solve the system identification problems based on quantized (binary) observations. In the case of binary outputs, i.e. using sign function as the quantizer block (Figure 2.4), this method can be formulated based on a least-mean-square algorithm in the form of:

$$\hat{\boldsymbol{\theta}}_{k+1} = \hat{\boldsymbol{\theta}}_k - \alpha_k\,(\hat{s}_k - s_k)\,\frac{\partial \tilde{s}_k}{\partial \hat{\boldsymbol{\theta}}_{\boldsymbol{k}}}, \tag{2.24}$$

where $\hat{\boldsymbol{\theta}}_k$ is the estimated system parameters at iteration k, $\alpha_k > 0$ is a regulative coefficient in order to ensure the stability and convergence of the algorithm and $\tilde{s}_k$ is a continuous approximation of the quantizer block (sign function). For instance, this approximation can be expressed as:

$$\tilde{s}_k = \frac{2}{\pi}\arctan\left(\frac{\hat{z}_k}{z_0}\right), \tag{2.25}$$

where z_0 is an arbitrary constant chosen based on prior knowledge of the amplitude of z. The quantity $\partial\tilde{s}_k/\partial\hat{\boldsymbol{\theta}}_{\boldsymbol{k}}$ is the so-called "pseudo gradient" of $\hat{s}_k$.

The author, then, related the updating equations of the algorithm to an associated ordinary differential equation (ODE) using a formal change of the time scale. Using the arguments from [113], local convergence of the algorithm is tied to local (linearized) stability of the associated ODE, whereas global convergence is linked to global Lyapunov stability of the associated ODE. The global convergence to the nominal parameters is finally proved for a finite impulse response (FIR) system with an arbitrary and known output quantizer under the assumption that the quantizer has at least one threshold value different from zero, building from [1, 114, 113] where Ljungs method of analysis is extended to the Wiener model case.

This approach can use not only online, but also offline by the minimization of continuous LS criteria in the form of:

$$W^N = \frac{1}{4N}\sum_{k=1}^{N}\left(s_k - \hat{s}_k\right)^2\left(\hat{s}_k\tilde{s}_k\right), \tag{2.26}$$

where N is the number of observations (see Figure 2.5 for an illustration). In this method, an approximation of the quantizer has been introduced that makes it possible to define an approximate gradient of the LS criteria [107, 4].

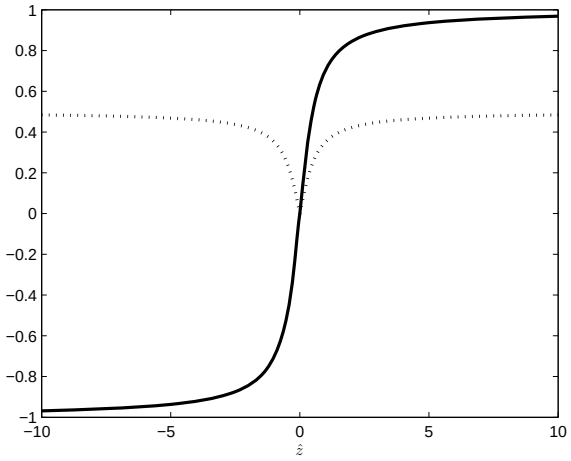

Figure 2.5: Illustration of $f(\hat{z}) = \frac{1}{2}\left(\hat{s}_k\tilde{s}_k\right)$ (dotted line) and of a continuous approximation of the quantizer block $\tilde{s}(\hat{z})$ (solid line) obtained from Wigren's method with $z_0 = 0.5$.

Recently, the theoretical framework of a Basic Identification Method using Binary Observations (called BIMBO) was introduced by Colinet and Juillard [5]. This method relies on an offline weighted least squares (WLS) approach for parameter estimation problems based on binary data. In the proposed framework (Figure 2.1), the known input signal u_k is filtered by a discrete-time invariant linear system H to produce the (scalar) value of the system output y_k at time k. H has a finite impulse response of length L, i.e. $\boldsymbol{\theta} = (\theta_k)_{k=1}^{L}$. The system output is then measured via a 1-bit ADC so that only the sign $s_k = sign(z_k)$ of the system output is known where $z_k = y_k + b_k$.

In [5], it is shown that the problem of estimation of system parameters $\boldsymbol{\theta}$ from $\hat{\boldsymbol{\theta}}$ based on N binary measurement can be treated by minimizing WLS criteria of the form:

$$J_p^N = \frac{1}{4}\frac{\sum_{k=1}^{N}\hat{z}_k^{2p}\left(s_k - \hat{s}_k\right)^2}{\sum_{k=1}^{N}\hat{z}_k^{2p}}, p \geq 1. \tag{2.27}$$

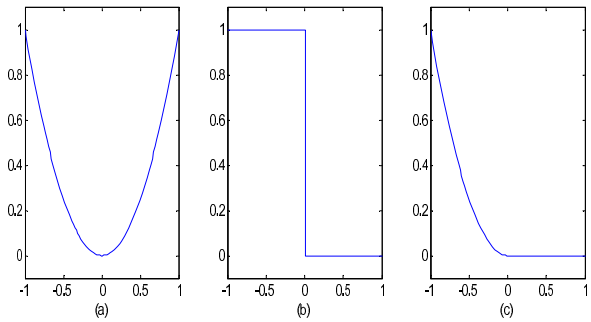

Figure 2.6: (a)$\hat{z}^2$, (b)$\frac{1}{4}(s - sign(\hat{z}))^2$ and (c) $\frac{1}{4}\hat{z}^2(s - sign(\hat{z}))^2$.

The term $\hat{z}_k^{2p}$ acts as a (positive) parameter dependent weight to the binary-valued error $(s_k - \hat{s}_k)^2$ in order to smooth out the discontinuities of the unweighted least-squares criterion (2.23). Because each of the terms under the sum sign in (2.27) is a continuous function of $\hat{\boldsymbol{\theta}}$, J_p^N is also continuous. Moreover, $\hat{z}_k^{2p}(s_k - \hat{s}_k)^2$ is continuously differentiable with respect to $\hat{z}_k$ (see Figure 2.6 for an illustration). Since $\hat{z}_k(\hat{\boldsymbol{\theta}})$ is continuously differentiable everywhere, $J_p^N(\hat{\boldsymbol{\theta}})$ is also continuously differentiable everywhere, except when:

$$\sum_{k=1}^{N} \hat{z}_k^{2p} = 0. \tag{2.28}$$

Since $\hat{z}_k^{2p}$ is positive, (2.28) is equivalent to:

$$\hat{z}_k = 0, 1 \leq k \leq N. \tag{2.29}$$

Since $(\hat{s}_k - s_k)^2$ takes only two values, 0 and 4, it is clear that $0 \leq J_p^N \leq 1$ and:

$$J_0^N = 0 \Longleftrightarrow J_p^N = 0, \tag{2.30}$$

where J_0^N is the (discontinuous) non-weighted least-squares criterion. In [5], the case when $p = 1$ is studied in depth and the properties of the corresponding WLS criterion, J_1^N, are established in a probabilistic framework, when N goes to infinity. In particular, it is shown that:

$$J_1^\infty(r) = \frac{1}{\pi}\left(\arccos(r) - r\sqrt{1 - r^2}\right), \tag{2.31}$$

$$J_0^\infty(r) = \frac{1}{\pi}\left(\arccos(r)\right), \tag{2.32}$$

where r is the correlation coefficient of z and $\hat{z}$ (Figure 2.7).
Furthermore, the authors proved that $J_1^\infty(\hat{\boldsymbol{\theta}})$ is convex in a neighborhood of its minimum and it is shown that the proposed criterion converges asymptotically to the optimal parameters regardless of the measurement noise provided the signal at the input of the quantizer $\hat{z}$ is Gaussian and centred [5].

Although, this offline method has been developed for using in the micro-applications [5], it bears some drawbacks in terms of storage requirement and computational complexity. It means that a large storage requirement is needed for this approach that is difficult

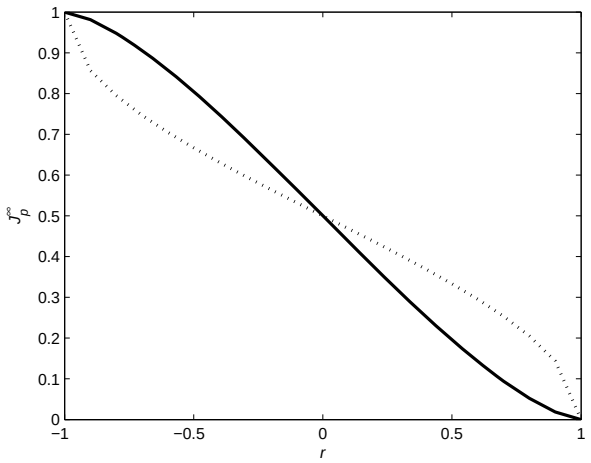

Figure 2.7: Illustration of $J_1^\infty(r)$ (solid line) and $J_0^\infty(r)$ (dotted line).

to provide in the context of microelectronics. Moreover, not only minimization algorithm used in this method has a high computational complexity but also its proposed criterion. These reasons make BIMBO difficult to implement on SoC.

2.3 Summary and discussion

Different identification methods based on quantized or binary outputs have been studied in the previous sections with various principals, advantages and drawbacks. We concentrate on the advantages and limitations of these methods in the context of microsystems at this section.

Starting from the first group (probabilistic methods), in our opinion, although the hypotheses on the quantizer's input and on the random threshold in Wang's methods are much less strict than those hypotheses in Rafajlowicz's method, the major constraint for these approaches in the context of our study is that the cumulative distribution function (cdf) of the threshold must be invertible which may only be achieved by using high-resolution ADCs. Furthermore, a matrix inversion step is used in Wang's method that makes this approach more complex in terms of calculation. Also, the Maximum Likelihood and EM-based algorithms [105] mostly suffer from high computational complexity because of their integrals evaluation process. Contrarily, one of the suitable approaches in this context is a pseudo-random testing method presented by Negreiros. This technique can be implemented in the SoC environment. However, the generation of a white Gaussian input requires a high-resolution digital-to-analog converter (DAC), whose implementation can be costly. These issues are partially solved in [104], where a white Bernoulli input is used as an exciting signal (thus requiring only a 1-bit DAC). Although this approach is fairly simple to implement [115], it relies on the mixing properties of the linear system, which may not be guaranteed a priori.

From the second group (deterministic approaches), we believe that Wigren's approach fits in the context of microsystem because it does not require a varying threshold (dithering signal), which can only be implemented with a high-resolution DAC or a surface-consuming analog component that increases the cost of the system (as opposed to Wang's or Rafajlowicz's methods). Furthermore, it can be used not only offline but also online and without specific input design. However, it does rely on an approximation of the quantizer. Thus, it is not an exact method as opposed to BIMBO.

Two distinguishing features of BIMBO are that no approximation of the quantizer is made, and the asymptotical convergence of the algorithm to the nominal system parameters can somehow be guaranteed, even in the presence of measurement noise. Although, this method bears some likeness to Wigren's methods, in the sense that it is based on the minimization of a least-squares criterion, it is more general than [3, 98, 116, 99] in the sense that it requires no specific input design. However, this offline method suffers some drawbacks in terms of storage requirements and computational complexity in the implementation context of microdevices like the other existing batch-data-based methods.

2.4 Conclusion

Most classical system identification methods cannot be used in the field of microdevices because of their implementation issues. Due to this fact, estimation methods based on quantized (ideally binary) outputs can play an important role in this context because they can be easily implemented with low-resolution ADCs on a small silicon surface. Thus, some important methods based on quantized or binary observations have been studied in this chapter. We investigated the advantages and limitations of these approaches in the context of MEMS integration and compared them in terms of storage requirements and implementation complexity.

We can conclude that although the methods using a dithering signal at the input of the quantizer may be useful in several macro scale applications, it is difficult to scale down these methods to the context of integrated microelectronics. Because all these methods rely on the fact that the cumulative probability distribution function of the dithering signal must be invertible that may only be achieved by using high-resolution ADCs. On the contrary, the approaches working without the use of a dithering signal such as pseudo gradient-based methods are easier to downscale.

Based on the advantages and drawbacks of these techniques, we try to propose new methods in order to relax some of these limitations in the context of microdevices. As a consequence, an alternative WLS criterion is presented in Chapter 3 that relies on the criterion introduced for BIMBO. However, the proposed criterion is easier to implement than (2.27) in the context of microelectronics. Furthermore, a new recursive estimation method is proposed in Chapter 4 which can be used as an inexpensive test method, requiring only little memory storage with a low computational complexity (as opposed to an offline method e.g. BIMBO) and amenable to implementation on FPGAs or small processor cores as used in System-on-Chip applications. The practical application of this

method is also presented in Chapter 5.

Chapter 3

An offline WLS method

In this chapter, we present an adaption of the BIMBO method, presented in chapter 2, for parameter estimation based on binary data. This represents the first contribution of this thesis, chronologically speaking. The asymptotical properties of the proposed criterion are established in a probabilistic framework. These asymptotical results are then illustrated by simulations in various contexts.

We compare the proposed criterion with the one presented for BIMBO [5]. We show that these two criteria do not have the same asymptotical behavior although they are closely related, particularly, in the presence of noise.

Furthermore, we study the quality of the proposed WLS approach when only a finite number of samples are available. An upper bound of the number of samples that are necessary for identifying system with a given accuracy is theoretically derived. The accuracy is defined in the sense of correlation coefficient between the optimal system parameters and our estimated system parameters. Theoretical results are also compared with simulations in order to study the validity of the results.

3.1 Framework and notations

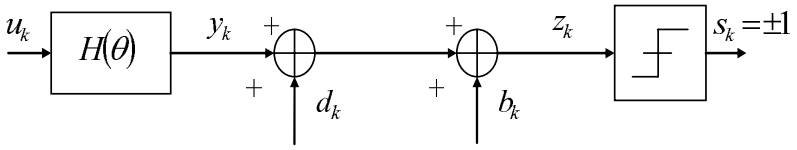

Figure 3.1: System framework.

Let us consider a discrete-time invariant linear system H. We assume H has a finite impulse response of length L, i.e. the impulse response can be represented by a column vector $\boldsymbol{\theta} = (\theta_k)_{k=1}^{L}$. Let u_k be the known scalar value of the system input at time k and y_k be the (scalar) value of the system output, so that:

$$y_k = \boldsymbol{\phi}_k^\top \boldsymbol{\theta}, \tag{3.1}$$

where $\boldsymbol{\phi_k} = (u_l)_{l=k-L+1}^{k}$ is the (column) vector of observations at time k. Let d_k be an additive dithering signal and b_k an additive noise at the quantizer's input. Let m_x and σ_x^2 denote the first- and second-order moments of any signal x. The system output is then measured via a 1-bit ADC so that only the sign $s_k = S(z_k)$ of the system output is known, where

$$\begin{cases} S(x) = 1, & \text{if } x \geq 0 \\ S(x) = -1, & \text{otherwise.} \end{cases}, \tag{3.2}$$

and $z_k = y_k + d_k + b_k$.

We are interested in finding an estimate $\hat{\boldsymbol{\theta}}$ of $\boldsymbol{\theta}$, based on N observations of u_k, s_k and, if need be, d_k. The estimated quantities are denoted by a hat (e.g. $\hat{z}_k = \hat{y}_k + d_k$) and $\hat{\boldsymbol{\theta}}$ has also length L. These notations are summed up in Figure 3.1.

3.2 The proposed WLS criterion

Recall that the classical LS criterion faces some issues, when applied to binary observations, that results in optimization problems. In [5], the authors tackle these issues by introducing new method, called BIMBO (see Chapter 2). However, this method suffers some drawbacks in the context of microsystem implementation as mentioned in the last chapter. The optimization algorithm used for minimizing the criteria has a high computational and implementation complexity and requires a large storage requirement like other batch-data-based methods. Moreover, the proposed criteria J_p^N (2.27) is difficult to implement on SoC.

Thus, an alternative method for BIMBO having binary measurements, is to define criteria with a lesser computational and implementation complexity comparing with (2.27). We propose the criteria in the form of:

$$G_f^N = \frac{1}{4N} \sum_{k=1}^{N} f(\hat{z}_k) \, (s_k - \hat{s}_k)^2, \tag{3.3}$$

where $f(.)$ is a continuously differentiable function that satisfies $f(0) = f'(0) = 0$ and $f'(x) > 0, \forall x \in \Re^+$, in order to ensure continuous differentiability of G_f^N. In the case when $f(x) = x^{2p}$, the corresponding criteria is derived as:

$$G_p^N = \frac{1}{4N} \sum_{k=1}^{N} \hat{z}_k^{2p} \left(s_k - \hat{s}_k\right)^2, p \geq 1 \tag{3.4}$$

in which the term $\hat{z}_k^{2p}$ acts as a (positive) weight to the binary valued error $(s_k - \hat{s}_k)^2$ and smooths out the discontinuities of the unweighted classical criterion (see Figure 3.2 for an illustration). In addition, it is clear that:

$$G_0^N = 0 \Longleftrightarrow G_p^N = 0, \forall p \geq 1, \tag{3.5}$$

i.e. that G_0^N and G_p^N are equivalent in the noise-free case [5] in the sense that all the $\hat{\boldsymbol{\theta}}$ that minimize G_0^N also minimize G_p^N and vice versa (Figure 3.2).

In the next sections, we focus on the following criterion (for $p = 1$ as an example):

$$G_1^N = \frac{1}{4N} \sum_{k=1}^{N} \hat{z}_k^2 \left(s_k - \hat{s}_k\right)^2. \tag{3.6}$$

and establish its properties in a probabilistic framework, when N goes to infinity. This criterion is then compared with J_1^N by simulation results. Furthermore, we study some non-asymptotical properties of G_p^N in order to investigate the estimation quality and performance efficiency of the proposed WLS criteria.

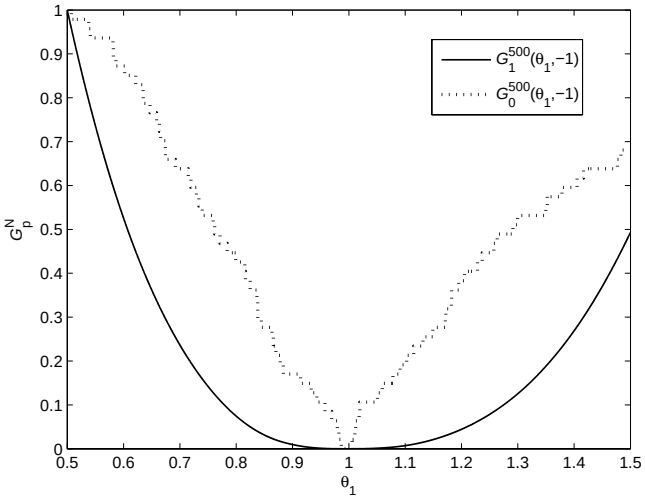

Figure 3.2: Comparison of G_1^N and unweighted classical criterion (G_0^N) for $N = 500$ and $\boldsymbol{\theta} = [1, -1]$.

3.3 Asymptotic properties of G_1^N

In order to perform the asymptotic analysis of G_1^N, let us consider that u_k, d_k and b_k are stationary processes. Let R_u^{LL} be the $L \times L$ covariance matrix of u. Since H is LTI, y_k and z_k are stationary and so are $\hat{y}_k$ and $\hat{z}_k$. The binary signals s_k and $\hat{s}_k$ are also stationary. This can be inferred from the fact that $S(a)S(b) = S(ab)$ and thus,

$$E\left(S\left(x(t)\right)S\left(x(t+\tau)\right)\right) = E\left(S\left(x(t)x(t+\tau)\right)\right) = 2P\left(x(t)x(t+\tau) \geq 0\right) - 1, \tag{3.7}$$

where, $E(.)$ denotes the expected value and $P(.)$ the probability. Provided x is stationary, the right-hand side of (3.7) depends only on τ and, thus, $S(x)$ is stationary. It follows that sums and/or products (as those appearing in (3.6)) of these processes are also stationary.

It is possible to interpret G_1^N as the empirical mean of a stationary process. Thus,

$$G_1^\infty = \lim_{N\to\infty} G_1^N = \frac{1}{4} E\left(\hat{z}_k^2 \left(s_k - \hat{s}_k\right)^2\right). \tag{3.8}$$

An analytical expression for (3.8) is then, established when z_k and $\hat{z}_k$ are jointly Gaussian with mean zero[1]. Thus, one may write:

$$\begin{aligned} G_1^\infty &= \frac{1}{4}\int_{-\infty}^{+\infty}\int_{-\infty}^{+\infty} \hat{z}^2 \left(S(z) - S(\hat{z})\right)^2 p\left(\hat{z}, z\right)\, d\hat{z}\, dz \\ &= \frac{1}{4}\left(\int_{-\infty}^{0}\int_{0}^{+\infty} \hat{z}^2 p\left(\hat{z}, z\right)\, d\hat{z}\, dz + \int_{0}^{+\infty}\int_{-\infty}^{0} \hat{z}^2 p\left(\hat{z}, z\right)\, d\hat{z}\, dz\right), \end{aligned} \tag{3.9}$$

with

$$p\left(\hat{z}, z\right) = \frac{1}{2\pi\sigma_{\hat{z}}\sigma_z\sqrt{1-r^2}} \exp\left(\frac{-1}{2\left(1-r^2\right)}\left(\frac{\hat{z}^2}{\sigma_{\hat{z}}^2} + \frac{z^2}{\sigma_z^2} - \frac{2r\hat{z}z}{\sigma_{\hat{z}}\sigma_z}\right)\right), \tag{3.10}$$

where r is the correlation coefficient of z and $\hat{z}$:

$$r = \frac{E\left(z\hat{z}\right)}{\sigma_z\sigma_{\hat{z}}}. \tag{3.11}$$

For the sake of simplicity, we assume u_k, d_k and b_k are not cross-correlated. (3.11) can then be expanded into:

$$r(\hat{\boldsymbol{\theta}}) = \frac{\sigma_d^2 + \boldsymbol{\theta}^\top \boldsymbol{R_u} \hat{\boldsymbol{\theta}}}{\sqrt{\sigma_b^2 + \sigma_d^2 + \boldsymbol{\theta}^\top \boldsymbol{R_u} \boldsymbol{\theta}}\sqrt{\sigma_d^2 + \hat{\boldsymbol{\theta}}^\top \boldsymbol{R_u} \hat{\boldsymbol{\theta}}}}. \tag{3.12}$$

The calculations are tedious but straightforward. One obtains:

$$G_1^\infty = \frac{\sigma_{\hat{z}}^2}{\pi}\left(\arccos(r) - r\sqrt{1-r^2}\right) = \sigma_{\hat{z}}^2 J_1^\infty, \tag{3.13}$$

[1] For example, this is the case if u, d and b are Gaussian with mean zero. In practice, a less stringent condition on u is simply $m_u = 0$: provided the mixing properties of $\hat{\boldsymbol{\theta}}$ and $\boldsymbol{\theta}$ are "good", one may consider that z_k and $\hat{z}_k$ are close to Gaussian.

where $J_1^\infty = \frac{1}{\pi}\left(\arccos(r) - r\sqrt{1-r^2}\right)$ that has been studied in chapter 2. Note that the asymptotic expression of the classical least-squares criterion can be also calculated as:

$$G_0^\infty = \lim_{N\to\infty} G_0^N = \frac{1}{\pi}\left(\arccos(r)\right). \tag{3.14}$$

As a consequence, the optimal $\hat{\boldsymbol{\theta}}$ is found by differentiating (3.13). This yields:

$$\frac{\partial G_1^\infty}{\partial \hat{\boldsymbol{\theta}}} = \mathbf{0} \Leftrightarrow 2J_1^\infty \boldsymbol{R_u}\hat{\boldsymbol{\theta}} + \sigma_{\hat{z}}^2 \frac{\partial J_1^\infty}{\partial r}\frac{\partial r}{\partial \hat{\boldsymbol{\theta}}} = \mathbf{0}, \tag{3.15}$$

where

$$\frac{\partial J_1^\infty}{\partial r} = -\frac{2}{\pi}\sqrt{1-r^2}, \tag{3.16}$$

and

$$\sigma_{\hat{z}}^2 \frac{\partial r}{\partial \hat{\boldsymbol{\theta}}} = \frac{\sigma_{\hat{z}}}{\sigma_z}\boldsymbol{R_u}\boldsymbol{\theta} - r\boldsymbol{R_u}\hat{\boldsymbol{\theta}}. \tag{3.17}$$

Thus, (3.15) is equivalent to:

$$\arccos(r)\boldsymbol{R_u}\hat{\boldsymbol{\theta}} - \sqrt{1-r^2}\frac{\sigma_{\hat{z}}}{\sigma_z}\boldsymbol{R_u}\boldsymbol{\theta} = \mathbf{0}. \tag{3.18}$$

If $\boldsymbol{R_u}$ has full rank, (3.18) reduces to:

$$\arccos(r)\hat{\boldsymbol{\theta}} = \sqrt{1-r^2}\frac{\sigma_{\hat{z}}}{\sigma_z}\boldsymbol{\theta}. \tag{3.19}$$

Thus the optimal $\hat{\boldsymbol{\theta}}$ is (at least) collinear to $\boldsymbol{\theta}$. Two cases must now be distinguished, depending on whether a dithering signal is present at the quantizer's input or not:

3.3.1 Case 1: $\sigma_d^2 \neq 0$

We suppose now that $r = 1$: in this case, $\arccos(r) = \sqrt{1-r^2} = 0$ and (3.18) is verified. In other words, any vector $\hat{\boldsymbol{\theta}}$ such that $r = 1$ minimizes G_1^∞. Now, it is clear that r can be equal to 1 if and only if:

$$\begin{cases} \sigma_b^2 = 0 \\ \hat{\boldsymbol{\theta}} = \boldsymbol{\theta} \end{cases} \tag{3.20}$$

Thus the following property holds.

Property 1- Provided $\boldsymbol{R_u}$ has full rank, the minimum of G_1^∞ is reached for $\hat{\boldsymbol{\theta}} = \boldsymbol{\theta}$ if $\sigma_d^2 \neq 0$ and $\sigma_b^2 = 0$.

Consider now that $\sigma_b^2 \neq 0$ and, as a consequence, that $r \neq 1$. (3.19) can be rewritten as:

$$\hat{\boldsymbol{\theta}} = \frac{\sqrt{1-r^2}}{\arccos(r)}\frac{\sigma_{\hat{z}}}{\sigma_z}\boldsymbol{\theta}. \tag{3.21}$$

Let

$$\lambda = \frac{\sqrt{1-r^2}}{\arccos(r)}\frac{\sigma_{\hat{z}}}{\sigma_z} = g(r)\frac{\sigma_{\hat{z}}}{\sigma_z}. \tag{3.22}$$

Taking the square of (3.22) and multiplying by σ_z^2 yields:

$$\begin{aligned} &\lambda^2\left(\sigma_b^2+\sigma_d^2+\boldsymbol{\theta}^\top \boldsymbol{R_u}\boldsymbol{\theta}\right) = g(r)^2\left(\sigma_d^2+\lambda^2\boldsymbol{\theta}^\top \boldsymbol{R_u}\boldsymbol{\theta}\right) \\ &\Leftrightarrow \lambda^2\left(\sigma_b^2+\sigma_d^2+\left(1-g(r)^2\right)\boldsymbol{\theta}^\top \boldsymbol{R_u}\boldsymbol{\theta}\right) = g(r)^2\sigma_d^2 \end{aligned} \tag{3.23}$$

and therefore:

$$\lambda = \frac{g(r)\sigma_d}{\sqrt{\sigma_b^2+\sigma_d^2+\left(1-g(r)^2\right)\boldsymbol{\theta}^\top \boldsymbol{R_u}\boldsymbol{\theta}}}. \tag{3.24}$$

We know that $0 \leq g(r) < 1$, $\forall r < 1$ and that $\sigma_b \neq 0$. From (3.24), it is straightforward that:

$$0 < \lambda < 1. \tag{3.25}$$

Thus, in the presence of measurement noise at the quantizer's input, one cannot achieve a consistent estimation of the nominal parameters $\boldsymbol{\theta}$ even with an infinite number of samples.

Property 2- Provided $\boldsymbol{R_u}$ has full rank, the minimum of G_1^∞ is reached for $\hat{\boldsymbol{\theta}} = \lambda\boldsymbol{\theta}$, $\lambda < 1$ if $\sigma_d^2 \neq 0$ and $\sigma_b^2 \neq 0$.

3.3.2 Case 2: $\sigma_d^2 = 0$

In the simpler case when $\sigma_d^2 = 0$, it is simple to show the following properties:

Property 3- Provided $\boldsymbol{R_u}$ has full rank, the minimum of G_1^∞ is reached for:

- $\hat{\boldsymbol{\theta}} = \lambda\boldsymbol{\theta}$, $\forall\lambda \geq 0$, if $\sigma_d^2 = 0$ and $\sigma_b^2 = 0$.
- $\hat{\boldsymbol{\theta}} = \mathbf{0}$, if $\sigma_d^2 = 0$ and $\sigma_b^2 \neq 0$.

As shown in the second and third properties, the proposed method results in a systematic error in the more realistic case ($\sigma_b \neq 0$) as opposed to BIMBO. Thus, in the next section, simulation results for the proposed method are compared with the results obtained from BIMBO under different scenarios. We also discuss the estimated value of λ in the various cases (to see if it is close to 1 or not).

3.4 Simulation results

In this section, we compare the results obtained with two WLS criteria, G_1^N and J_1^N. For the sake of simplicity, we choose $\boldsymbol{\theta} = [1 \quad 1]$ (i.e. $L = 2$). The signals u_k, d_k and b_k have

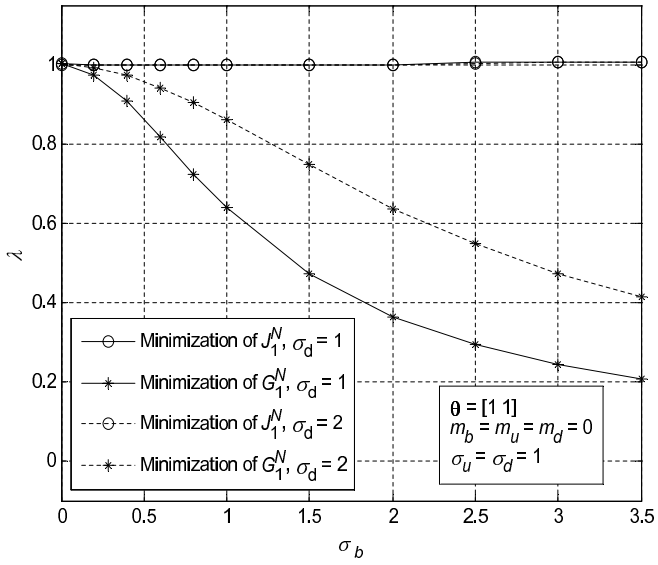

Figure 3.3: $\tilde{\lambda}$ vs. σ_b when u_k, d_k and b_k are Gaussian and centred.

Gaussian distributions with zero mean: σ_u is set equal to 1, whereas σ_d and σ_b may vary. In order to satisfy the asymptotic conditions, one must impose $N >> L$ [5]. For each experiment, $\hat{\boldsymbol{\theta}}$ is estimated with G_1^N and J_1^N thanks to a BFGS quasi-Newton method [117], implemented by the *fminunc* function of Matlab. Each experiment is repeated a large number of times, in order to estimate $\tilde{\lambda}$, the expected value of λ, for different values of σ_d and σ_b . More precisely, for given σ_d and σ_b, $\tilde{\lambda}$ is defined as:

$$\tilde{\lambda} = \frac{1}{P} \sum_{p=1}^{P} \frac{\|\hat{\boldsymbol{\theta}}_p\|}{\|\boldsymbol{\theta}\|}, \tag{3.26}$$

where $\hat{\boldsymbol{\theta}}_p = \arg\min\left(G_1^N\right)$ or $\arg\min\left(J_1^N\right)$, depending on which criterion is tested and P is the number of experiments. P is chosen so that the standard deviation of $\tilde{\lambda}$ is small. Note that the angle between $\hat{\boldsymbol{\theta}}_p$ and $\boldsymbol{\theta}$ must be small for (3.26) to give a meaningful estimation of λ. Since $N >> L$, this should indeed be the case: as a measure of precaution, one can verify that the correlation coefficient between $\hat{\boldsymbol{\theta}}_p$ and $\boldsymbol{\theta}$ is very close to 1, for all experiments.

The results are shown in Figure 3.3. The value of λ estimated with J_1^N is always very close to 1, regardless of the value of σ_d and σ_b: this shows that it is possible to properly estimate the system parameters regardless of the level of noise at the quantizer input, when J_1^N is selected as the criterion.

Conversely, when G_1^N is used, λ is equal to 1 only when $\sigma_b = 0$. When σ_b increases, the estimated value of λ decreases, which illustrates Property 2 of this criterion. This shows that this criterion is not suitable for parameter estimation in a noisy context. Moreover, λ is not only a function of σ_b but also of σ_d : as can be expected, the larger σ_d is with respect to σ_b, the closer λ is to 1.

Several other scenarios can be tested in which the constraints on the distributions of

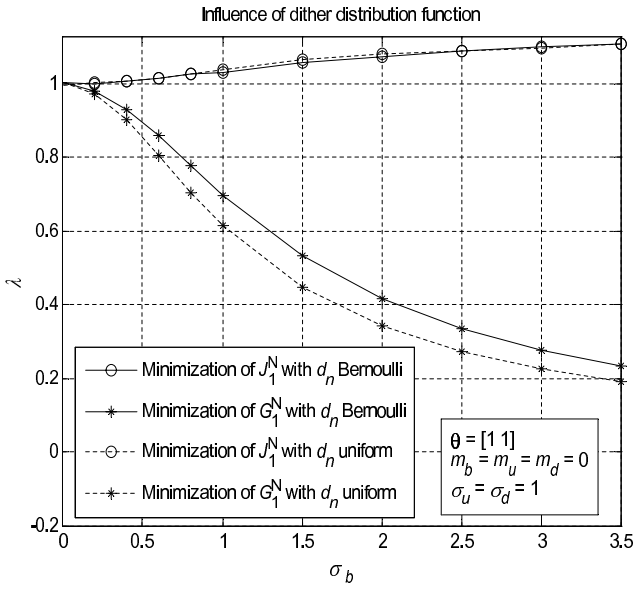

Figure 3.4: $\tilde{\lambda}$ vs. σ_b when u_k and b_k are Gaussian and centred, whereas d_k is uniform or Bernoulli.

u_k, d_k and b_k are made less strict. In Figure 3.4, u_k and b_k are Gaussian and centred, whereas d_k is uniform or Bernoulli. This test shows that, when σ_b increases, λ becomes larger than 1 when J_1^N is used. In Figure 3.5 (left), d_k and b_k are Gaussian and centred, whereas u_k is Gaussian with nonzero mean: simulations show that λ becomes smaller than 1 when J_1^N is used. Finally, in Figure 3.5 (right), u_k and d_k are Gaussian and centred, whereas b_k is Gaussian with nonzero mean. However, this does not seem to have any influence on λ, which stays very close to 1 when J_1^N is used. In these last three scenarios, the qualitative behavior of λ when G_1^N is used does not differ much from the case when all signals are Gaussian and centred. One can also notice that the bias is always larger when G_1^N is used.

These simulations tend to show that the hypotheses made for obtaining Properties 1-3 for the proposed criterion may somehow be relaxed when $\sigma_b = 0$: G_1^N and J_1^N give equally good results regardless of the distribution of d_k or of the mean value of u_k or b_k. When $\sigma_b \neq 0$, G_1^N and J_1^N fail in correctly estimating $\|\boldsymbol{\theta}\|$ when d_k is Bernoulli or uniform. This is also the case when u_k has nonzero mean. This goes to show that, if $\sigma_b \neq 0$, the only hypothesis that may be relaxed concerns the measurement noise b_k. The simulation results concerning the consistency of the two criteria are summarized in Table 3.1.

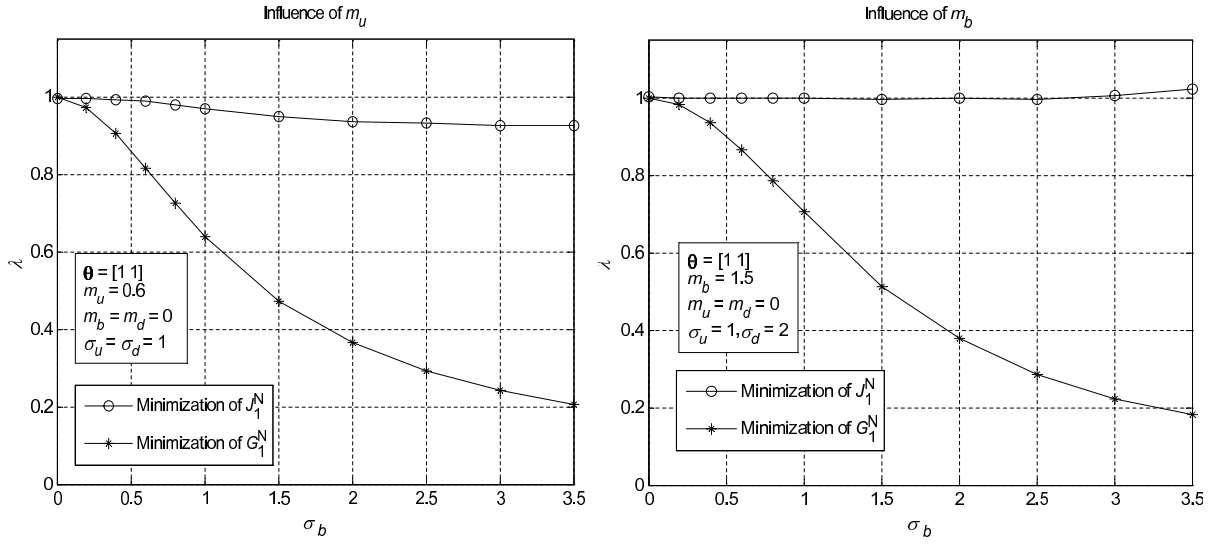

Figure 3.5: $\tilde{\lambda}$ vs. σ_b: when d_k and b_k are centred Gaussian and u_k is Gaussian with nonzero mean (left), when u_k and d_k are centred Gaussian and b_k is Gaussian with nonzero mean (right).

Table 3.1: Comparison of the consistency of the two criteria under different scenarios.

	J_1^∞		G_1^∞	
	$\sigma_b^2 = 0$	$\sigma_b^2 \neq 0$	$\sigma_b^2 = 0$	$\sigma_b^2 \neq 0$
u_k, d_k, b_k Gaussian centered with $\sigma_d \neq 0$	Consistent	Consistent	Consistent	Not consistent
u_k, d_k Gaussian centered, b_k Gaussian non centered	Consistent	Consistent	Consistent	Not consistent
u_k, b_k Gaussian centered, d_k uniform or Bernoulli	Consistent	Not Consistent	Consistent	Not consistent

3.5 Estimation quality of the proposed method

Due to the fact that our goal is to propose a method that can be well adapted to the context of microsystem, it is interesting to estimate the number of necessary samples (i.e. memory requirements) to achieve a desirable estimation quality. As a consequence, it is possible to make a compromise between storage requirements and our estimation quality.

In the previous sections, we showed that the problem of parameter estimation from binary measurement in the noise-free environment can be treated by minimizing WLS criteria of the form:

$$G_p^N\left(\hat{\boldsymbol{\theta}}\right) = \frac{1}{4N}\sum_{k=1}^{N} \hat{z}_k^{2p}\left(s_k - \hat{s}_k\right)^2, p \geq 1. \tag{3.27}$$

We already established the properties of G_1^N such as estimator consistency under a probabilistic framework, when N goes to infinity. The equivalence between G_0^N and G_P^N has been also shown in Section 3.2. Based on this equivalence between the two criteria (3.5), we study in this section some non-asymptotical properties of G_0^N and see how they apply to G_p^N in order to investigate the estimation quality of the proposed approach based on the number of necessary samples to identify the system. It should be mentioned that, in [3, 98, 90], the authors used the Cramer-Rao bound (CRB) to determine the efficiency and quality of their estimation methods. However, the CRB is difficult to establish in our proposed approach, because there exists no analytical expression of the optimal parameters in this technique. Therefore, we define another criterion to analyze the quality and performance of this method based on estimation accuracy and the number of necessary samples to identify the system in the noise-free case.

3.5.1 Consequence of a finite number of samples

In order to investigate the quality of our WLS approach introduced in previous sections, the relation between accuracy (in the sense of correlation coefficient between z and $\hat{z}$) and the number of necessary samples N for identifying a system is figured out.

The purpose of this section is to determine how many samples N are necessary to estimate a given system with length L by a given "accuracy". To ensure the quality of the estimation, a sufficient condition is that:

$$\forall \hat{\boldsymbol{\theta}}, G_p^N\left(\hat{\boldsymbol{\theta}}\right) \approx G_p^\infty\left(\hat{\boldsymbol{\theta}}\right). \tag{3.28}$$

Or, in other words, a sufficient condition is that we are "close" to the limiting case while N goes to infinity ($N \longrightarrow \infty$). Regarding $G_p^N\left(\hat{\boldsymbol{\theta}}\right)$ with a fixed $\hat{\boldsymbol{\theta}}$ as a random variable (the value of which changes from one experiment to the other), one can consider that the number of necessary samples N is large enough when:

$$\frac{\mathrm{var}\left(G_p^N\left(\hat{\boldsymbol{\theta}}\right)\right)}{\mathrm{E}\left(G_p^N\left(\hat{\boldsymbol{\theta}}\right)\right)^2} < 1. \tag{3.29}$$

We have not been able to obtain a satisfactory expression for any of these quantities except in the case $p = 0$. However, because of the "equivalence" between G_p^N and G_0^N (3.5), reasonably good results can be expected if G_0^N is used instead of G_p^N in (3.29). Therefore, from (3.5) and (3.29), we can consider that N is large enough when:

$$\frac{\mathrm{var}\left(G_0^N\left(\hat{\boldsymbol{\theta}}\right)\right)}{\mathrm{E}\left(G_0^N\left(\hat{\boldsymbol{\theta}}\right)\right)^2} < 1. \tag{3.30}$$

As it is illustrated in Figure 3.6, when N is small, the probability that $G_0^N = 0$ for $\hat{\boldsymbol{\theta}} \neq \boldsymbol{\theta}$ is non zero. Increasing N reduces the variance of G_0^N which reduces the misestimating

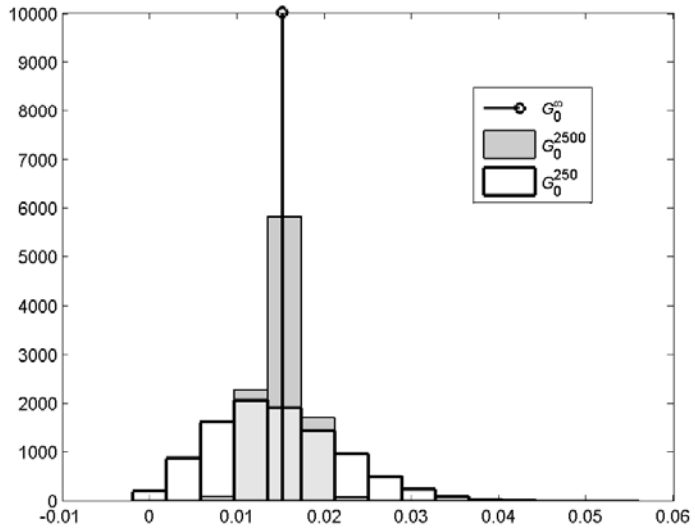

Figure 3.6: Histogram of G_0^{∞}, G_0^{2500} and G_0^{250} for $\boldsymbol{\theta} = [1, -1]$ and $\hat{\boldsymbol{\theta}} = [1.1, -1]$.

probability of $\boldsymbol{\theta}$.

Since $1/4\left(s_k - \hat{s}_k\right)^2$ takes only two values (0 or 1), it can be considered as a Bernoulli random variable with parameter q. The value of q is equal to:

$$\begin{aligned} q = \mathrm{E}\left(\frac{1}{4}\left(\hat{s}_k\left(\hat{\boldsymbol{\theta}}\right) - s_k\right)^2\right) &= \mathrm{E}\left(\frac{1}{2} - \frac{1}{2}\hat{s}_k s_l\right) \\ &= \frac{1}{2} - \frac{1}{2}\mathrm{cov}\left(\hat{s}_k, s_k\right). \end{aligned} \tag{3.31}$$

From [118], (3.31) reduces to:

$$q = \frac{1}{2}\left(1 - \frac{2}{\pi}\arcsin\left(\mathrm{cov}\left(\hat{z}_k, z_k\right)\right)\right) = \frac{1}{\pi}\arccos(r) = G_0^{\infty}(r). \tag{3.32}$$

Thus,

$$\mathrm{E}\left(G_0^N\left(\hat{\boldsymbol{\theta}}\right)\right) = \frac{1}{N}\sum_{k=1}^{N}\mathrm{E}\left(\frac{1}{4}\left(\hat{s}_k\left(\hat{\boldsymbol{\theta}}\right) - s_k\right)^2\right) = G_0^{\infty}(r). \tag{3.33}$$

The numerator of (3.30) is also given by:

$$\begin{aligned} \mathrm{var}\left(G_0^N\left(\hat{\boldsymbol{\theta}}\right)\right) &= \frac{1}{N^2}\mathrm{var}\left(\sum_{k=1}^{N}\frac{\left(\hat{s}_k\left(\hat{\boldsymbol{\theta}}\right) - s_k\right)^2}{4}\right) \\ &= \frac{1}{N^2}\mathrm{var}\left(\sum_{k=1}^{N}\Delta(k)\right). \end{aligned} \tag{3.34}$$

Expanding the right-hand side of (3.34) leads to:

$$\mathrm{var}\left(G_0^N\left(\hat{\boldsymbol{\theta}}\right)\right) = \frac{1}{N^2}\sum_{k=1}^{N}\mathrm{var}\left(\Delta(k)\right) + \frac{1}{N^2}\sum_{k=1}^{N}\sum_{l=1,l\neq k}^{N}\mathrm{cov}\left(\Delta(k),\Delta(l)\right). \tag{3.35}$$

Because of the stationarity hypothesis, this can be further transformed into:

$$\mathrm{var}\left(G_0^N\left(\hat{\boldsymbol{\theta}}\right)\right) = \frac{1}{N^2}\left(N\mathrm{var}\left(\Delta(t)\right)\right) + \frac{2}{N^2}\sum_{k=1}^{N-1}\left(N-k\right)\mathrm{cov}\left(\Delta\left(t\right),\Delta\left(t+k\right)\right). \tag{3.36}$$

The second term on the right-hand side is split in two parts:

$$\begin{aligned}\sum_{k=1}^{N-1}(N-k)\mathrm{cov}\left(\Delta(t),\Delta(t+k)\right) = &\sum_{k=1}^{L}(N-k)\mathrm{cov}\left(\Delta(t),\Delta(t+k)\right) + \\ &\sum_{k=L+1}^{N-1}(N-k)\mathrm{cov}\left(\Delta(t),\Delta(t+k)\right).\end{aligned} \tag{3.37}$$

Since H has length L and the input signal u is white, the second term of the right-hand side of (3.37) equals 0. The Cauchy-Schwartz inequality is then used to yield:

$$\sum_{k=1}^{L}(N-k)\mathrm{cov}\left(\Delta(t),\Delta(t+k)\right) \leq \sum_{k=1}^{L}(N-k)\mathrm{var}\left(\Delta(t)\right) = L\left(N-\frac{L+1}{2}\right)\mathrm{var}\left(\Delta(t)\right). \tag{3.38}$$

This can be injected into (3.36):

$$\mathrm{var}\left(G_0^N\left(\hat{\boldsymbol{\theta}}\right)\right) \leq \frac{N(2L+1)-L(L+1)}{N^2}\mathrm{var}\left(\Delta(t)\right). \tag{3.39}$$

Now $\mathrm{var}\left(\Delta(t)\right)$ can be split into:

$$\mathrm{var}\left(\Delta(t)\right) = \mathrm{var}\left(\frac{1}{4}\left(\hat{s}_k\left(\hat{\boldsymbol{\theta}}\right)-s_k\right)^2\right). \tag{3.40}$$

As $1/4\left(\hat{s}_k\left(\hat{\boldsymbol{\theta}}\right)-s_k\right)^2$ is a Bernoulli random variable with parameter $q = G_0^\infty(r)$, thus, we obtain:

$$\mathrm{var}(\Delta(t)) = G_0^\infty(r) - G_0^{\infty 2}(r). \tag{3.41}$$

As a consequence, (3.41) can be injected into (3.39):

$$\mathrm{var}\left(G_0^N\left(\hat{\boldsymbol{\theta}}\right)\right) \leq \frac{N(2L+1)-L(L+1)}{N^2} \times G_0^\infty(r)\left(1-G_0^\infty(r)\right). \tag{3.42}$$

When N is large with respect to L, (3.42) reduces to:

$$\mathrm{var}\left(G_0^N\left(\hat{\boldsymbol{\theta}}\right)\right) \leq \frac{2L+1}{N}G_0^\infty(r)\left(1-G_0^\infty(r)\right). \tag{3.43}$$

Thus, a sufficient condition for (3.30) to hold is (in the limit of large N):

$$\frac{N}{2L+1} > \frac{1}{G_0^{\infty}(r)} - 1. \tag{3.44}$$

When r is close to 1, assuming $\frac{N}{2L+1} >> 1$, a Taylor series expansion can be applied to (3.44), which yields:

$$e = 1 - r \approx \frac{\pi^2}{2}\left(\frac{2L+1}{N}\right)^2, \tag{3.45}$$

where $e = 1-r$ is the error on the correlation coefficient, i.e. the accuracy of the method.

Suppose, for example, that we want to make sure that the error on the correlation coefficient between the nominal and estimated system parameters is about 0.01. Letting $e = 0.01$ in (3.45) yields:

$$N \approx \frac{10\pi}{\sqrt{2}}(2L+1) \approx 22(2L+1). \tag{3.46}$$

Choosing N according to (3.46) thus ensures that $\hat{\boldsymbol{\theta}}$, the parameter vector resulting from the optimization, is "close" to $\boldsymbol{\theta}$ in the sense that their correlation coefficient (given by (3.12)) is about $r = 0.99$. Simulation results are shown in the next subsection to confirm the theoretical results.

3.5.2 Validation of the theoretical results by simulation

In this subsection, the validity of the results established in section (3.5.1) is put to the test. Four impulse responses of lengths 2, 4, 8 and 16 are analyzed: they consist of repetitions of the sequence [1,-1] (oscillatory behavior is commonplace in MEMS devices). A sequence of N samples of a white Gaussian noise with zero mean and unit variance is applied at the system input. A dithering signal (of the same nature as the input signal) is applied at the input of the comparator. A parameter vector is estimated thanks to the gradient algorithm proposed in [5] and its correlation coefficient with the nominal parameter vector is calculated and stored. The algorithm is stopped when $G_1^N = 0$, which is always achievable in the noise-free case. This experiment is repeated a large number of times (typically 10^4) in order to precisely determine the average value of r for a given number of samples and thus, the accuracy of the method ($e = 1 - r$).

Figure 3.7 illustrates the accuracy of the estimation e versus $N/(2L+1)$ obtained for $\sigma_d = 0$. These simulation results for different lengths of impulse response L are obtained from G_1^N. Note that the same simulation results can be also obtained with G_p^N, $p \geq 0$ because of (3.5). The simulations agree rather well with the theoretical results obtained in the previous section. It confirms that e is inversely proportional to $(N/2L+1)^2$. However, it should be noted that the experimental value of the accuracy is not only a function of $N/(2L+1)$ but also of L (Figure 3.7), i.e. the error behaves as:

$$e = 1 - r = K(L)\left(\frac{2L+1}{N}\right)^2, \tag{3.47}$$

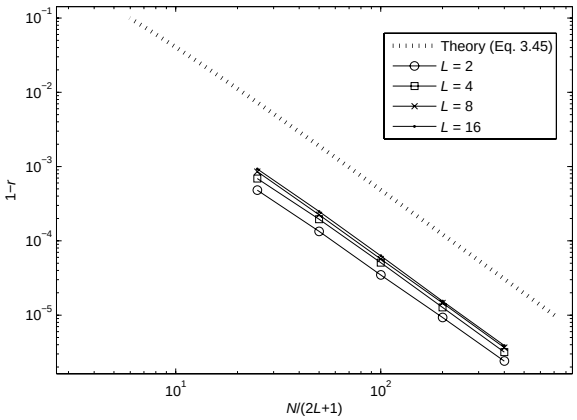

Figure 3.7: Plot $1-r$ vs. $\frac{N}{2L+1}$ for different values of L obtained from G_1^N and comparison with the theoretical prediction derived from (3.45).

where $K(L)$ is a factor which depends on the filter that should be identified and its impulse response length. In the presence case, the number of necessary samples for reaching a given accuracy is overestimated by (3.45). This is a consequence of using the Cauchy-Schwartz inequality for going from (3.37) to (3.39).

When $\sigma_d \neq 0$, the same results as in Figure 3.7 are obtained. However, one must keep in mind that in this case, r represents the correlation between z and $\hat{z}$, not $\boldsymbol{\theta}$ and $\hat{\boldsymbol{\theta}}$. Thus, supposing σ_d is large with respect to $\boldsymbol{\theta}^T\boldsymbol{\theta}$ and $\hat{\boldsymbol{\theta}}^T\hat{\boldsymbol{\theta}}$, r (3.12) can be close to 1 regardless of whether $\hat{\boldsymbol{\theta}}$ is actually "close" to $\boldsymbol{\theta}$. Consequently, it is also interesting to plot the cosine of the angle made by $\hat{\boldsymbol{\theta}}$ and $\boldsymbol{\theta}$:

$$c = \frac{\boldsymbol{\theta}^T\hat{\boldsymbol{\theta}}}{\sqrt{\boldsymbol{\theta}^T\boldsymbol{\theta}}\sqrt{\hat{\boldsymbol{\theta}}^T\hat{\boldsymbol{\theta}}}}, \tag{3.48}$$

versus σ_d compared with r versus σ_d (Figure 3.8-a). These results show that as σ_d decreases, thus the angle made by $\hat{\boldsymbol{\theta}}$ and $\boldsymbol{\theta}$ becomes smaller. On the other hand, too large or too small dither is detrimental to the quality of the identification as it is shown in Figure 3.8.

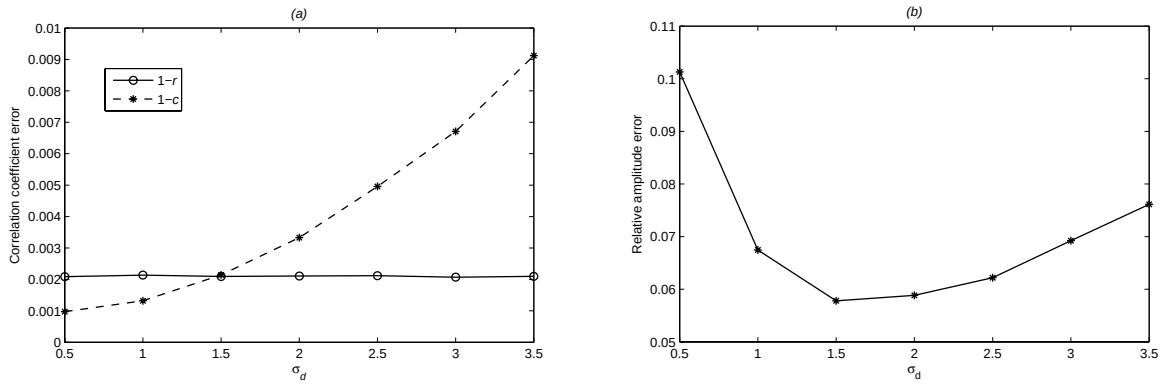

Figure 3.8: (a) Correlation coefficient error ($1-r$ and $1-c$) vs σ_d, (b) Relative amplitude error $\left(1-\frac{\|\hat{\boldsymbol{\theta}}\|}{\|\boldsymbol{\theta}\|}\right)$ vs σ_d for $L=2$ and $\frac{N}{2L+1}=20$.

3.6 Conclusion

In this chapter, we presented WLS criteria for parameter estimation problems based on binary observations: this method is an alternative to the one presented in [5]. These two approaches can be integrated to a given microsystem as a self-test algorithm to estimate the microsystem parameters in order to compensate the operation condition variations or fabrication dispersions. In the noise-free case, the proposed criterion G_1^N is as efficient as J_1^N [5] for estimating the optimal system parameters. It can be also implemented on SoC environment more easily than the compared method. However, in the presence of noise, using G_1^N for determining the system parameters leads to an underestimation of the parameters.

The quality of the estimation has been also investigated based on the number of samples that are necessary for identifying system with a given accuracy. Thus, one can make a good compromise between the estimation accuracy and the number of necessary samples (i.e. storage requirements) in order to reduce the cost and complexity of implementation in the field of microsystems.

As mentioned before, complexity of optimization algorithm and of the proposed criteria are two issues faced BIMBO in the context of microdevices. We partially solved the second problem by introducing a criterion that is easier to implement in this context (i.e. less cost and calculation time). However, this offline algorithm still suffers some issues in terms of storage requirements. Moreover, the proposed criteria cannot properly estimate the system parameters in the presence of measurement noise. As a consequence, our goal is to develop an online method for practical applications with a low complexity and small storage requirements so that it can be easily implemented on SoC. This online approach, relied on our offline criteria (3.4), is presented in the next chapter.

Chapter 4

LMS-based Identification Method using Binary Observations (LIMBO)

An online approach to parameter estimation problems based on binary observations is presented in this chapter. This recursive identification method with low-storage requirements and computational complexity relies on a least-mean squares approach which makes it possible to estimate the coefficients of a finite-impulse response system knowing only the system input and the sign of the system output. Without the use of dithering signal, the impulse response can be identified up to a positive multiplicative constant. However, using a dithering signal to identify the gain of the impulse response is addressed in the next chapter for a practical application.

In this chapter, we prove the convergence of this method provided that the input signal satisfies a strong mixing property. Some simulation results are then given in order to illustrate the properties of this method under various scenarios. The role of the regulative coefficient is also investigated thanks to simulated data. The proposed method is compared with Wigren's approach [107]: it is shown that the proposed method is competitive with the other one in terms of estimation quality and of calculation complexity.

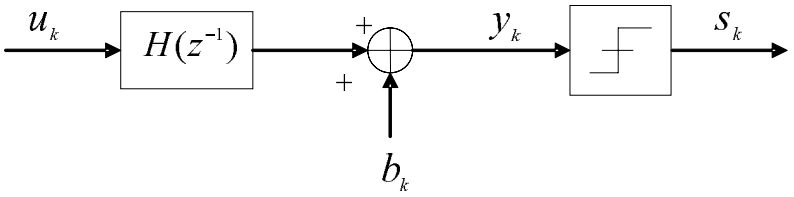

Figure 4.1: Block diagram of the system model. Signal y_k is not available for measurement.

4.1 Framework and notations

The known input signal u_k is filtered by a discrete-time invariant linear system $H(z^{-1})$ to produce the system output y_k at time k (Figure 4.1). H has an impulse response of length L, i.e. it can be represented by a column vector $\boldsymbol{\theta} = (\theta_k)_{k=1}^{L}$.

Let $\hat{\boldsymbol{\theta}}_k$ be the estimated vector of parameters (of length L) at time k and $\hat{\boldsymbol{\theta}}_1$ be the initial estimate. Let also, b_k be an additive noise at the system output. The output and the estimated output can be expressed as:

$$\begin{cases} y_k = \boldsymbol{\theta}^\top \boldsymbol{\phi}_k + b_k \\ \hat{y}_k = \hat{\boldsymbol{\theta}}_k^\top \boldsymbol{\phi}_k \end{cases}, \tag{4.1}$$

where $\boldsymbol{\phi}_k = [u_k, u_{k-1}, ..., u_{k-L+1}]^\top$ is the vector of inputs at time k. The system output then goes through a 1-bit ADC so that only the sign $s_k = S(y_k)$ of the system output is known, where

$$\begin{cases} s_k = 1, & \text{if } y_k \geq 0 \\ s_k = -1, & \text{otherwise.} \end{cases} \tag{4.2}$$

As mentioned in Chapter 3 (Section 3.6), the proposed offline identification method still suffers some drawbacks in terms of storage requirements and algorithm complexity in the context of microdevice implementation (such as the other existing batch-data-based approaches). Thus, it is interesting to develop an online estimation method to solve these issues faced to the offline identification approaches.

As a consequence, our goal is to develop a recursive estimation method to estimate $\boldsymbol{\theta}$ based on N observations of the binary output s_k knowing u_k. Note that because of the absence of dither signal at the comparator input, it is only possible to identify $\boldsymbol{\theta}$ up to a positive multiplicative constant. However, it is possible to use a dithering signal in practical applications in order to identify the gain of the impulse response. This subject is discussed in Chapter 5. Without loss of generality, we then consider $\|\boldsymbol{\theta}\| = 1$ in the rest of this chapter.
In summary, we are going to estimate the coefficients $\boldsymbol{\theta}$ of a FIR filter (of length L) such that $\|\boldsymbol{\theta}\| = 1$ using

- the binary observations s_k of the sign of the filter output.

- the inputs u_k of the filter (not necessarily binary).

We assume the following prior information on the system. However, we show in the next section that these assumptions do not need to be stringently verified for more realistic applications in order to obtain an appropriate performance of the proposed method.

Assumption 1 $v_1 = \hat{\boldsymbol{\theta}}_1^\top \boldsymbol{\theta} \geq 0$.

Remark 1 *It is rather simple to verify assumption 1. For example, a positive constant signal is used as input. If the sign of the output is positive, it means that the sign S_g of the static gain is positive ($S_g = 1$), otherwise $S_g = -1$. Choosing*

$$\hat{\boldsymbol{\theta}}_1 = \frac{S_g}{L} \times [1, 1, ..., 1]^\top \tag{4.3}$$

then ensures that assumption 1 is verified.

Assumption 2 *$\boldsymbol{\phi}_k$ is a random process such that*

- *the probability density function (pdf) of $\frac{\boldsymbol{\phi}_k}{\|\boldsymbol{\phi}_k\|}$ is non-zero on the unit sphere.*
- *$\boldsymbol{\phi}_k$ verifies the α-mixing condition[1] [119, 120, 121].*

Remark 2 *The first condition in assumption 2 ensures that $\boldsymbol{\phi}_k$ may be in any angular sector of R^L and the second condition guarantees that $\boldsymbol{\phi}_k$ and $\boldsymbol{\phi}_{k+l}$ can be considered as independent for large enough l. An input signal verifying assumption 2 is a sequence of i.i.d. random variables with a continuous pdf whose support contains an interval of the form $[-a, a]$, $a > 0$ (e.g. uniform and centered[2]) [112].*

In the following section, our approach is presented and we study the convergence of sequences $\hat{\boldsymbol{\theta}}_k$ to $\boldsymbol{\theta}$ based on an LMS treatment of the offline method presented in the previous chapter. The proof of the convergence is first established in the noise-free case:

Assumption 3 $b_k = 0$,

then the convergence of the algorithm in the more realistic case when $b_k \neq 0$ is shown by Monte Carlo simulations.

[1] The α-mixing condition is introduced by Rosenblatt in order to prove the central limit theorem for weakly dependent random variables.

[2] It is rather simple to generate signals meeting this condition (such as a sequence of i.i.d. uniform and centered random variables). In practice, this input signal is generated with a maximal linear feedback shift register, the implementation of which is fairly straightforward.

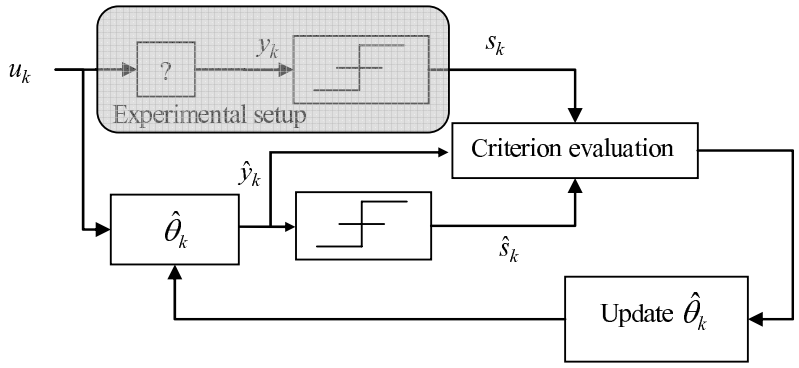

Figure 4.2: Block diagram of LIMBO. A parametric model of the real system is built so as to maximize the similarity between $\boldsymbol{\theta}$ and $\hat{\boldsymbol{\theta}}_{\boldsymbol{k}}$.

4.2 Identification algorithm and its convergence

4.2.1 Basic approach to the problem

In classical offline identification methods (i.e. when the output of the system is not quantized [1, 2]), the quadratic error is defined as $\sum_k (y_k - \hat{y}_k)^2$. Thus, the instantaneous estimation error is $\tilde{E}_k = y_k - \hat{y}_k$. As a consequence, the following algorithm is used in the classical LMS approach [122, 123]:

$$\hat{\boldsymbol{\theta}}_{k+1} = \hat{\boldsymbol{\theta}}_k - \alpha_k \frac{\partial \tilde{E}_k^2}{\partial \hat{\theta}}, \tag{4.4}$$

where $\alpha_k > 0$ must verify some conditions to guarantee the stability and convergence of the algorithm. However, in the framework of system identification based on binary observations, we only have access to s_k and the unweighted instantaneous error,

$$\tilde{E}_k = (s_k - \hat{s}_k), \tag{4.5}$$

is not differentiable with respect to $\hat{\boldsymbol{\theta}}_{\boldsymbol{k}}$.

In the previous chapter, we showed that, given N observations, the offline identification of $\boldsymbol{\theta}$ based on binary outputs can be achieved by minimizing a quadratic error of the form:

$$E^2 = \frac{1}{4} \sum_{k=1}^{N} \hat{y}_k^2 \, (s_k - \hat{s}_k)^2. \tag{4.6}$$

Thus, we propose to extend our offline method to an online approach (Figure 4.2) by using (4.4) and the following definition of the instantaneous error:

$$\tilde{E}_k = \frac{1}{2} |s_k - \hat{s}_k| \hat{y}_k, \tag{4.7}$$

which is differentiable with respect to $\hat{\boldsymbol{\theta}}_{\boldsymbol{k}}$ as opposed to (4.5).

Using (4.1), (4.7) and the fact that $|s_k - \hat{s}_k|^2 = 2|s_k - \hat{s}_k|$, (4.4) can be developed as

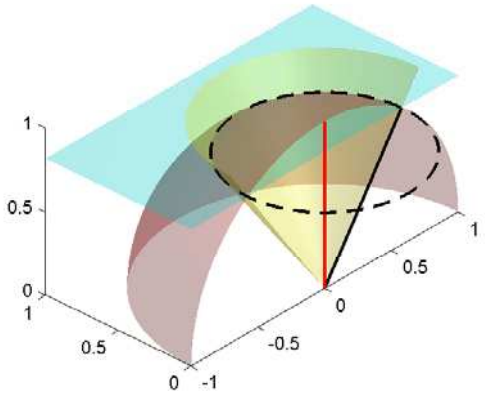

Figure 4.3: As k goes to infinity, $\hat{\boldsymbol{\theta}}_k$ revolves around $\boldsymbol{\theta}$ on a circle orthogonal to $\boldsymbol{\theta}$, defined as the intersection of the unit sphere and a cone of revolution with axis $\boldsymbol{\theta}$ and half-angle $\cos^{-1}(v_\infty)$.

the basic approach to the problem:

$$\hat{\boldsymbol{\theta}}_{k+1} = \hat{\boldsymbol{\theta}}_k - \alpha_k |s_k - \hat{s}_k| \hat{y}_k \boldsymbol{\phi}_k. \tag{4.8}$$

Equation (4.8) above is equivalent to

$$\begin{cases} \hat{\boldsymbol{\theta}}_{k+1} = \hat{\boldsymbol{\theta}}_k - 2\alpha_k \hat{y}_k \boldsymbol{\phi}_k, & \text{if } s_k \neq \hat{s}_k \\ \hat{\boldsymbol{\theta}}_{k+1} = \hat{\boldsymbol{\theta}}_k, & \text{otherwise.} \end{cases} \tag{4.9}$$

Since it is impossible to estimate the static gain of $\boldsymbol{\theta}$ in the absence of dither, we shall choose α_k so that $\|\hat{\boldsymbol{\theta}}_k\|$ remains constant. To this end, we use

$$\alpha_k = \frac{1}{\boldsymbol{\phi}_k^\top \boldsymbol{\phi}_k}, \tag{4.10}$$

for which it is possible to verify that $\|\hat{\boldsymbol{\theta}}_{k+1}\| = \|\hat{\boldsymbol{\theta}}_k\|$. Without loss of generality, we impose $\|\hat{\boldsymbol{\theta}}_k\| = 1$.

Let us consider the sequence

$$v_k = \hat{\boldsymbol{\theta}}_k^\top \boldsymbol{\theta}. \tag{4.11}$$

Projecting (4.8) on $\boldsymbol{\theta}$ under assumption 3, we obtain:

$$v_{k+1} = v_k - \alpha_k |s_k - \hat{s}_k| \hat{y}_k y_k. \tag{4.12}$$

The product $\hat{y}_k y_k$ being negative if $s_k \neq \hat{s}_k$, this sequence is monotonically increasing. Furthermore, the Cauchy-Schwartz inequality

$$\hat{\boldsymbol{\theta}}_k^\top \boldsymbol{\theta} \leq \|\hat{\boldsymbol{\theta}}_k\| \|\boldsymbol{\theta}\| = \|\boldsymbol{\theta}\| \tag{4.13}$$

implies that the sequence (v_k) is bounded from above and thus, converges to a limit v_∞. This means that:

- either $\hat{\boldsymbol{\theta}}_k$ converges to a limit $\hat{\boldsymbol{\theta}}_\infty$.
- or $\hat{\boldsymbol{\theta}}_k$ is drawn towards a cone whose axis is oriented by $\boldsymbol{\theta}$ with half-angle $\cos^{-1}(v_\infty)$ (Figure 4.3) without converging, for example, orbiting around $\boldsymbol{\theta}$ on and on.

Although simulations seem to show that the second case is never met in practice, for a wide class of inputs, we have not been able to prove the convergence of (4.8) without resorting to overly strong hypotheses (see Appendix B). However, one may construct another sequence of $\hat{\boldsymbol{\theta}}_k$ in order to avoid getting stuck on a cone. Intuitively, this sequence may be constructed from a combination of $\hat{\boldsymbol{\theta}}_k$ and of the $\hat{\boldsymbol{\theta}}_{k+1}$ derived from (4.8). If k is large enough so that $\hat{\boldsymbol{\theta}}_k$ and $\hat{\boldsymbol{\theta}}_{k+1}$ are close to the limit cone, the angle between $\boldsymbol{\theta}$ and the vector resulting from any convex combination of $\hat{\boldsymbol{\theta}}_k$ and $\hat{\boldsymbol{\theta}}_{k+1}$ will necessarily be smaller than $\cos^{-1}(v_\infty)$. Thus, it should be possible to relax (4.8) to ensure convergence. This is studied in the next subsection.

4.2.2 Relaxed approach

The following relaxed algorithm is considered:

$$\hat{\boldsymbol{\theta}}_{k+1} = \frac{\hat{\boldsymbol{\theta}}_k - \mu\alpha_k|s_k - \hat{s}_k|\hat{y}_k\boldsymbol{\phi}_k}{w_k}, \tag{4.14}$$

where $0 < \mu < 1$ and

$$w_k = \sqrt{1 - 2\mu(1-\mu)\alpha_k|s_k - \hat{s}_k|\hat{y}_k^2} \leq 1 \tag{4.15}$$

is a normalizing factor so that $\|\hat{\boldsymbol{\theta}}_k\| = 1, \forall k$.

Remark 3 *If $\mu = 1$, algorithm (4.8) is obtained (the basic approach). On the other hand, if $\mu = 0$, we get $\hat{\boldsymbol{\theta}}_k = \hat{\boldsymbol{\theta}}_1$, $\forall k$.*

Theorem 4.2.1 *Under assumptions 1, 2 and 3, the sequence defined by (4.14)-(4.15) and (4.10) converges surely to $\boldsymbol{\theta}$, $\forall \mu \in (0,1)$.*

PROOF. When $0 < \mu < 1$, the $\hat{\boldsymbol{\theta}}_{k+1}$ defined by (4.14) is a convex combination of $\hat{\boldsymbol{\theta}}_k$ (with weight $1-\mu$) and of the $\hat{\boldsymbol{\theta}}_{k+1}$ defined by (4.8) (with weight μ). Projecting (4.14) on $\boldsymbol{\theta}$, we get

$$v_{k+1} = \frac{v_k - \mu\alpha_k|s_k - \hat{s}_k|\hat{y}_k y_k}{w_k}. \tag{4.16}$$

Since,

$$\mu\alpha_k|s_k - \hat{s}_k|\hat{y}_k y_k \leq 0, \tag{4.17}$$

$0 \leq w_k \leq 1$ and $v_1 \geq 0$, the sequence (v_k) is monotonically increasing. As it is also bounded from above (4.13), it converges and then

$$\frac{v_k}{v_{k+1}} \xrightarrow{k\to\infty} 1. \tag{4.18}$$

From (4.16) and (4.15),

$$\frac{v_k}{v_{k+1}} \leq w_k \leq 1, \tag{4.19}$$

hence:

$$w_k \xrightarrow{k\to\infty} 1. \tag{4.20}$$

Considering the definition of w_k (4.15), this proves that

$$\alpha_k |s_k - \hat{s}_k| \hat{y}_k^2 \xrightarrow{k\to\infty} 0. \tag{4.21}$$

Furthermore, projecting (4.14) on $\hat{\boldsymbol{\theta}}_k$ yields:

$$\hat{\boldsymbol{\theta}}_{k+1}^\top \hat{\boldsymbol{\theta}}_k = \frac{1 - \mu\alpha_k |s_k - \hat{s}_k| \hat{y}_k^2}{w_k}. \tag{4.22}$$

As a consequence,

$$\hat{\boldsymbol{\theta}}_{k+1}^\top \hat{\boldsymbol{\theta}}_k \xrightarrow{k\to\infty} 1. \tag{4.23}$$

On the other hand, projecting (4.14) on $\hat{\boldsymbol{\theta}}_{k+1}$ yields:

$$1 = \frac{\hat{\boldsymbol{\theta}}_k^\top \hat{\boldsymbol{\theta}}_{k+1} - \mu\alpha_k |s_k - \hat{s}_k| \hat{y}_k \boldsymbol{\phi}_k^\top \hat{\boldsymbol{\theta}}_{k+1}}{w_k}, \tag{4.24}$$

which implies:

$$\alpha_k |s_k - \hat{s}_k| \hat{y}_k \boldsymbol{\phi}_k^\top \hat{\boldsymbol{\theta}}_{k+1} \xrightarrow{k\to\infty} 0, \tag{4.25}$$

since w_k and $\hat{\boldsymbol{\theta}}_k^\top \hat{\boldsymbol{\theta}}_{k+1}$ converge to 1 as seen above.
Furthermore, one proves that

$$\alpha_{k+1} |s_{k+1} - \hat{s}_{k+1}| \hat{y}_{k+1} \boldsymbol{\phi}_{k+1}^\top \hat{\boldsymbol{\theta}}_k \xrightarrow{k\to\infty} 0, \tag{4.26}$$

by projecting (4.14) on $\alpha_{k+1} |s_{k+1} - \hat{s}_{k+1}| \hat{y}_{k+1} \boldsymbol{\phi}_{k+1}^\top$ and using the Cauchy-Schwartz inequality on the second term of the right-hand side. Replacing k by $k+1$ in (4.14) and projecting the resulting equation on $\hat{\boldsymbol{\theta}}_k$, we obtain an expression of $\hat{\boldsymbol{\theta}}_{k+2}^\top \hat{\boldsymbol{\theta}}_k$ as a function of quantities whose convergence is already established. It is then straightforward that $\hat{\boldsymbol{\theta}}_{k+2}^\top \hat{\boldsymbol{\theta}}_k \xrightarrow{k\to\infty} 1$ and by induction,

$$\forall l, \quad \hat{\boldsymbol{\theta}}_{k+l}^\top \hat{\boldsymbol{\theta}}_k \xrightarrow{k\to\infty} 1. \tag{4.27}$$

Consequently, since

$$\|\hat{\boldsymbol{\theta}}_{k+l} - \hat{\boldsymbol{\theta}}_k\|^2 = 2\left(1 - \hat{\boldsymbol{\theta}}_{k+l}^\top \hat{\boldsymbol{\theta}}_k\right), \tag{4.28}$$

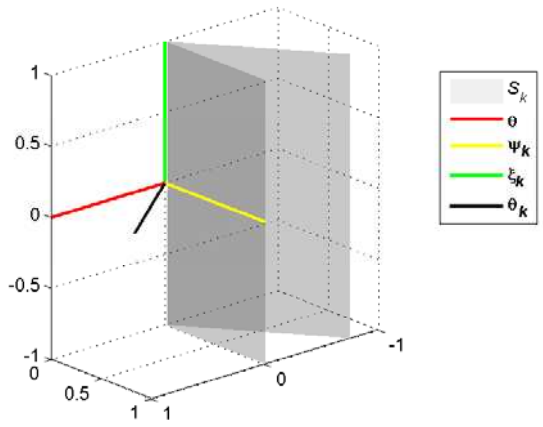

Figure 4.4: If $\boldsymbol{\phi}_k$ belongs to the sector S_k, $s_k \neq \hat{s}_k$.

the sequence $\hat{\boldsymbol{\theta}}_k$ is Cauchy. R^L being complete, $\hat{\boldsymbol{\theta}}_k$ converges to a limit $\hat{\boldsymbol{\theta}}_\infty$. Let us then show that, provided certain hypotheses hold,

$$v_\infty = \hat{\boldsymbol{\theta}}_\infty^\top \boldsymbol{\theta} = 1. \tag{4.29}$$

As v_k is necessarily smaller than 1, we try to determine under what circumstances v_k can be increased by $\epsilon\,(1 - v_k)$, $\epsilon \in (0, 1]$. The coefficient w_k being smaller than 1, a sufficient condition for

$$v_{k+1} - v_k \geq \epsilon\,(1 - v_k) \tag{4.30}$$

is that the right-hand term of the numerator of (4.16) should be greater than $\epsilon\,(1 - v_k)$ when $s_k \neq \hat{s}_k$, i.e.

$$2\mu\alpha_k \hat{y}_k y_k + \epsilon\,(1 - v_k) < 0. \tag{4.31}$$

Multiplying (4.31) by $\boldsymbol{\phi}_k^\top \boldsymbol{\phi}_k = \alpha_k^{-1}$ yields

$$\boldsymbol{\phi}_k^\top \left(\mu \left(\boldsymbol{\theta}\hat{\boldsymbol{\theta}}_k^\top + \hat{\boldsymbol{\theta}}_k \boldsymbol{\theta}^\top\right) + \epsilon\,(1 - v_k)\,\boldsymbol{I}_L\right) \boldsymbol{\phi}_k < 0, \tag{4.32}$$

where $\boldsymbol{I}_L$ is the $L \times L$ identity matrix. Let us decompose $\hat{\boldsymbol{\theta}}_k$ as

$$\hat{\boldsymbol{\theta}}_k = v_k \boldsymbol{\theta} + \sqrt{1 - v_k^2}\,\boldsymbol{\psi}_k, \tag{4.33}$$

where $\boldsymbol{\psi}_k$ is a unit vector orthogonal to $\boldsymbol{\theta}$, and $\boldsymbol{\phi}_k$ as

$$\boldsymbol{\phi}_k = a_k \boldsymbol{\theta} + b_k \boldsymbol{\psi}_k + c_k \boldsymbol{\xi}_k, \tag{4.34}$$

where $\boldsymbol{\xi}_k$ is a unit vector orthogonal to $\boldsymbol{\theta}$ and $\boldsymbol{\psi}_k$ (Figure 4.4). Then, the condition for $s_k \neq \hat{s}_k$ is derived as:

$$a_k \left(a_k v_k + b_k \sqrt{1 - v_k^2}\right) < 0 \tag{4.35}$$

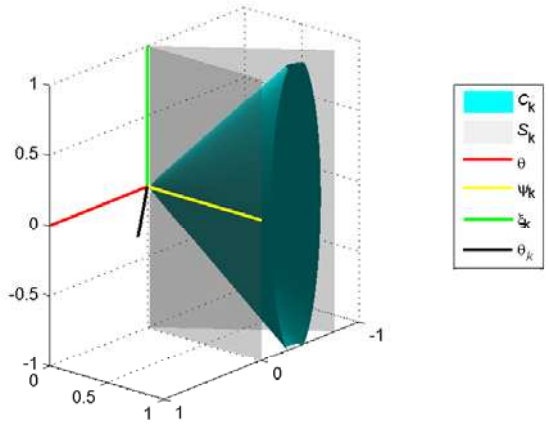

Figure 4.5: When $\boldsymbol{\phi}_k$ belongs to the elliptical cone $C_k^{1/2} \subset S_k$, then $s_k \neq \hat{s}_k$ and $-4\alpha_k \hat{y}_k y_k > 1 - v_k$.

and (4.32) can be rewritten as:

$$\begin{pmatrix} a_k & b_k & c_k \end{pmatrix} \mathbf{A}_k \begin{pmatrix} a_k \\ b_k \\ c_k \end{pmatrix} < 0, \tag{4.36}$$

where

$$\mathbf{A}_k = \begin{pmatrix} \epsilon(1-v_k) + 2\mu v_k & \mu\sqrt{1-v_k^2} & 0 \\ \mu\sqrt{1-v_k^2} & \epsilon(1-v_k) & 0 \\ 0 & 0 & \epsilon(1-v_k) \end{pmatrix}. \tag{4.37}$$

Condition (4.35) imposes that $\boldsymbol{\phi}_k$ should belong to a certain angular sector S_k to verify $s_k \neq \hat{s}_k$ (Figure 4.4). The condition (4.36) cannot be verified unless $\epsilon < \mu$. If such is the case, it imposes that $\boldsymbol{\phi}_k$ should belong to the inside of an elliptical cone[3] contained in S_k. For example, the elliptical cone $C_k^{1/2}$ corresponding to $\epsilon = \mu/2$ is represented in Figure 4.5. Its major half-angle is $\alpha = \frac{\pi}{4}$ and its minor half-angle is

$$\beta_k = \tan^{-1}\left(\sqrt{\frac{1-v_k}{3+v_k}}\right). \tag{4.38}$$

As k increases, $C_k^{1/2}$ shrinks (because β_k is a decreasing function of v_k) while revolving around $\boldsymbol{\theta}$. As $\hat{\boldsymbol{\theta}}_k$ is drawn to $\hat{\boldsymbol{\theta}}_\infty$, $C_k^{1/2}$ goes to a limiting cone $C_\infty^{1/2}$ with major half-angle α and minor half-angle β_∞.

Let us suppose $v_\infty < 1$. Since v_k converges, $\forall \eta > 0$ there exists K_0 large enough so that $\forall k > K_0$, $v_\infty - v_k < \eta$. For example, we take $\eta = \frac{\mu}{4}(1 - v_\infty)$. Since $v_\infty < 1$, the solid angle β_∞ defined by the limiting cone $C_\infty^{1/2}$ is greater than 0. Moreover, it is clear that $\exists K_1 > K_0$ such that

$$\bigcap_{k>K_1} C_k^{1/2} = C \neq \emptyset. \tag{4.39}$$

[3]If $L = 2$, the $\boldsymbol{\phi}_k$ verifying (4.31) are inside a two-dimensional angular sector contained in S_k. The rest of the proof is unaffected.

Consequently, for $k > K_1$, any $\boldsymbol{\phi}_k$ inside C would increase v_k by at least $\frac{\mu}{2}(1 - v_\infty) = 2\eta$, which would contradict our initial hypothesis that $v_\infty - v_k < \eta$.
A necessary condition for $v_\infty < 1$ is then that

$$\forall k > K_1, P(\boldsymbol{\phi}_k \in C) = 0. \tag{4.40}$$

However, $\boldsymbol{\phi}_k$ verifies assumption 2. This means that the probability that a given vector of inputs enters C in finite time after K_1 is 1. Thus (4.40) cannot hold and

$$v_\infty = 1 \Longleftrightarrow \hat{\boldsymbol{\theta}}_\infty = \boldsymbol{\theta}. \tag{4.41}$$

This completes the proof of the theorem.

4.2.3 Numerical results

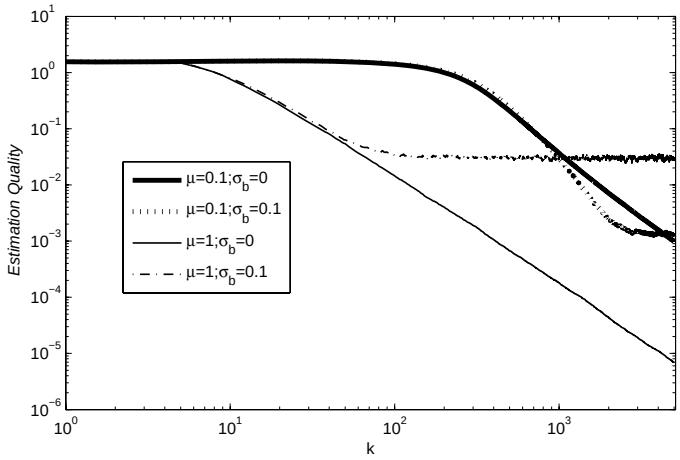

Figure 4.6: 80^{th} percentile of $(1 - v_k)$ for various values of μ and σ_b, using a uniformly distributed input signal.

In this subsection, we report simulation results which suggest that, in order to obtain an appropriate performance of the proposed method in real applications, assumptions 1, 2 and 3 used in the proof of the convergence do not need to be stringently verified. The influence of the relaxation coefficient μ on the convergence rate is also investigated.

We choose the same test case[4] as in [107]:

$$\boldsymbol{\theta} = [1 \quad -0.7 \quad 4 \quad -2.8].$$

Note that $\boldsymbol{\theta}$ is normalized before starting the LIMBO algorithm. The results of the Monte Carlo simulations presented in this section are based on 5000 realizations of the input signal (and of the measurement noise when $b_k \neq 0$). First, we study the influence of μ and

[4]We may also choose a test case consist of repetitions of the sequence $\boldsymbol{\theta} = [1 \quad -1 \quad 1 \quad -1]$ as oscillatory behaviour is commonplace in MEMS devices. However, the above test case is more general than this one and it also makes possible to compare the results of the proposed method with the ones obtained from Wigren's approach on the same test case as in [107]. This is addressed in Section 4.3

measurement noise. The signal u_k is uniformly distributed on $[-1, 1]$, b_k has a Gaussian distribution with zero mean and variance σ_b^2 and both signals are white. The algorithm is initialized with $\hat{\boldsymbol{\theta}}_1 = [0 \quad 0 \quad 0 \quad 1]$.

Figure 4.6 illustrates the estimation quality, measured by the 80^{th} percentile of $(1-v_k)$ from the Monte Carlo realizations, for two values of μ and σ_b. In the noise-free case ($\sigma_b = 0$), the larger μ is, the faster the convergence of the algorithm is. Moreover, the convergence is obtained even in the basic non-relaxed approach ($\mu = 1$). Regardless of the speed of convergence, the optimal parameters are found for all values of $0 < \mu \leq 1$ (Figure 4.6). As could be expected from the theorem proof and can also be seen from Figure 4.6, the rate of convergence decreases when v_k increases. This shows that choosing a white input sequence is clearly sub-optimal. A better strategy would be to pick the input based on the prior knowledge of the currently estimated $\hat{\boldsymbol{\theta}}_k$ and of the previous values of $\boldsymbol{\phi}_k$ which led to unsuccessful trials (i.e. did not result in a change of $\hat{\boldsymbol{\theta}}_k$).

When $\sigma_b \neq 0$, the algorithm estimates the system parameters more precisely if μ is small. In other words, when μ increases the algorithm speed increases, however the precision of the estimation decreases. Therefore, in the presence of measurement noise, it is necessary to make a good compromise between the rate of convergence and the desired estimation quality. Using an adaptive relaxation coefficient (for example, a decreasing sequence as in classical LMS approaches) may also yield good results.

Note that the starting point of the algorithm $\hat{\boldsymbol{\theta}}_1 = [0 \quad 0 \quad 0 \quad 1]$ does not verify assumption 1 (i.e. $v_1 < 0$). Nevertheless, the convergence takes place (Figure 4.6). Similar results are also obtained for different initial points, whether they verify assumption 1 or not, and regardless of the value of μ and σ_b. It means that even if the initial point is not chosen appropriately, the convergence of LIMBO is always obtained, although it may be non-monotonic in the first steps. This effect can be seen in Figure 4.7 that illustrates the estimation quality obtained from only one realization (of 5000 Monte Carlo realizations) with two different initial points.

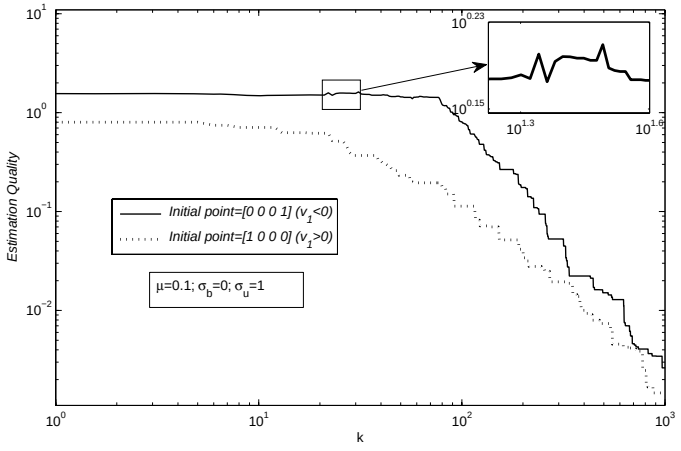

Figure 4.7: The convergence may be non-monotonic in the first steps for a "bad" initial guess $\left(\hat{\boldsymbol{\theta}}_1 = [0 \quad 0 \quad 0 \quad 1]\right)$ especially for small values of μ.

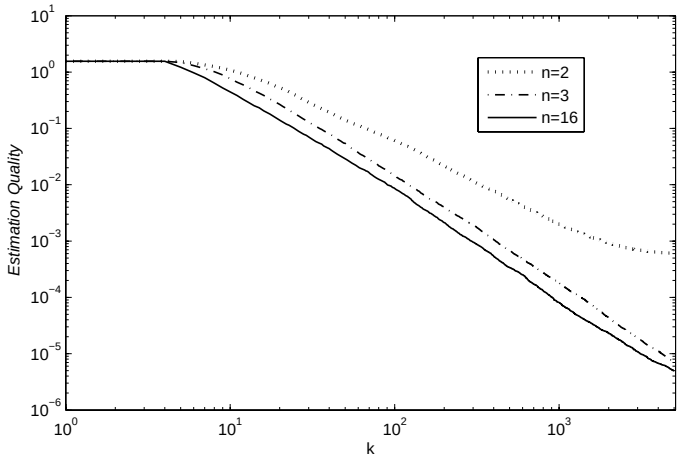

Figure 4.8: 80^{th} percentile of $(1 - v_k)$ for three values of n with $\mu = 1$ and $\sigma_b = 0$, using quantized input signals.

Now, assumption 2 is put to the test. The second part of this assumption (the α-mixing condition) is easy to obtain in practice by using an input sequence having a finite correlation length. On the other hand, if the input signal is quantized (on a finite number of bits, n), the first condition of assumption 2 cannot be verified, since there only exists 2^{nL} different $\boldsymbol{\phi}_k$. Note that the quantification levels of the input signal should not include zero, because the probability of having $\|\boldsymbol{\phi}_k\| = 0$, which causes α_k to be undefined, would then be non-zero. This problem can also be tackled by adding a small positive constant in the denominator of α_k as in the normalized LMS algorithm [122].

Figure 4.8 shows the estimation quality, defined as above, for $n = 2$, 3 and 16 bits, in the absence of measurement noise. As expected, the larger n is, the finer the estimation is. In the present example, $n = 3$ yields very satisfactory results, nonetheless. Finally, it should be noted that, when L is large, a very coarse quantization of the input signal can still yield some very good results (the number of possible ϕ_k increases exponentially with L, whereas the number of parameters to be estimated increases linearly). A result of similar nature was established and verified in [104].

The system may also excited by a white Gaussian input[5] with zero mean. The simulations (Figure 4.9) show that LIMBO converges also in this case as predicted by the theorem. However, the convergence seems to be faster than for a uniformly distributed input. On the other hand, a Bernoulli input signal does not satisfy the α-mixing condition. Thus, the convergence of the algorithm is not guaranteed as shown by the simulations (see Figure 4.10 for $L = 4$). However it is interesting to notice that the longer the impulse response of the system L is, the better the estimation quality is (Figure 4.10).

[5]It is true that a Gaussian input signal may not be easy to generate with only low resolution (say, 1-bit) DACs comparing with uniformly-distributed inputs, quantized with different DACs (2, 3 or 16-bit resolution), as illustrated in Figure 4.8. However, it is possible to obtain a good approximation through modulation techniques (such as PWM or $\sum\Delta$, provided the binary input signal has a large enough oversampling ratio compared to the bandwidth of the identified system).

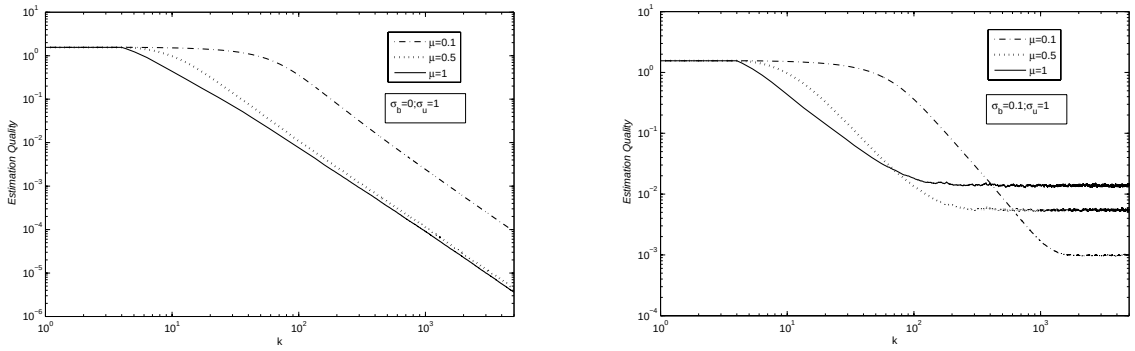

Figure 4.9: 80^{th} percentile of $(1-v_k)$ for various values of μ with $\sigma_b = 0$ (left) and $\sigma_b = 0.1$ (right) using a white Gaussian input.

Finally, we have performed several simulations illustrating the robustness of the proposed estimation algorithm with respect to under-modeling. we consider a system with a 150-sample-long impulse response (a damped sine wave) and try to estimate, using LIMBO, the 64 first parameters. A typical result, obtained with a white uniform input, $\mu = 0.1$, $N = 10^4$ samples and $\hat{\boldsymbol{\theta}}_{\mathbf{1}} = [1 \quad 0 \quad 0 \quad 0]$, is presented in Figure 4.11 hereafter. Note that, out of the 10^4 samples, only 1208 were such that s_k differed from $\hat{s}_k$, so that the estimated parameters were only updated 1208 times by LIMBO. We have presented in Figure 4.12 the results obtained with the classical normalized non-quantized LMS algorithm on this same test-case, after 1208 samples (and updates) and 10^4 samples, which may show the fundamental difference between the convergence behavior of the two approaches. After 1208 samples, the LMS algorithm yields roughly the same estimation quality as LIMBO after the same number of updates.

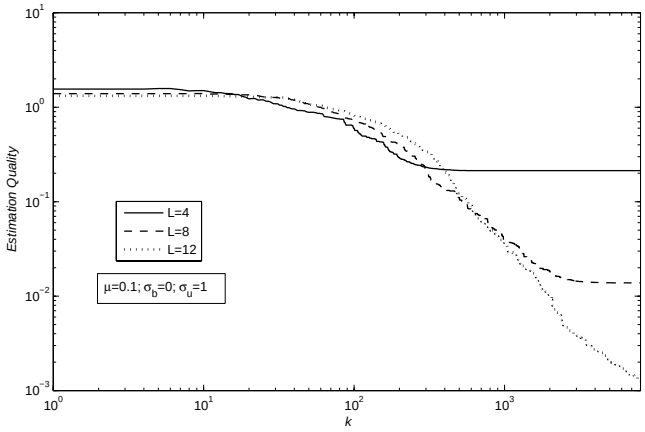

Figure 4.10: 80^{th} percentile of $(1 - v_k)$ for various lengths of system impulse response (L) consisting of repetitions of the sequence $\boldsymbol{\theta} = [1 \quad -0.7 \quad 4 \quad -2.8]$ for $\mu = 0.1$ using a Bernoulli input signal.

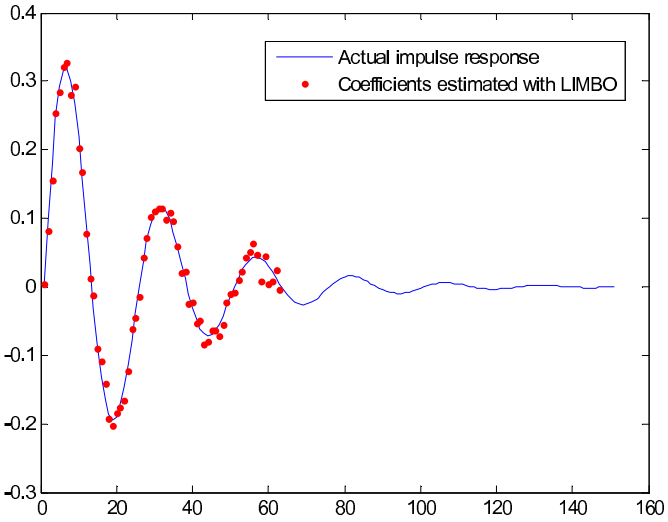

Figure 4.11: Impulse response (continuous line) and results obtained with LIMBO (dots) after 10^4 samples (1208 updates).

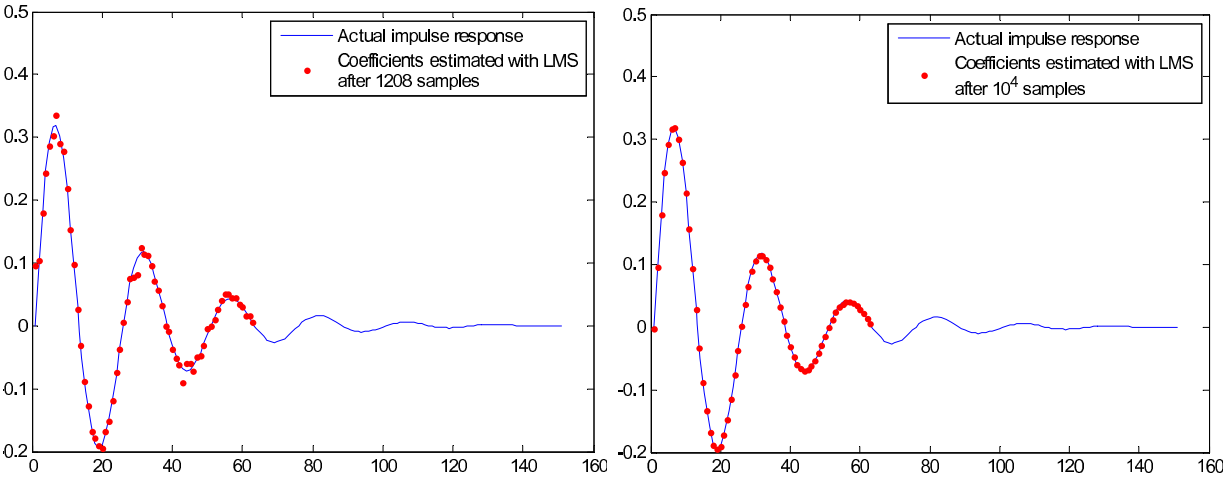

Figure 4.12: Actual impulse response (continuous line) and results obtained with the normalized LMS algorithm (dots) after 1208 samples (left) and 10^4 samples (right).

4.3 Comparison of LIMBO with Wigren's method

We believe that Wigren method is an appropriate method which can be well adapted to the context of microsystems as mentioned in Chapter 2. The low-cost implementation of the algorithm on SoC makes it more appealing for practical micro-applications comparing to other existing approaches in the literature (see Chapter 2). Moreover, this online method does not need large storage requirements as opposed to offline methods (e.x. BIMBO). Thus, it is interesting to compare this algorithm with the method proposed in this chapter. The comparison is addressed in two subsections. The first subsection includes a theoretical comparison between the algorithms. The second one compares two methods by simulation under various scenarios. The complexity of each method and their ease of implementation in the field of microdevices are also addressed in this subsection.

4.3.1 Theoretical comparison

Recall that when used in the context of binary observations, Wigren's method reduces, in its simplest form, to:

$$\hat{\boldsymbol{\theta}}_{\mathbf{1}} = [1 \quad 0 \quad 0 \quad ... \quad 0 \quad 0], \tag{4.42a}$$

$$\hat{\boldsymbol{\theta}}_{\boldsymbol{k+1}} = \hat{\boldsymbol{\theta}}_{\boldsymbol{k}} - \alpha_k \left(\hat{s}_k - s_k\right) \frac{\partial \tilde{s}_k}{\partial \hat{\boldsymbol{\theta}}_{\boldsymbol{k}}}, \tag{4.42b}$$

where

$$\hat{s}_k = S\left(\hat{y}_k\right), \tag{4.43a}$$

$$\hat{y}_k = \hat{\boldsymbol{\theta}}_{\boldsymbol{k}}^{\top} \boldsymbol{\phi}_{\boldsymbol{k}}, \tag{4.43b}$$

$$\tilde{s}_k \approx \frac{2}{\pi} \arctan\left(\frac{\hat{y}_k}{y_0}\right), \tag{4.43c}$$

and y_0 is an arbitrary constant [107]. The quantity $\partial \tilde{s}_k / \partial \hat{\boldsymbol{\theta}}_{\boldsymbol{k}}$ is the so-called pseudo-gradient of $\hat{s}_k$. Comparison of (4.42) and (4.8) results in:

$$\hat{\boldsymbol{\theta}}_{\boldsymbol{k+1}} = \hat{\boldsymbol{\theta}}_{\boldsymbol{k}} - \alpha_k \left(\hat{s}_k - s_k\right) \frac{\partial \tilde{s}_k}{\partial \hat{\boldsymbol{\theta}}_{\boldsymbol{k}}}, \tag{4.44}$$

where $\tilde{s}_k = \hat{s}_k \hat{y}_k^2$ for LIMBO and $\tilde{s}_k \approx \frac{2}{\pi} \arctan\left(\frac{\hat{y}_k}{y_0}\right)$ for Wigren's approach (see Figure 4.13 for an illustration).

This qualitative comparison shows that these two methods can be reformulated as a kind of pseudo-gradient approaches with some similar characteristics, despite of several distinctions between two algorithms. These distinctions range from the difference between the proposed criteria, the regulative coefficients to the assumptions made on the system[6]

[6]For example, Wigren supposed that the quantizer has at least one threshold value different from zero.

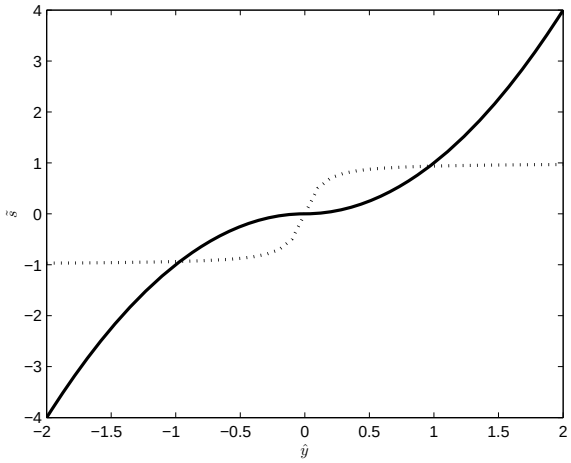

Figure 4.13: A typical Illustration of $\tilde{s}_k = \hat{s}_k \hat{y}_k^2$ for LIMBO (solid line) and of $\tilde{s}_k \approx \frac{2}{\pi} \arctan\left(\frac{\hat{y}_k}{y_0}\right)$ for Wigren's approach with $y_0 = 0.1$ (dotted line).

and the methodology used for the proof of the algorithm (see Appendix B). In the next subsection, we compare the behaviour of these algorithms under different scenarios for practical application in the implementation context of microsystems.

4.3.2 Simulation results comparison

In this subsection, the results obtained with LIMBO (4.14) are compared with those obtained with Wigren's approach (4.42) [107]. The quality of the estimation for the compared method can be also defined as $1 - w_k$:

$$w_k = \hat{\boldsymbol{\theta}}_{\boldsymbol{k}}^{\top} \boldsymbol{\theta}. \tag{4.45}$$

Furthermore the role of the regulative coefficient (α_k) for both methods as well as the optimal choice of y_0 for Wigren's approach and of μ for LIMBO are addressed. We also discuss the efficiency and the complexity of each method and their ease of implementation in the field of microdevices.

In (4.14) or (4.42), the regulative coefficient (α_k) can be chosen with different strategies (constant or adaptive step size [124]). For instance, in [107], the convergence of the pseudo-gradient LMS approach is proved with $\alpha_k = 1/k$, whereas $\alpha_k = \left(\boldsymbol{\phi}_k^{\top} \boldsymbol{\phi}_k\right)^{-1}$ is used for the proof of the algorithm convergence in LIMBO. However, it should be noted that this choice of regulative coefficients ($\alpha_k = 1/k$ or $\alpha_k = \left(\boldsymbol{\phi}_k^{\top} \boldsymbol{\phi}_k\right)^{-1}$) may not be perfectly adjusted to the integration context of microdevices, because division, being one of the most complicated and expensive arithmetic operations, is costly to implement. This is the reason why we first investigate the use of a constant regulative coefficient in (4.14) and (4.42) and we then, use the proposed regulative coefficients for each method. Simulation results are studied under different scenarios in noise-free case and noisy environment:

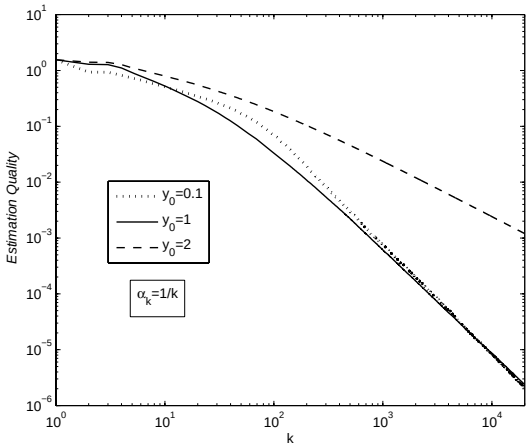

Figure 4.14: 80^{th} percentile of $(1 - w_k)$ with $\alpha_k = 1/k$ and $\sigma_b = 0$ for different values of y_0.

Noise-free case ($\sigma_b = 0$)

The methods are compared, without measurement noise, on the same test case as in the previous section. u_k is a Gaussian white noise with zero mean and unit standard deviation. The value of y_0 in Wigren's method is set by trial-and-error to $y_0 = 1$ when $\alpha_k = 1/k$ and to $y_0 = 10^3\alpha_k$ while $\alpha_k = \alpha$ (using a constant regulative coefficient), so that a good compromise between convergence speed and estimation quality is reached. Typical results are shown in Figure 4.14. The value of μ for LIMBO is also set to $\mu = 1$, because of the noise-free case (as discussed in subsection 4.2.3).

When a constant regulative coefficient ($\alpha_k = \alpha$) is used, we find that $\alpha < 0.2$ yield reasonable results for both methods, in terms of convergence speed and estimation quality (Table 4.1), with a notable advantage for LIMBO in terms of estimation quality. The

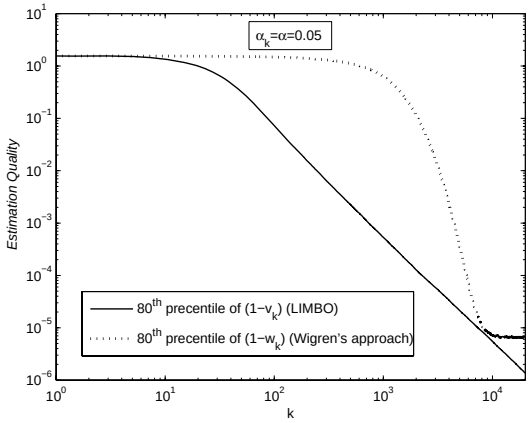

Figure 4.15: Comparison of LIMBO and Wigren's method with $\sigma_b = 0$, using a constant regulative coefficient ($\alpha = 0.05$) for two methods.

Table 4.1: Comparison of estimation quality between LIMBO and Wigren's method with $\sigma_b = 0$ for different regulative coefficients.

	80^{th} percentile of $(1 - v_{10^5})$	80^{th} percentile of $(1 - w_{10^5})$
$\alpha_k = 1/k$	$6.4e-4$	$2.5e-8$
$\alpha = 0.01$	$7.04e-8$	$7.7e-6$
$\alpha = 0.05$	$5.99e-9$	$1.74e-5$
$\alpha = 0.1$	$3.54e-6$	$1.93e-5$
$\alpha = 0.15$	$1.18e-6$	$1.77e-5$
$\alpha = 0.2$	$3.5e-3$	$7.7e-5$

reason for this difference is that when a constant regulative coefficient is chosen, Wigren's approach applied to binary observations stops converging after reaching a certain accuracy (dependent on the choice of y_0). On the other hand, the LIMBO approach converges to the nominal parameters within the limits of finite machine precision. This is illustrated in Figure 4.15.

When a monotonously decreasing regulative coefficient is used for both methods (in the present case, when $\alpha_k = 1/k$), there is a distinct advantage to using Wigren's approach: (4.14) converges very slowly, as is shown in Figure 4.16. On the other hand, (4.42) converges faster to the nominal parameters. However, the convergence speed and the estimation quality of LIMBO when an appropriate constant regulative coefficient ($\alpha_k = \alpha$) or the proposed adaptive one $\alpha_k = \left(\boldsymbol{\phi}_k^\top \boldsymbol{\phi}_k\right)^{-1}$ is used are completely competitive to those obtained with Wigren's approach while $\alpha_k = 1/k$ (Figure 4.17).

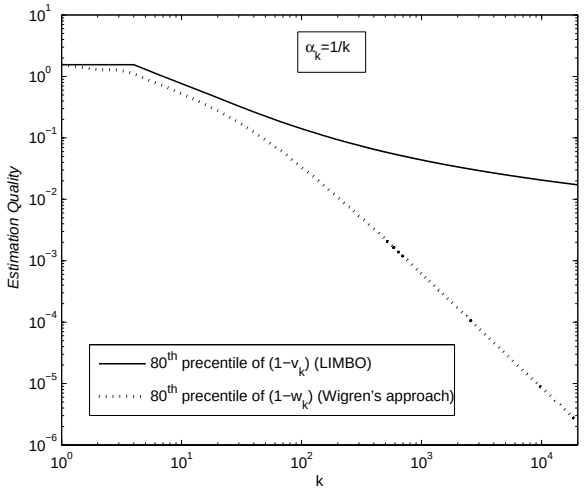

Figure 4.16: Comparison of LIMBO and Wigren's method with $\sigma_b = 0$, using $\alpha_k = 1/k$ for two methods.

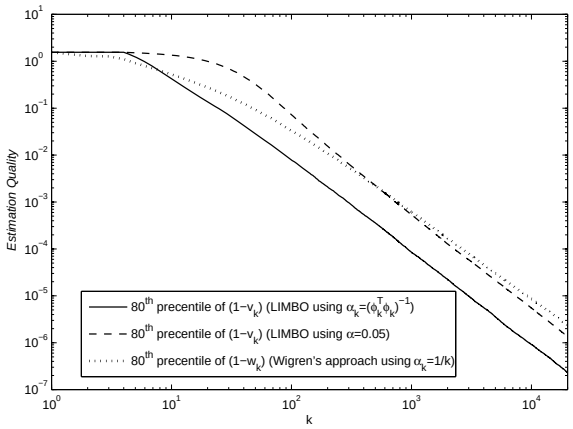

Figure 4.17: Comparison of LIMBO and Wigren's method with $\sigma_b = 0$, using $\alpha_k = 1/k$ for Wigren's approach while using $\alpha_k = \left(\boldsymbol{\phi}_k^\top \boldsymbol{\phi}_k\right)^{-1}$ and $\alpha = 0.05$ for the proposed method.

When using $\alpha_k = 1/k$ for (4.42) and a constant regulative coefficient (α) for (4.14), the parameters of both methods (y_0 for Wigren's approach, α for LIMBO) can always be adjusted so that they converge to the nominal system parameters with a similar speed (Figure 4.17). However, the computational cost of (4.14) is always smaller than that of (4.42): only one division (for normalization step) is required in LIMBO with a constant coefficient, whereas Wigren's approach with a monotonously decreasing coefficient requires at least two or three divisions, depending on whether the pseudogradient $\partial \tilde{s}_k / \partial \tilde{\boldsymbol{\theta}}_{\boldsymbol{k}}$ is actually computed or tabulated.

When $\alpha_k = 1/k$ is used for Wigren's approach and $\alpha_k = \left(\boldsymbol{\phi}_k^\top \boldsymbol{\phi}_k\right)^{-1}$ for LIMBO, the convergence takes place for both methods. However, LIMBO may overcome the compared method in terms of estimation quality and convergence speed (see Figure 4.17). In this case, the computational cost of (4.14) using $\alpha_k = \left(\boldsymbol{\phi}_k^\top \boldsymbol{\phi}_k\right)^{-1}$ may be equal to (4.42) using $\alpha_k = 1/k$.

Qualitatively similar results can also be obtained by using a uniformly distributed input signal with zero mean and unit standard deviation (Figure 4.18). The only difference is that the speed of the convergence for both methods are generally slower than using a Gaussian input signal. However, one can notice that the influence of the input signal distribution is more important for Wigren's approach than LIMBO: it means that although the convergence speed of both methods decreases while using a uniformly distributed input signal, however the convergence speed of Wigren's approach decreases much more than that of LIMBO (Figure 4.18).

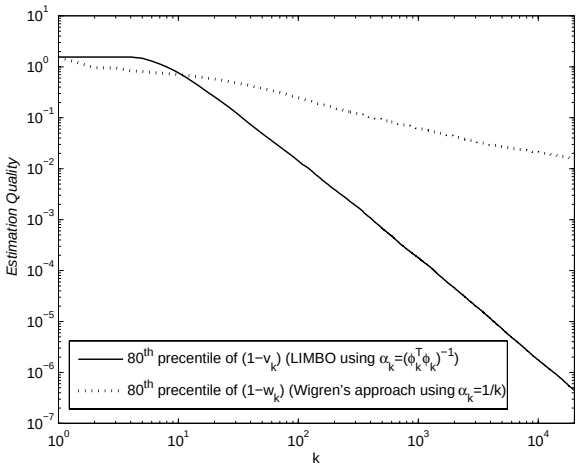

Figure 4.18: Comparison of LIMBO and Wigren's method for $\sigma_b = 0$ using a uniformly distributed input signal.

Noisy case ($\sigma_b \neq 0$)

The methods are now compared in a more realistic case for practical applications in a noisy environment ($\sigma_b \neq 0$). The simulations are performed on the same test case as in the previous subsection for two different input signal distributions. The values of y_0 adjusted in the previous section are also valid to make a good compromise between convergence speed and estimation quality. The value of μ for LIMBO is set to $\mu = 0.01$ because in a noisy case, one should choose a small relaxation coefficient to ensure an appropriate estimation quality as discussed in section 4.2.3.

While using a constant regulative coefficient, $\alpha < 0.2$ provides also some good results for both methods as obtained in the noise-free case. A typical result for $\alpha = 0.05$ is shown in Figure 4.19. In this case, two methods can properly estimates the optimal system parameters by adjusting (α, μ) for LIMBO and (α, y_0) for Wigren's approach, regardless of the input signal distribution (Figure 4.19).

When using the proposed adaptive regulative coefficients for each method ($\alpha_k = 1/k$ for (4.42) and $\alpha_k = \left(\boldsymbol{\phi}_k^\top \boldsymbol{\phi}_k\right)^{-1}$ for (4.14)), Wigren's algorithm converges to the optimal parameters faster than LIMBO in first iterations, regardless of the input signal distribution. However, the convergence of LIMBO and its estimation quality is completely competitive having enough number of iterations (Figure 4.20).

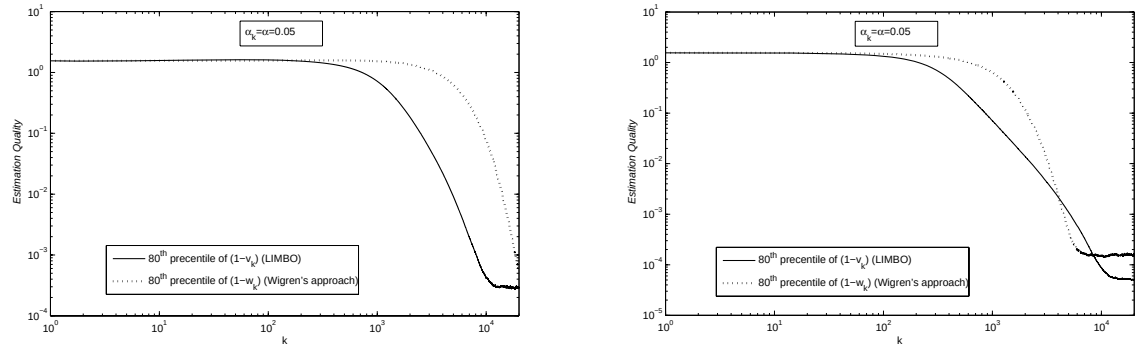

Figure 4.19: Comparison of LIMBO and Wigren's method for $\sigma_b = 0.1$, $\sigma_u = 1$ and a constant regulative coefficient ($\alpha = 0.05$), using a uniformly distributed input signal (left) and a Gaussian input signal (right).

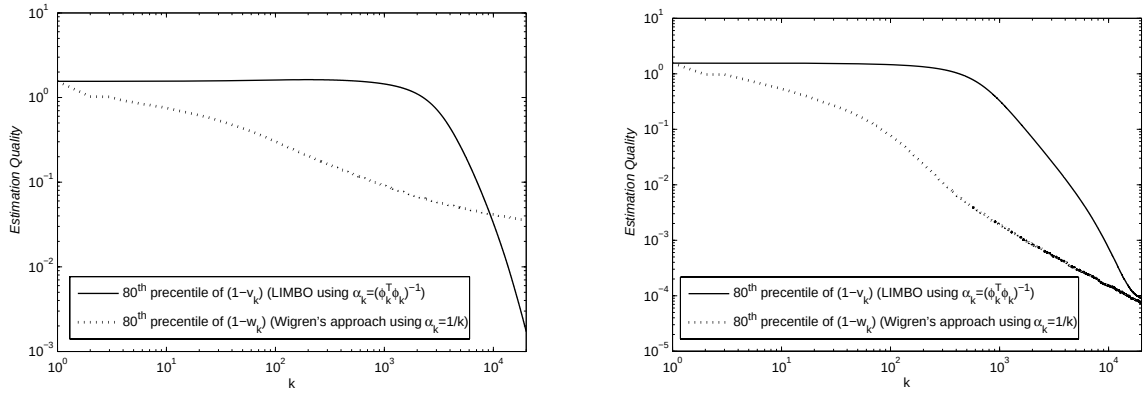

Figure 4.20: Comparison of LIMBO and Wigren's method for $\sigma_b = 0.1$, $\sigma_u = 1$ and the proposed adaptive regulative coefficients, using a uniformly distributed input signal (left) and a Gaussian input signal (right).

4.3.3 Summary

Based on the simulations in the previous subsections, one can conclude that two compared methods may provide some good results under different scenarios by using constant or adaptive regulative coefficient. Using a constant regulative coefficient may be less expensive and easier to implement in the context of microdevices. However one must adjust two parameters for each method to achieve a satisfactory results (for LIMBO, (α, μ) and (α, y_0) for Wigren's method).

On the other hand, when using the proposed adaptive regulative coefficients, we can properly estimate the optimal system parameters by adjusting only one parameter for each algorithm under different conditions (μ and y_0). However, the implementation cost and its complexity of the methods may increase.

4.4 Conclusion

In this chapter, LIMBO, a basic LMS-like approach for estimating system parameters based on binary observations, has been derived from the offline WLS approach presented in Chapter 3. We then relaxed the basic approach by using a relaxation coefficient (μ) to ensure its rigorous mathematical convergence. The asymptotical convergence of the approach has been also studied. In particular, we gave some assumptions under which the convergence of the algorithm to the optimal system parameters is theoretically guaranteed. We showed by simulation that these assumptions do not necessarily have to be met in practice in order to obtain a good performance of the method.

Furthermore the robustness of the proposed estimation algorithm with respect to under-modeling and its main difference with classical normalized LMS approach have been illustrated by simulations. Besides, simulations showed that the results obtained with LIMBO are comparable, in terms of convergence speed and of estimation quality, to those obtained with the approach presented in [107], with a lesser computational complexity. The computational complexity of LIMBO is also much lower than that of ML algorithms (no integral to evaluate). Moreover, our approach is online and has low computational storage requirements, as opposed to offline techniques based on batch-data methods (e.x. BIMBO method [5]). This makes LIMBO an inexpensive test method with a very low computational complexity, requiring only little memory storage and amenable to implementation on small processor cores as used in SoC applications.

In the next Chapter, we develop an experimental application of the proposed method for a micromachined sensor. We estimate the microdevice impulse response and its offset by only using binary inputs and outputs that can easily be implemented on an FPGA with low power consumption and minimal silicon area [125]. Using a dithering signal to identify the gain of the impulse response of the microdevice is also addressed in this Chapter.

Chapter 5

Experimental application of LIMBO dedicated to microsystem integrated self-testing

Microsystems have emerged in the early 90s. Since then most scientific researchers have focused on fabrication technology and design. Thus, unlike other domains of test research and developments, the microsystem testing field is still young and not mature enough for mass production. Recently, the importance of integrated testing approaches has arisen and some significant contributions on microsystem testability have been developed as studied in Chapter 1.

In this chapter, we show with a real-world example how the LIMBO algorithm can be applied to the design of a low-cost Built-In Self-Test (BIST). The tested MEMS device is a microwire used as a heating resistor, inserted in a Wheatstone bridge. We show how the impulse response and the offset of the microdevice are estimated only using binary inputs and outputs and straightforward calculations, which can easily be implemented on an FPGA. The estimation, using a dithering signal, of the gain of the microdevice impulse response is also addressed in this chapter. This low-cost Built-In Self-Test (BIST) approach only requires a 1-bit ADC and a 1-bit DAC, which makes it very amenable to integration and highlights its suitability for the test of systems based on resistive sensor and actuator.

5.1 A new low-cost BIST method for resistive MEMS sensors based on LIMBO

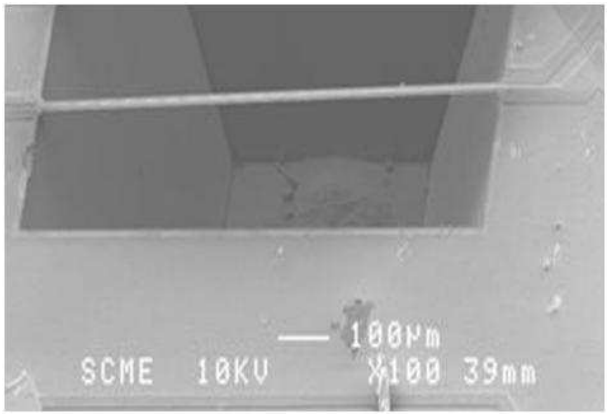

Figure 5.1: Scanning Electron Micrograph (SEM) of the microwire used for the evaluation of LIMBO.

This work being focused on the evaluation of the performances of the LIMBO method, the start candidate is here a MEMS microwire used as a heating resistor, chosen with regards to its great ease of use. The trial device is a $1.5k\Omega$, $5\mu m \times 20\mu m \times 1500\mu m$ Silicon-On-Insulator (SOI) processed microwire, deeply under-etched (Figure 5.1). Under-etching enables the microwire to be set over a $300\mu m$ thick gas layer. When heated by a current $i(t)$, where t denotes time, the temperature of the wire increases. The transient excess temperature of the wire, $\Theta(t)$ can be expressed by

$$\Theta(t) \propto h(t) * i^2(t), \tag{5.1}$$

where $*$ denotes the convolution operator and $h(t)$ is the unity gain impulse response of the wire, expressed in the time domain. Following [126, 127], we have:

$$h(t) = \sum_{n=0}^{\infty} g_n \exp\left(-\frac{t}{t_n}\right) \cong g_0 \exp\left(-\frac{t}{t_0}\right); \quad \int_{t=0}^{\infty} h(t).d(t) = 1, \tag{5.2}$$

where g_n and t_n are respectively the n^{th} gain and time constants given by a Fourier analysis of the transient heat equation in the wire. In the present case, only the first mode is significant.

Our objective is to use a system identification method in order to monitor the variations of this impulse response, induced by changes in the operating conditions, ageing, etc. First, we describe how the LIMBO algorithm is used for fitting the model of the tested MEMS. Loosely, LIMBO requires the generation of a spectrally rich signal, here a one-bit binary white noise, at the input of the unknown system. The sign s_k of the system output y_k is then measured through a 1-bit ADC (i.e. the available data is u_k and $s_k = sign(y_k)$). Using an internal parametric model of the system, its estimated output $\hat{y}_k$ and $\hat{s}_k = sign(\hat{y}_k)$ are calculated. The parametric model is then adjusted with LIMBO,

in order to minimize $(s_k - \hat{s}_k)^2$. The outputs of LIMBO are the estimations of Y_o, the offset at the input of the 1-bit ADC, and of $h(pT_s), \quad p = 0, ..., P-1$, the P-sample long discrete-time impulse response of the wire, where T_s is the sampling period. These outputs, collected in a single vector

$$\hat{\boldsymbol{\theta}} = [Y_0, h(0), ..., h((P-1)T_s)]^\top,$$

are estimated according to the following iterative procedure:

- At the k^{th} sample, the observation vector $\boldsymbol{\phi}_k$ is defined as $\boldsymbol{\phi}_k = [1 \quad u_k \quad ... \quad u_{(k-P+1)}]^\top$. In the present case, vector $\boldsymbol{\phi}_k$ is filled with binary samples $u_k = +1$ or -1.
- The system's analog output $\hat{y}_k$ is then estimated using $\hat{y}_k = \boldsymbol{\phi}_k^\top \hat{\boldsymbol{\theta}}_k$ where $\hat{\boldsymbol{\theta}}_k$ are the parameters estimated at the k^{th} iteration.
- Now, if the measured sign $s_k = sign(y_k)$ of the system's analog output is the same as $\hat{s}_k = sign(\hat{y}_k)$, the estimated impulse response $\hat{\boldsymbol{\theta}}_k$ is assumed to be correctly estimated, so that $\hat{\boldsymbol{\theta}}_{k+1} = \hat{\boldsymbol{\theta}}_k$. In the other case, $\hat{\boldsymbol{\theta}}_k$ is assumed to be incorrect. It is then updated using the following correction:

$$\hat{\boldsymbol{\xi}}_{\boldsymbol{k+1}} = \hat{\boldsymbol{\theta}}_{\boldsymbol{k}} - 2\mu \frac{\hat{y}_k}{\boldsymbol{\phi}_k^\top \boldsymbol{\phi}_k} \boldsymbol{\phi}_k, \tag{5.3a}$$

$$\hat{\boldsymbol{\theta}}_{\boldsymbol{k+1}} = \frac{\hat{\boldsymbol{\xi}}_{\boldsymbol{k+1}}}{\left\| \hat{\boldsymbol{\xi}}_{\boldsymbol{k+1}} \right\|}, \tag{5.3b}$$

  where $\mu \in]0, 1[$ is a relaxation parameter scaling the convergence of the algorithm, which will be discussed in subsection 5.1.3.

The LIMBO algorithm features straightforward calculations, fixed-size buffer and low memory storage, which eases its implementation on a Digital Signal Processor (DSP). Following the description of the read-out electronics and of the experimental setup, subsection 5.1.3 illustrates the performance of the proposed method based on experimental results.

5.1.1 Interface circuitry

In resistive based sensors, there exists a functional relationship between the resistance of the material and the corresponding physical quantity to be measured (q) such as force, temperature or light intensity. Thus, we can establish a functional relationship as:

$$R_W = f(q), \tag{5.4}$$

where R_W is the value of the resistance of the sensor. However, the primary issue in the context of the use of data acquisition (DAQ) hardware is that what we need is voltage,

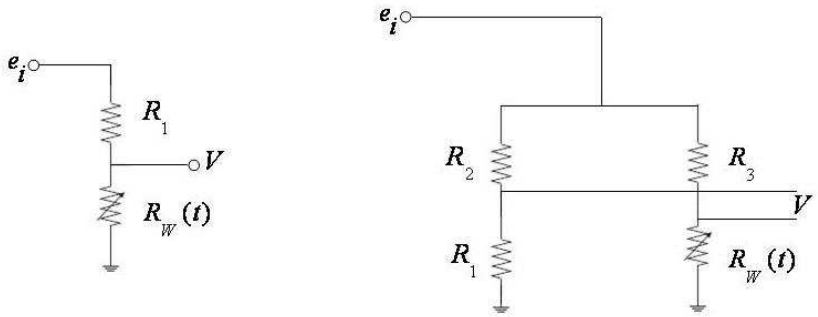

Figure 5.2: Two basic types of interface circuitry: voltage divider (left) and Wheatstone bridge (right).

not resistance. It means that it is required to obtain a functional relationship between voltage of the sensing circuit V and the measured physical parameter:

$$V = f(q). \tag{5.5}$$

As a consequence, it is essential to use additional circuitry around the resistive microwire, in order to extract the measured signal as a voltage and to interface with DAQ hardware. With this additional circuit, we obtain a functional relationship between the output voltage of the circuit and the resistance of the sensor:

$$V = f(R_W), \tag{5.6}$$

which can be then reformulated by using (5.4), as a relationship between the output voltage of the circuit used by DAQ hardware and the physical parameter measured by the sensor.

For a wide range of resistive sensors, a simple voltage divider is employed as interface circuitry (Figure 5.2-left). In this case, R_W is a resistive sensor (the microwire) and R1 kept as a fixed resistor. Thus, the voltage developed on the sensor that is the output voltage of the divider circuit, can be expressed as a functional relationship of the sensor resistance:

$$V = e_i \frac{R_W}{R_1 + R_W}, \tag{5.7}$$

where e_i is the input voltage.

In the case of using the voltage divider, the choice of the resistance for the fixed resistor is usually a common issue. It is clear that when the resistance of the sensor changes from 0 to infinity, the output voltage may vary from 0 to e_i, regardless of the value of R_1. However, the resistance of the sensor may normally vary from a minimum value (R_{Wmin}) to a maximum value (R_{Wmax}). An appropriate first approximation is then to choose the mean value as the value for the fixed resistor:

$$R_1 = \frac{R_{Wmin} + R_{Wmax}}{2}. \tag{5.8}$$

However, when the relative variations of the sensor resistance in response to changes of physical parameter are very small, this simple interface circuitry is not practical. One

can then usually use a Wheatstone bridge (Figure 5.2-right). As it is illustrated in the figure, R_W is the resistive microwire inserted in a Wheatstone bridge with three other resistance (R_1, R_2 and R_3). Thus, one can easily obtain a functional relationship between the output voltage and the resistance of the sensor:

$$V = e_i \left(\frac{R_W}{R_W + R_3} - \frac{R_1}{R_1 + R_2} \right). \tag{5.9}$$

It is important to mention that the microwire used in Wheatstone bridge as in Figure 5.2(left), provides a too small voltage signal which is not practically useful to be interfaced with data acquisition hardware. Thus, one must amplify the output signal from the bridge in order to perform further processes. A differential amplifier is then used that makes our experimental setup for evaluation of LIMBO as shown in Figure 5.3. In the next subsection, we will discuss how to use this setup to evaluate LIMBO algorithm.

5.1.2 Read-Out Electronics - Micro Wire inside a Wheatstone Bridge

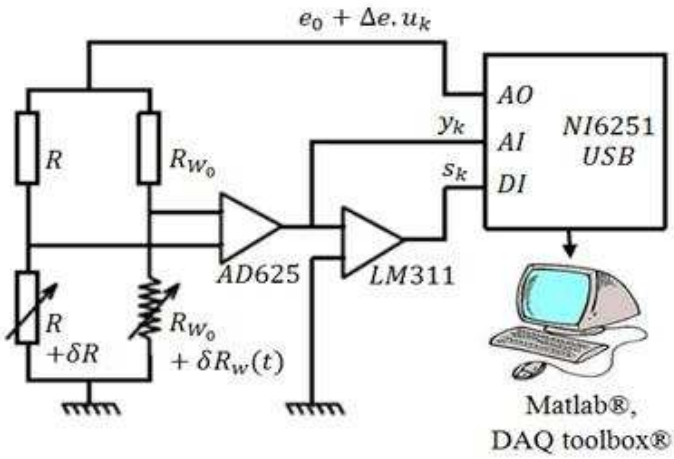

Figure 5.3: Experimental setup. The microwire is placed on the bottom-right side in the Wheatstone bridge. The bottom-left side variable resistor is used to control the offset of the bridge.

This section shows how to use a Wheatstone bridge whose differential output can be processed with LIMBO, in order to sense the changes in one of the resistances (the microwire) composing the bridge. For reasonable values of the current going through the bridge, over heating of the microwire is low. The value of the resistance of the microwire $R_W(t)$ can then be expressed with a first order expansion as:

$$R_W(t) = R_{W_0} \left(1 + \beta \Theta(t)\right), \tag{5.10}$$

where R_{W_0}, in Ω, is the nominal value of the resistance of the wire at ambient temperature and β the Temperature Coefficient of Resistivity (TCR) of the microwire, in K^{-1}. The Wheatstone bridge (Figure 5.3) is biased by a voltage

$$e(t) = e_0 + \Delta e.u(t), \tag{5.11}$$

where e_0 and Δe are constant, $e_0 > \Delta e$ and $u(t) = \pm 1$ is a binary pseudo-random sequence with sampling period T_s. Note that, since $e_0 > \Delta e$, we have $e(t) > 0$. The voltage drop $\delta V(t)$ across the differential branch can be expressed at the first order as:

$$\delta V(t) \approx \left(\beta \Theta(t) + \frac{\delta R_{W_0}}{R_{W_0}} - \frac{\delta R}{R} \right) e(t), \tag{5.12}$$

where δR_{W_0} and δR denote resistance mismatch between the upper and lower branches of the bridge, due to fabrication process or ageing variation. Since

$$\Theta(t) \propto h(t) * i^2(t) \propto h(t) * e^2(t), \tag{5.13}$$

and $u(t)^2 = 1$, using (5.11) leads to:

$$\Theta(t) \propto \left(\Delta e^2 + e_0^2 \right) + 2 e_0 \Delta e h(t) * u(t). \tag{5.14}$$

Substitution of (5.14) into (5.12) finally gives the nonlinear expression:

$$\begin{aligned} \delta V(t) &\propto \left[\beta \left(\Delta e^2 + e_0^2 \right) + \frac{\delta R_{W_0}}{R_{W_0}} - \frac{\delta R}{R} + 2\beta e_0 \Delta e h(t) * u(t) \right] e(t) \\ &\propto \left(Y_o + h(t) * u(t) \right) e(t) = y(t) e(t). \end{aligned} \tag{5.15}$$

Since $e(t) > 0$, it follows that:

$$sign\left(\delta V(t)\right) = sign\left(y(t)\right). \tag{5.16}$$

Thus, in spite of the nonlinear input-output relationship, LIMBO can be used to estimate both the offset Y_o and the coefficients $h(pT_s)$ of the discrete-time impulse response, from the (discrete-time) 1 bit signals u_k and s_k. However, note that if the offset is too large (i.e. the bridge is very unbalanced), s_k will be constant and there will be no way to identify the system.

From a practical point of view, the Wheatstone bridge is supplied with a 10kHz binary digital signal ($e_0 = 1V, \Delta e = 0.5V$) through the NI6251USB 16-bit data acquisition hardware Analog Output, for convenience. The differential output signal $\delta V(t)$ of the resistor bridge is amplified using the AD625 instrumentation amplifier, with gain 300. The system's analog output is then recorded through the Analog Input of the NI6251USB. An LM311 voltage comparator provides the binary signal s_k to the Digital Input of the NI6251USB. The data acquisition hardware is remote-controlled by the Data Acquisition Toolbox® software of Matlab®, where the LIMBO algorithm is running online, either as a post-processing tool using Matlab® script programming, or in real-time using Simulink® features. Recording of the system's analog output (Figure 5.4) is made in order to provide a comparison of accuracy of the system identification of LIMBO to that of other standard parameter estimation methods relying on high-resolution output signals, as shown in the next subsection.

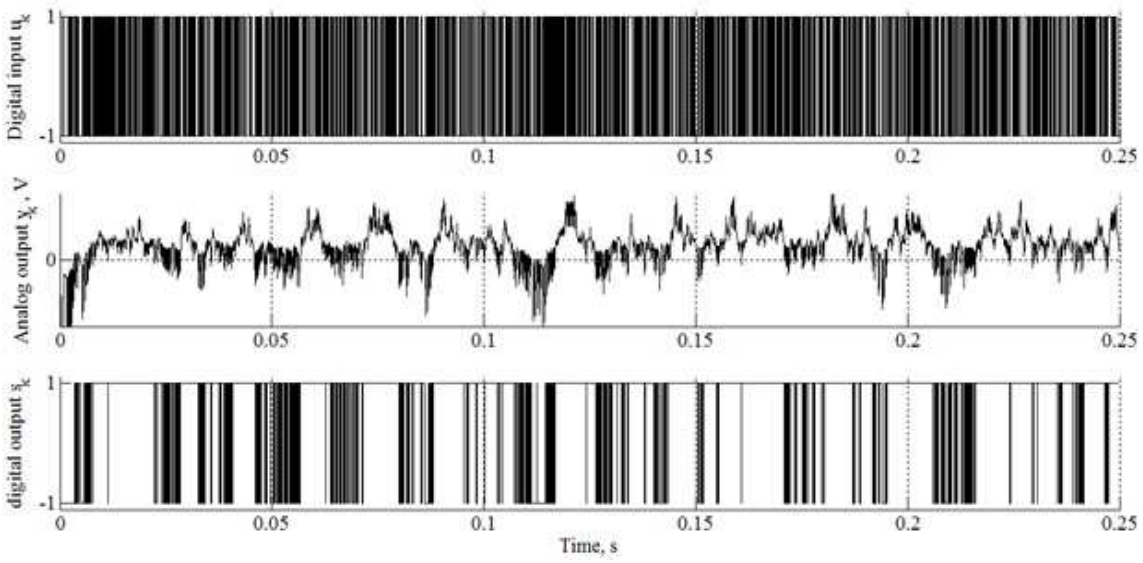

Figure 5.4: 250 ms long signal record of the binary input u_k, of the analog output y_k and of the digital output s_k versus time (from top to bottom).

5.1.3 Experimental Results - Evaluation of the performances

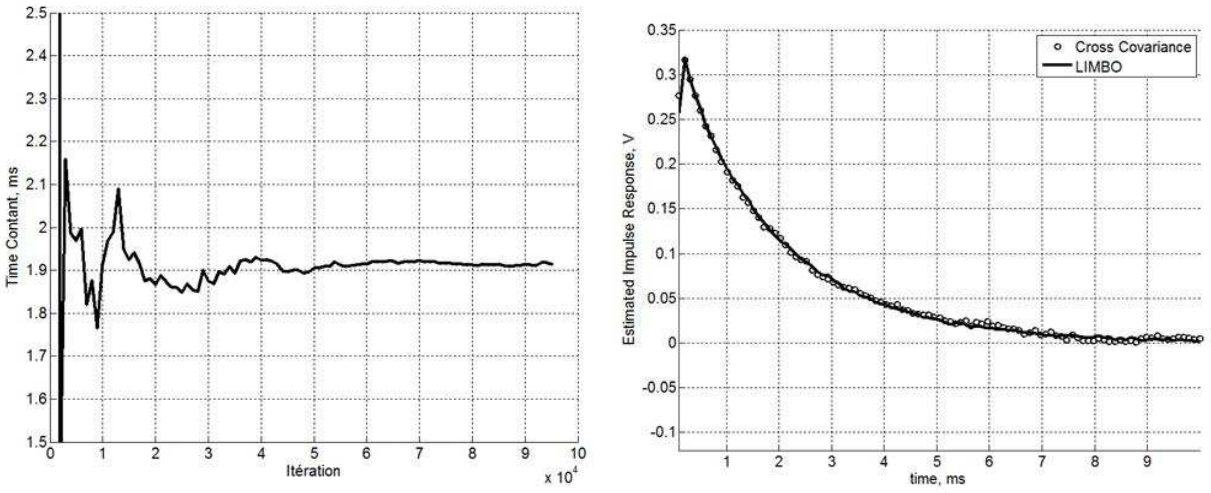

Figure 5.5: Convergence status of LIMBO, in terms of time constant t_0 (left) and comparison of the impulse response estimated online with LIMBO with that obtained from the cross-covariance of y_k with u_k (batch method), using a 16−bit DAC and 20000 samples (right).

This section illustrates the accuracy and the rate of convergence of the LIMBO algorithm. As mentioned before, the rate of convergence of LIMBO is determined by the relaxation parameter μ. The value of μ is crucial to the trade-off between speed and accuracy: a large value of μ results in fast convergence, but poor accuracy. On the other hand a very small value results in very good accuracy but in a very slow convergence. In

the present case, we start with $\mu = 0.5$ and we multiply it by 0.97 every 1000 iterations. The impulse response is calculated using $P = 100$ parameters, which corresponds to a duration of $10ms$. The time constant t_0 can then be estimated from the impulse response coefficients, using (5.2).

Convergence is shown in Figure 5.5(left) in terms of time constant t_0. 20000 iterations (i.e. $2s$) are needed here to provide a good estimation of the impulse response of the microwire. The time constant is estimated with about than 0.2% accuracy and the offset voltage with $1.0mV$ resolution over a $\pm 350mV$ full scale. Figure 5.5(right) represents the impulse responses estimated after $2s$ with LIMBO, on one hand, and with a batch estimation of the cross-covariance of u_k and 16-bit signal y_k, on the other hand. This clearly shows that LIMBO provides results comparable to those obtained using full-scale 16-bit measurements. Note that the impulse response of the complete system is not purely exponential, as (5.2) would have led us to think: the rising slope at the beginning of the impulse response is in fact due to the limited bandwidth of the instrumentation amplifier, which filters out the high frequency components of the signal.

It should be stressed that LIMBO, as presented so far, does not allow us to identify the gain of the impulse response (since multiplying y_k by any positive constant leaves s_k unchanged). However, this can be achieved by adding a known voltage reference (a dithering signal $d(t)$) at the input of the comparator. In this case, it is possible to write:

$$\tilde{y}(t) = y(t) + d(t), \tag{5.17}$$

where $y(t) = e(t)\,(h(t) + Y_0)$ and Y_0 is the offset of the output. One can then establish the nonlinear expression as in (5.15) for the case of using a dithering signal:

$$\begin{aligned} \delta V(t) &\propto \left[\beta\left(\Delta e^2 + e_0^2\right) + \frac{\delta R_{W_0}}{R_{W_0}} - \frac{\delta R}{R} + 2\beta e_0 \Delta e h(t) * u(t) + d(t)\right] e(t) \\ &\propto \left(Y_o + h(t) * u(t) + d(t)\right) e(t) = \tilde{y}(t) e(t). \end{aligned} \tag{5.18}$$

Since $e(t) > 0$, it yields:

$$sign\left(\delta V(t)\right) = sign\left(\tilde{y}(t)\right) = sign\left(\frac{d(t)}{e(t)} + h(t) * u(t) + Y_0\right). \tag{5.19}$$

Figure 5.6 illustrates estimations of the gain of the impulse response versus the temperature for $d(t) = \pm 1v$. This shows that although it is possible to estimate the gain of the impulse response by using a dithering signal, our estimations are affected by temperature changes. When the temperature of the operating condition increases, the estimated gain of the impulse response is increased as well. The result of fitting our set of estimated points with linear LS regression are also shown in Figure 5.6. By using this LS fit, the temperature effects on the gain of the impulse response can be compensated and calibrated by adjusting the resistance R.

Although the gain of the impulse response can be estimated by using a dithering signal, the value of dithering signal is also an important factor. Figure 5.7 illustrates estimations of the impulse response gain versus the temperature for different values of dithering signal. These results show that as $d(t)$ is too large or too small, thus the sensitivity of

estimations against temperature changes decreases. It means that, too large or too small dither is detrimental to the sensitivity of estimations. The results of the same nature are also established by simulations in Chapter 3 for the offline proposed method (see Section 3.5.2).

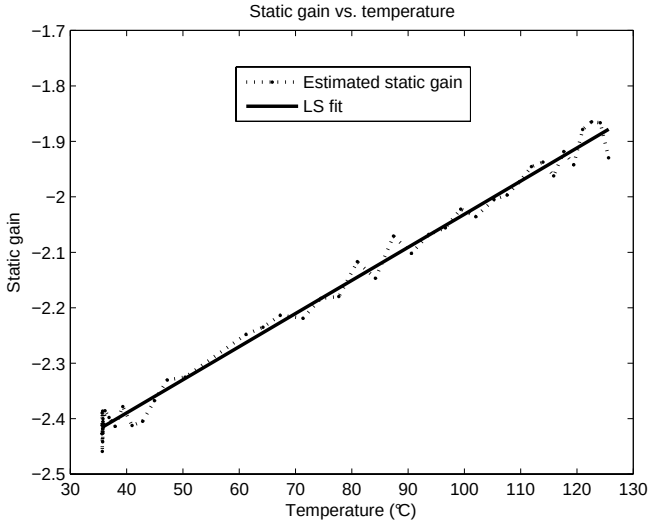

Figure 5.6: Estimated gain of the impulse response versus the temperature for $d(t) = \pm 1v$.

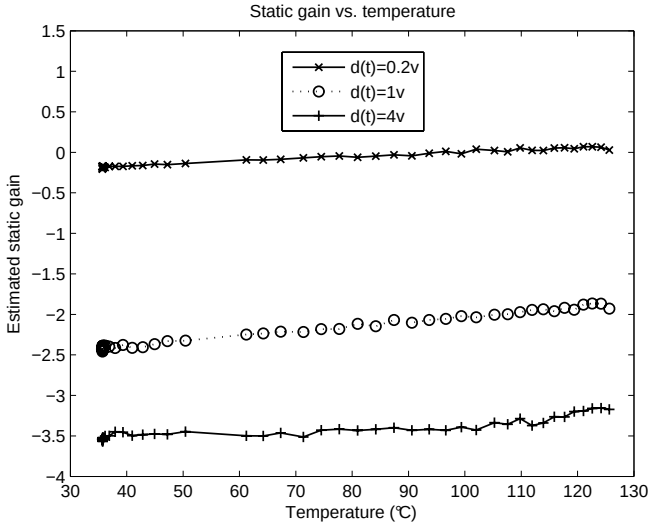

Figure 5.7: Estimated gain of the impulse response versus the temperature for different values of $d(t) = \pm 0.2v$, $d(t) = \pm 1v$ and $d(t) = \pm 4v$.

5.2 Conclusion

We have presented in this chapter how the LIMBO algorithm can be used to estimate several characteristics (namely offset and response time) of resistive microwires, with a minimal number of analog components and very low digital requirements. We also showed how it is possible to estimate the gain of the impulse response by using a dithering signal. The choice of an optimal dithering signal was also discussed. The proposed method and measurement setup could be easily extended to actual resistive sensors or to other sorts of impulse responses (not purely exponential). The BIST method considered in this work requires only low-resolution analog-to-digital (A/D) or digital-to-analog (D/A) converting blocks, so that the silicon area necessary for their co-integration with the MEMS is as small as possible.

Chapter 6

General conclusions and future works

6.1 Dissertation contributions

While the characteristic dimensions of electronic systems scale down to micro or nano world, their performance is greatly influenced. Microfabrication process or variations of the operating situation such as temperature, humidity or pressure are usual cause of dispersion. Therefore, it seems essential to co-integrate self-testing or self-adjustment routines for these microdevices. For this feature, most existing system parameter estimation methods are based on the implementation of high-resolution digital measurements of the system's output that require the use of N-bit ($N >> 1$) Analog-to-Digital Converters (ADC). Thus, long design time and large silicon areas are needed, which increases the cost of the microfabricated devices. The parameter estimation problems based on binary (or quantized) outputs can be introduced as alternative self-test identification methods, requiring only an (ideally) 1-bit ADC that can be implemented in a small silicon surface with minimal energy consumption. Moreover, in the case of online methods, it does not require large storage resources. As a consequence, although the use of such identification methods is one of the absorbing domains in a wide range of applications, the approaches studied in this dissertation are aimed at the test of micro electronic devices, such as MEMS. The details of our contributions are described hereafter:

- We presented a new WLS criterion for parameter estimation based on binary data: this offline approach is an alternative to the one presented in [5]. We have shown that these two criteria, although closely related, do not have the same asymptotical behaviour. Particularly, in the presence of noise, using the proposed criterion for determining the system parameters results in an underestimation of the optimal system parameters. However, the proposed method is easier to implement than the compared one in the context of MEMS integration. The established asymptotical results have also been confirmed by simulations performed in a Gaussian context. Other scenarios, where not all signals are Gaussian or centred, have been tested:

these simulations showed that the hypotheses made for obtaining the theoretical results can somehow be relaxed. Furthermore, the estimation quality of the proposed approach in a noise-free environment has been investigated in the case of the existence of only a finite number of samples. The relation between accuracy and the number of samples needed for identifying a system was figured out. Moreover, the simulation results were compared with good agreement to the theoretical results.

- LIMBO, a recursive parameter estimation method using binary observations based on the LMS algorithm was derived from our offline approach. The asymptotical convergence of this online method was investigated. In particular, we gave some assumptions under which the convergence of the algorithm to the optimal system parameters is theoretically guaranteed. We showed by simulations that these assumptions do not necessarily have to be met in practice in order to obtain a good performance of the method. Furthermore, simulations illustrated that the results obtained with LIMBO were comparable, in terms of convergence speed and of estimation quality, to those obtained with an appropriate approach in the field of microdevices [107]. Finally, we concluded that LIMBO has a very low computational complexity and implementation cost, making it an inexpensive test method, requiring only little memory storage (as opposed to offline approaches) and amenable to implementation on FPGAs or small processor cores as used in the context of micro electronics.

- We presented an experimental application of LIMBO dedicated to the self-test of integrated micro electronic mechanical systems. We used a MEMS microwire as a heating resistor, derived by a Wheatstone bridge. The impulse response and the offset of the microdevice have been estimated only using binary inputs and outputs and straightforward calculations which made it easy to implement in the context of integrated MEMS self-testing. The proposed online Built-In Self-Test method is very amenable to integration for the self-testing of systems relying on resistive sensor and actuator, because it requires low memory storage, only a 1-bit ADC and a 1-bit DAC which can be easily implemented in a small silicon area with minimal energy consumption.

6.2 Perspective for future works

There are several interesting areas for future works on the LIMBO algorithm and its applications. It is our belief that the LIMBO algorithm can be extended to more complex systems such as Infinite Impulse Response (IIR) or nonlinear systems. The design of an optimal input signal for LIMBO is also the subject of future works. Furthermore, some other practical applications of LIMBO can be investigated. In the following, we address some of these interesting challenges.

6.2.1 Theoretical scope

Extension to IIR systems

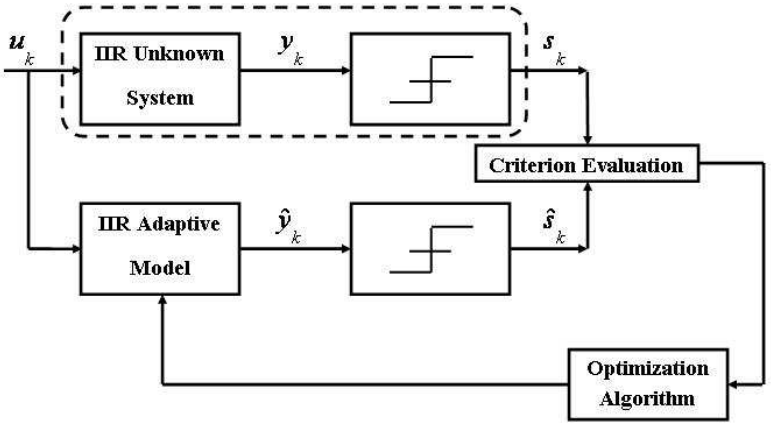

Figure 6.1: General schematic of LIMBO used for IIR systems.

In the most general formulation of discrete-time infinite impulse response models, an input function u_k and the system output sequence y_k are related by the following linear difference equation:

$$y_k = \sum_{i=1}^{P} b_i u_{k-i} - \sum_{j=1}^{Q} a_j y_{k-j}, \tag{6.1}$$

where b_i and a_i are, respectively, feedforward and feedback system coefficients with orders of P and Q. Thus, the transfer function is defined as:

$$H(z) = \frac{\sum_{i=1}^{P} b_i z^{-i}}{1 + \sum_{j=1}^{Q} a_j z^{-j}}. \tag{6.2}$$

The goal is then to develop a recursive estimation method to estimate the coefficients b_i and a_j based on observations of the input signal and the binary output of the comparator

(Figure 6.1). The first simulation results shows that LIMBO adapted to IIR systems can properly estimate the nominal system coefficients for simple systems (i.e. first order systems); however the convergence of the method is not at all ensured in the case of more complex IIR systems. How to guarantee convergence of the algorithm in this case is an appealing subject for future work.

Extension to nonlinear systems

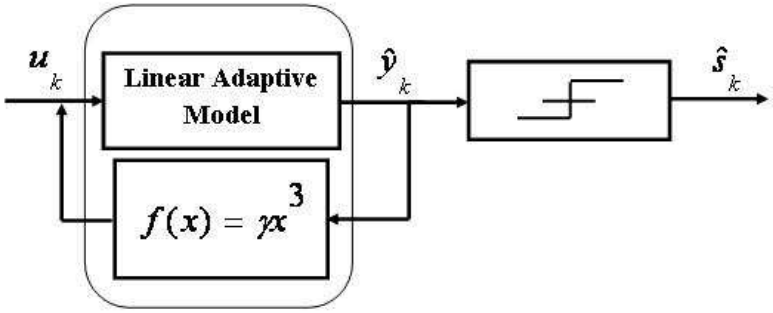

Figure 6.2: Schematic of a model that can be used for extension of LIMBO to the nonlinear case. The goal is to estimate the linear system parameters and the Duffing coefficient (γ).

Nonlinear problems are always interesting for scientific researchers because most physical systems are inherently nonlinear in nature. Thus, we also consider extending our LIMBO to nonlinear systems. The schematic of this setup is shown in Figure 6.2 where the type of nonlinearity is supposed to be the Duffing nonlinearity, because several nonlinear systems can be represented by various forms of the Duffing equations such as the nonlinear behaviour of some isolators, beams, cables and electrical circuits [128]. The objective for future work is thus to develop a recursive estimation method to estimate the linear system parameters as well as the Duffing coefficient based on observations of the input signal and the binary output of the comparator.

6.2.2 Application scope

The first application of LIMBO presented in this dissertation was aimed at the test of microfabricated devices. We believe that it is also possible to develop a low-cost measurement system based on an integrated multifunction reconfigurable sensor by using the LIMBO algorithm (Figure 6.3). The user can reconfigure the multifunction sensor to measure different condition changes such as temperature, pressure and humidity. The LIMBO algorithm is used to recalibrate the MEMS sensor in order to compensate the influences of other condition changes on the performance of the MEMS sensor. For example, when

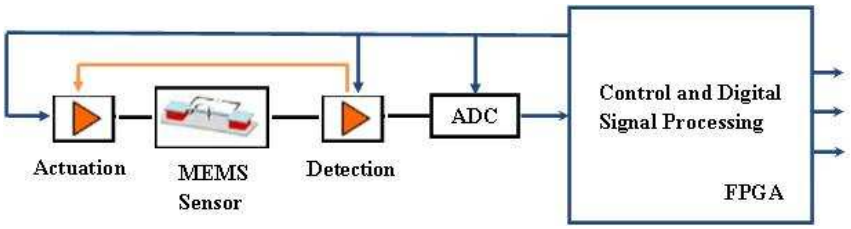

Figure 6.3: General schematic of a low-cost measurement system based on an integrated multifunction reconfigurable sensor using the LIMBO algorithm.

the user configures the MEMS sensor to measure the temperature, the LIMBO algorithm is used to recalibrate the system and its interface against other changes such as pressure, humidity and so on. Thus, the measurement system is precisely calibrated to sense temperature changes and other operating changes do not affect it. The development of this multifunction reconfigurable measurement system is the subject of an ongoing project [35].

Appendix A

Barriers to microsystems low-cost test methods

The multiple energy domains inherent to high-volume microsystems create several issues that impose important limitations against developing low-cost test methods for these microsystems. Some of these issues are:

- **Special environmental requirements:** It is difficult to implement an integrated tester for microsystems that require special environmental conditions. For instance, a mechanical shaker is required in an accelerometer, while a temperature sensor needs a heat source. Such customized environmental requirements make it difficult to develop Built-In Self-Test (BIST) features for microsystems.

- **Conflicting interference:** In integrated microsystems, the closeness of different microdevices may result in conflicting interference. For instance, heat generated by signal processing subsystems may lead to thermal expansion of a mechanical sensor that causes an error in the microsystem output results.

- **Functional diversity:** This means that it is required to develop different test approaches for different modules within the microsystem (such as sensors, actuators, analog and digital signal processing circuits).

- **Limited electrical Input/Output access:** Because of limited electrical I/O access for typical microsystems, access to internal nodes is difficult. As a consequence, both controllability and observability of internal parameters are limited.

- **Packaging influence:** The packaging of a multi-module system causes mechanical stresses that may change the device functionality (e.g. a changed spring constant caused by stress in springs that may also result in bending).

- **Lack of knowledge of device dynamics:** It is difficult to develop robust designs that may be more reliable, because of the lack of complete knowledge of device dynamics. In other words, inaccurate modeling of the complex interactions may affect the test process.

Appendix B

Discussion on the proof of convergence of some existing methods

In this section, some existing proofs of convergence for classical recursive estimation algorithms are briefly addressed and we discuss their similarities and differences with the methodology proposed in Chapter 4.
Some ODE-based techniques and convergence in mean methodologies used for proof of classical LMS approaches are addressed in [124, 122, 106, 107]. For instance, Wigren's proof of convergence for his own pseudo-gradient based method relies on the ordinary differential equation approach (see Chapter 2). The algorithm convergence to the nominal parameters is then proved for a finite impulse response (FIR) system with an arbitrary and known output quantizer under the assumption that the quantizer has at least one threshold value different from zero. It means that Wigren did not extend his proof to the case when the threshold of the ADC is unknown or equal to zero as opposed to our method (see Section 4.2). The regulative coefficient in this method is also supposed to become infinitesimally small as time increases which is not the case in our method since it uses a non-decreasing regulative coefficient.
In addition, the approaches based on convergence in mean rely on the independence of the vector of inputs at each instant and the vector of estimated parameters. This assumption does not hold in the context of our study. Thus, we believe that using the same methodology as can be found in the literature for classical LMS algorithms (ODE approach, convergence in the mean) leads to theoretical dead-ends that we are able to circumvent by using the approach presented in Chapter 4.
Another category of classical approaches for the proof of convergence is related to neural network theory. However, these methods rely on some approximations or assumptions on the system that do not hold in the context of our study. For example, Haykin presented the perceptron convergence theorem in [123, 122]. In fact, the first step of our proof is similar to that of the perceptron convergence theorem: the estimated parameter vector $\hat{\boldsymbol{\theta}}_k$ at the k^{th} update is projected on the nominal one $\boldsymbol{\theta_k}$, and the sequence $v_k = \hat{\boldsymbol{\theta}}_k^\top \boldsymbol{\theta}$ (4.11) is shown to be increasing. However, the perceptron proof then uses the hypothesis that the training set (our inputs) is absolutely (linearly) separable, i.e. that there exists $\eta > 0$ such that, for all k, $|y_k| > \eta$. Using this hypothesis, it is possible to show that at every update the sequence v_k is bounded from below by $\bar{v}_k \propto \eta^2 k^2$ and from above by $\bar{v}_k \propto k$. As a

consequence one may conclude that, for a finite training set to which the perceptron is repeatedly applied, the algorithm converges after a finite number of updates. In the context of our work, the hypothesis that there exists such a η can clearly not be made. Furthermore, repeatedly going over the training set requires storing this very training set, opposite to our goal of developing an online identification method, with as little storage requirements as possible.
Finally, as addressed in Chapter 4, we believe that it is necessary to look for a proof of convergence with hypotheses as close to the actual conditions of use of the method as possible. However, the proposed assumptions can be somewhat relaxed in more realistic cases as shown in Chapter 4.

Bibliography

[1] L. Ljung, *System identification - theory for the user*, Prentice Hall, Upper Saddle River, 1999.

[2] E. Walter and L. Pronzato, *Identification of parametric models from experimental data*, Springer - Verlag., 1997.

[3] L.Y. Wang, J.F. Zhang, and G.G. Yin, "System identification using binary sensors," *IEEE Transactions on Automatic Control*, vol. 48, no. 11, pp. 1892–1907, 2003.

[4] T. Wigren, "Approximate gradients, convergence and positive realness in recursive identification of a class of non-linear systems," *International Journal of Adaptive Control and Signal Processing*, vol. 9, pp. 325–354, 1995.

[5] E. Colinet and J. Juillard, "A weighted least-squares approach to parameter estimation problems based on binary measurements," *IEEE Transactions on Automatic Control*, vol. 55, no. 1, pp. 148–152, 2010.

[6] E. Colinet, *Nouvelles architectures et méthodes de conception de microsystemes sigma-delta et de microsystemes résonants*, Ph.D. thesis, Université de Paris-Sud 11, 2005.

[7] Cornelius T. Leondes, *MEMS/NEMS Handbook - Techniques and Applications*, Springer - Verlag., 2006.

[8] Srinivas A. Tadigadapa and N. Najafi, "Developments in Microelectromechanical Systems (MEMS): A Manufacturing Perspective," *Journal of Manufacturing Science and Engineering*, vol. 125, pp. 816–823, 2003.

[9] B. Charlot, S. Mir, F. Parrain, and B. Courtois, "Electrically Induced Stimuli For MEMS Self-Test," in *Proceedings of the 19th IEEE VLSI Test Symposium*, 2001, pp. 210–215.

[10] G. Kovacs, *Micromachined transducers source book*, McGraw-Hill, 1998.

[11] M. Bao and W. Wang, "Future of microelectromechanical systems (MEMS)," *Journal of Sensors and Actuators*, vol. 56, pp. 135–141, 1996.

[12] M. Madou, *Fundamentals of Microfabrication*, New York: CRC Press LLC, 2002.

[13] G. Delapierre, "Micromachining: A Survey of the Most Commonly Used Processes," *Journal of Sensors and Actuators*, vol. 17, pp. 123–138, 1989.

[14] W. Benecke, "Silicon Micromachining for Microsensors and Microactuators," *Journal of Microelectronic Engineering*, vol. 11, pp. 73–82, 1990.

[15] G. L. enavides, L. F. Bieg, and M. P. Saavedra, "High Aspect Ratio Mesoscale Parts Enabled by Wire Micro-EDM," *Microsystem Technologies*, vol. 8, no. 6, pp. 395–401, 2002.

[16] M. A. Schmidt, "Water-to-wafer bonding for microstructure formation," *Proceedings of the IEEE*, vol. 86, no. 8, pp. 1575–1585, 1998.

[17] W. Bacher, W. Menz, and J. Mohr, "The LIGA Technique and Its Potential for Microsystems A Survey," *IEEE Transactions on Industrial Electronics*, vol. 42, no. 5, pp. 431–441, 1995.

[18] M. Nadim, *An introduction to microelectromechanical systems engineering*, Artech House, 1999.

[19] H. Aeidel, "The mechanism of anisotropic silicon etching and its relevance for micromachining," in *Proceedings of the international conference on Solid-State Sensors and Actuators*, 1987, pp. 120–125.

[20] G. T. A. Kovacs, N. I. Maluf, and K. E. Petersen, "Bulk Micromachining of Silicon," *Proceedings of the IEEE*, vol. 86, pp. 1536–1551, 1998.

[21] P. T. Docker, P. Kinnell, and M. C. L. Ward, "A dry single-step process for the manufacture of released MEMS structures," *Journal of Micromechanics and Microengineering*, vol. 13, no. 5, pp. 790–794, 2003.

[22] E. Fatikow and U. Rembold, *Microsystem Technology and Microrobotics*, Springer-verlag, 1997.

[23] C. Linder, L. Paratte, M. A. Gretillat, V. P. Jaecklin, and N. F. De Rooij, "Surface Micromachining," *Journal of Micromechanics and Microengineering*, vol. 2, pp. 122–132, 1992.

[24] Ch. Kharrat, *Application des techniques de contrôle sur les réseaux de micro et nanostructures.*, Ph.D. thesis, Université Joseph Fourier Grenoble I, 2009.

[25] K. Gilleo, *MEMS/MOEMS Packaging*, McGraw-Hill, 2005.

[26] M.H. Bao, *Handbook of sensors and actuators*, Elsevier, 2000.

[27] Samaun, K.D. Wise, and J.B. Angell, "An IC piezoresistive pressure sensor for biomedical instrumentation," *IEEE Transactions on Biomedical Engineering*, vol. 20, pp. 101–109, 1973.

[28] J. Wen H. Ko Hynecek and S.F. Boettcher, "Development of a miniature pressure transducer for biomedical applications," *IEEE Transactions on Electron Devices*, vol. 26, no. 12, pp. 1896–1905, 1979.

[29] W.H. Ko, M.H. Bao, and Y.D. Hong, "A high-sensitivity integrated-circuit capacitive pressure transducer," *IEEE Transactions on Electron Devices*, vol. 29, no. 1, pp. 48–56, 1982.

[30] L.M. Roylance and J.B. Angell, "A batch-fabricated silicon accelerometer," *IEEE Transactions on Electron Devices*, vol. 26, no. 12, pp. 1911–1917, 1979.

[31] J.D. Zook, D.W. Burns, H. Guckel, J.J. Sniegowski, R.L. Engelstad, and Z. Feng, "Resonant microbeam strain transducers," in *Proceedings of International Conference on Solid-State Sensors and Actuators*, 1991, pp. 529–532.

[32] Y. Omura, Y. Nonomura, and O. Tabata, "New resonant accelerometer based on rigidity change ," in *Proceedings of International Conference on Solid-State Sensors and Actuators*, 1997, pp. 855–858.

[33] K. Petersen, F. Pourahmadi, J. Brown, P. Parsons, M. Skinner, and J. Tudor, "Resonant beam pressure sensor fabricated with silicon fusion bonding," in *Proceedings of International Conference on Solid-State Sensors and Actuators*, 1991, pp. 664–667.

[34] T.A. Roessig, R.T. Howe, A.P. Pisano, and J.H. Smith, "Surface-micromachined resonant accelerometer," in *Proceedings of International Conference on Solid-State Sensors and Actuators*, 1997, pp. 859–862.

[35] H. Mathias, A. Glascott-Jones, G. Amendola, A. Exertier, J. Juillard, M. Roger, and E. Colinet, "Low-cost measurement system based on integrated multi-purpose reconfigurable sensor," in *Technical Report for the French National Research Agency*, 2009.

[36] H Fujita, "Future of actuators and microsystems," *Journal of Sensors and Actuators*, vol. A56, pp. 105–111, 1996.

[37] Stephen D. Senturia, *Microsystem design*, Springer, 2000.

[38] W. C. Tang, C. H. Nguyen, and R. T. Howe, "Laterally driven polysilicon resonant microstructures," *Journal of Sensors and Actuators*, vol. A20, pp. 25–32, 1989.

[39] W. C. Tang, M. G. Lim, and R. T. Howe, "Electrostatic Comb Drive Levitation and Control Method," *Journal of Microelectromechanical Systems*, vol. 1, no. 4, pp. 170–178, 1992.

[40] Ph. Lerch, C. Kara Slimane, B. Romanowicz, and Ph. Renaud, "Modelization and characterization of asymmetrical thermal microactuators," *Journal of Micromechanics and Microengineering*, vol. 6, no. 1, pp. 134–137, 1996.

[41] Q. Huang and N. K. Sh. Lee, "Analysis and design of polysilicon thermal flexure actuator," *Journal of Micromechanics and Microengineering*, vol. 9, no. 1, pp. 64–70, 1999.

[42] J. H. Comtois and V. M. Bright, "Applications for surface-micromachined polysilicon thermal actuators and arrays," *Journal of Sensors and Actuators*, vol. 58, no. 1, pp. 19–25, 1997.

[43] D. L. Devoe and A. Pisano, "Modeling and optimal design of piezoelectric cantilever microactautors," *Journal of Microelectromechanical systems,*, vol. 6, no. 3, pp. 266–270, 1997.

[44] I. Ivan, M. Rakotondrabe, P. Lutz, and N. Chaillet, "Quasistatic displacement self-sensing method for cantilevered piezoelectric actuators," *Review of Scientific Instruments*, vol. 80, no. 6, pp. 065102–1–065102–8, 2009.

[45] H. Ishihara, F. Arai, and T. Fukuda, "Micro Mechatronics and Micro Actuator," *IEEE/ASME Transactions on Mechatronics*, vol. 1, no. 1, pp. 68–79, 1996.

[46] O. Brand, Gary K. Fedder, C. Hierold, Jan G. Korvink, O. Tabata, and T. Tsuchiya, *Reliability of MEMS: Testing of Materials and Devices*, WILEY, 2007.

[47] J. A. Connally and S. B. Brown, "Slow crack growth in single-crystal silicon," *Science*, vol. 256, pp. 1537–1539, 1992.

[48] S.B. Brown, W. van Arsdell, and C.L. Muhlstein, "Materials reliability in MEMS devices," in *Proceedings of International Conference on Solid State Sensors and Actuators*, 1997, pp. 591–593.

[49] S. Nakao, T. Ando, M. Shikida, and K. Sato, "Mechanical properties of a micron-sized SCS film in a high-temperature environment ," *Journal of Micromechanics and Microengineering*, vol. 16, pp. 715–720, 2006.

[50] T. Olbrich, A. Richardson, W. Vermeiren, and B. Straube, "Integrating Testability into Microsystems," *Microsystem Technologies*, pp. 72–79, 1997.

[51] A. Dhayni, *Pseudorandom Built-In Self-Test for Microsystems*, Ph.D. thesis, Institut National Polytechnique de Grenoble, 2006.

[52] N. Deb, *Defect Oriented Test of Inertial Microsystems*, Ph.D. thesis, Carnegie Mellon University, 2005.

[53] A. Hartzell and D. Woodilla, "Reliability Methodology for Prediction of Micromachined Accelerometer Stiction," in *Proceedings of Reliability Physics Symposium*, 1999, pp. 202–205.

[54] R.W. Beegle, R.W. Brocato, and R.W. Grant, "IMEMS Accelerometer Testing - Test Laboratory Development and Usage," in *Proceedings of International Test Conference*, 1999, pp. 338–347.

[55] D.M. Tanner, J.A. Walraven, K.S. Helgesen, L.W. Helgesen, D.L. Gregory, J.R. Stake, and N.F. Smith, "MEMS Reliability in a Vibration Environment," in *Proceedings of Reliability Physics Symposium*, 2000, pp. 139–145.

[56] D.M. Tanner, J.A. Walraven, K.S. Helgesen, L.W. Irwin, F. Brown, N.F. Smith, and N. Masters, "MEMS Reliability in Shock Environments," in *Proceedings of Reliability Physics Symposium*, 2000, pp. 129–138.

[57] A. Kolpekwar, C. Kellen, and R.D. Blanton, "MEMS Fault Model Generation using CARAMEL," in *Proceedings of International Test Conference*, 1998, pp. 557–566.

[58] T. Jiang and R.D. Blanton, "Particulate Failures for Surface-Micromachined MEMS," in *Proceedings of International Test Conference*, 1999, pp. 329–337.

[59] T. Jiang, C. Kellon, and R.D. Blanton, "Inductive Fault Analysis of a Microresonator," in *Proceedings of Modeling and Simulation of Microsystems*, 1999, pp. 498–501.

[60] V. Beroulle, Y. Bertrand, L. Latorre, and P. Nouet, "Test and Testability of a Monolithic MEMS for Magnetic Field Sensing," *Journal of Electronic Testing, Theory and Applications*, pp. 439–450, 2001.

[61] A. Castillejo, D. Veychard, S. Mir, J.M. Karam, and B. Courtois, "Failure Mechanisms and Fault Classes for CMOS-Compatible Microelectromechanical Systems," in *Proceedings of International Test Conference*, 1998, pp. 541–550.

[62] B.C. Kim and K. Marella, "A Novel Test Methodology for MEMS Magnetic Micromotors," in *Proceedings of VLSI Test Symposium*, 1999, pp. 284–289.

[63] B. Charlot, S. Mir, E.F. Cota, M. Lubaszewski, and B. Courtois, "Fault Simulation of MEMS Using HDLs," in *Proceedings of Symposium on Design, Test and Microfabrication of MEMS/MOEMS*, 1999, pp. 70–77.

[64] B. Charlot, S. Moussouris, S. Mir, and B. Courtois, "Fault Modeling of Electrostatic Comb-drives for MEMS," in *Proceedings of Symposium on Design, Test and Microfabrication of MEMS/MOEMS*, 1999, pp. 398–405.

[65] B. Charlot, S. Mir, E.F. Cota, M. Lubaszewski, and B. Courtois, "Fault modeling of suspended thermal MEMS," in *Proceedings of International Test Conference*, 1999, pp. 319–328.

[66] P. Durr, U. Dauderstadt, D. Kunze, M. Auvert, and H. Lakner, "Reliability Test and Failure Analysis of Optical MEMS," in *Proceedings of Physical and Failure Analysis of Integrated Circuits*, 2002, pp. 201–206.

[67] H.V. Allen, S.C. Terry, and D.W. De Bruin, "Self-Testable Accelerometer Systems," in *Proceedings of Micro Electro Mechanical Systems*, 1989, pp. 113–115.

[68] T. Olbrich, A. Richardson, and D. Bradley, "Built-in-Self-Test and Diagnostics for Safety Critical Microsystems," *Microelectronics Reliability*, vol. 36, no. 7/8, pp. 1125–1136, 1996.

[69] V. Beroulle, Y. Bertrand, L. Latorre, and P. Nouet, "Evaluation of the Oscillation-based Test Methodology for Micro-Electro-Mechanical Systems," in *Proceedings of VLSI Test Symposium*, 2002, pp. 439–444.

[70] D. De Bruyker, A. Cozma, and R. Puers, "A Combined Piezoresistive/Capacitive Pressure Sensor with Self-test Function based on Thermal Actuation," in *Proceedings of Solid State Sensors and Actuators*, 1997, pp. 1461–1464.

[71] B. Charlot, S. Mir, F. Parrain, and B. Courtois, "Generation of Electrically Induced Stimuli for MEMS Self-Test," *Journal of Electronic Testing, Theory and Applications*, pp. 459–470, 2001.

[72] V. Beroulle, Y. Bertrand, L. Latorre, and P. Nouet, "On the use of an Oscillation-based Test Methodology for CMOS Micro-Electro-Mechanical Systems," in *Proceedings of Symposium on Design, Automation and Test in Europe*, 2002, p. 1120.

[73] M. Aikele, K. Bauer, W. Ficker, F. Neubauer, U. Prechtel, J. Schalk, and H. Seidel, "Resonant Accelerometer with Self-test," *Journal of Sensors and Actuators A*, vol. 92, no. 1-3, pp. 161–167, 2001.

[74] R. Puers and S. Reyntjens, "RASTAReal-Acceleration-for-Self-Test Accelerometer: A New Concept for Selftesting Accelerometers," *Journal of Sensors and Actuators A*, vol. 97-98, pp. 359–368, 2002.

[75] T. Maudie and J. Wertz, "Pressure Sensor Performance and Reliability," *IEEE Industry Applications Magazine*, vol. 3, no. 3, pp. 37–43, 1997.

[76] T. Maudie, A. Hardt, R. Nielsen, D. Stanerson, R. Bleschke, and M. Miller, "MEMS Manufacturing Testing: An Accelerometer Case Study," in *Proceedings of International Test Conference*, 2003, pp. 843–849.

[77] R. Rosing, A. Lechner, A. Richardson, and A. Dorey, "Fault Simulation and Modelling of Microelectromechanical Systems," *Computing and Control Engineering Journal*, vol. 11, no. 5, pp. 242–250, 2000.

[78] X. Xiong, Y.L. Wu, and W.B. Jone, "A Dual-Mode Built-In Self-Test Technique for Capacitive MEMS Devices," in *Proceedings of VLSI Test Symposium*, 2004, pp. 148–153.

[79] N. Dumas, F. Azais, L. Latorre, and P. Nouet, "Electrically-Induced Thermal Stimuli for MEMS Testing," in *Proceedings of* 9^{th} *IEEE European Test Symposium*, 2004, pp. 60–65.

[80] K. J. Astrom and P. Eykhoff, "System identification–a survey," *Automatica*, vol. 7, pp. 123–167, 1971.

[81] S. A. Billings, "Identification of nonlinear systems–A survey," *Proceedings of IEEE*, vol. 127, pp. 272–285, 1980.

[82] K. S. Narendra and J. H. Taylor, *Frequency domain criteria for absolute stability*, Academic Press, NY, 1973.

[83] M. Vidyasagar, *Nonlinear system analysis*, Prentice Hall, NJ, 1978.

[84] S. Dasgupta, G. Johnson, and A.M. Baksho, "Sign-Sign LMS convergence with independent stochastic inputs," *IEEE Transactions on Information Theory*, vol. 36, no. 1, pp. 197–201, 1990.

[85] C. Ion, G. Yin, and V. Krishnamurthy, "Sign-regressor adaptive filtering algorithms using averaged iterates and observations," in *Stochastic Theory and Control*, Bozenna Pasik-Duncan, Ed., vol. 280 of *Lecture Notes in Control and Information Sciences*, pp. 223–238. Springer Berlin / Heidelberg, 2002.

[86] G. Yin and H. Chen, "On asymptotic properties of a constant-step-size sign-error algorithm for adaptive filtering," *Science in China Series F: Information Sciences*, vol. 45, no. 5, pp. 321–334, 2002.

[87] H. F. Chen and G. Yin, "Asymptotic properties of sign algorithms for adaptive filtering," *IEEE Transactions on Automatic Control*, vol. 48, no. 9, pp. 1545–1556, 2003.

[88] P. Billingsley, *Convergence of Probability Measures*, Wiley, NY, 1968.

[89] L.Y. Wang and G.G. Yin, "Asymptotically efficient parameter estimation using quantized output observations," *Automatica*, vol. 43, no. 7, pp. 1178–1191, 2007.

[90] Y.L. Zhao, L.Y. Wang, G.G. Yin, and J.F. Zhang, "Identification of Wiener systems with binary-valued output observations," *Automatica*, vol. 43, no. 10, pp. 1752–1765, 2007.

[91] Y.L. Zhao, J.F. Zhang, L.Y. Wang, and G.G. Yin, "Identification of hammerstein systems with set-valued observations," in *Proceedings of the 17th IFAC World Congress*, 2008, pp. 6458–6465.

[92] L.Y. Wang, G.G. Yin, Y. Zhao, and J.F. Zhang, "Sufficient excitation conditions for system identification using binary-valued observations," in *Proceedings of the 2006 American Control Conference*, 2006, pp. 3777–3782.

[93] L.Y. Wang and G.G. Yin, "Information characterization of communication channels for system identification," *Journal of Systems Science and Complexity*, vol. 20, pp. 251–261, 2007.

[94] L.Y. Wang, G.G. Yin, J.F. Zhang, and Y.L. Zhao, "Space and time complexities and sensor threshold selection in quantized identification," *Automatica*, vol. 44, no. 12, pp. 3014–3024, 2008.

[95] G. Xu, L.Y. Wang, and G.G. Yin, "State reconstruction for linear time-invariant systems with binary-valued output observations," in *Proceedings of the 46th IEEE Conference on Decision and Control (CDC)*, 2007, pp. 4305–4310.

[96] L.Y. Wang, G.G. Yin, and C. Xu, "Identification of cascaded systems with linear and quantized observations," in *Proceedings of the 46th IEEE Conference on Decision and Control (CDC)*, 2007, pp. 3616–3621.

[97] L.Y. Wang, G.G. Yin, and G. Xu, "State estimation of systems with binary-valued observations," in *Proceedings of the 46th IEEE Conference on Decision and Control (CDC)*, 2007, pp. 5545–5549.

[98] L.Y. Wang, G.G. Yin, and J.F. Zhang, "Joint identification of plant rational models and noise distribution functions using binary-valued observations," *Automatica*, vol. 42, no. 4, pp. 535–547, 2006.

[99] E. Rafajlowicz, "System identification from cheap, qualitative output observations," *IEEE Transactions on Automatic Control*, vol. 41, no. 9, pp. 1381–1385, 1996.

[100] R. E. Kalman and J. E. Bertram, "Control system analysis and design via the second method of Lyapunov," *Transactions of the ASME, Journal of Basic Engineering*, vol. 82, pp. 394–400, 1960.

[101] K. H. Keinitz, "Guaranteed cost control approach to the stabilization of uncertain linear discrete-time systems," *International Journal of Systems Science*, vol. 21, no. 4, pp. 643–652, 1990.

[102] M. Negreiros, L. Carro, and A.A. Susin, "Ultimate low cost analog BIST," in *Proceedings of the 40th Conference on Design Automation*. ACM New York, NY, USA, 2003, pp. 570–573.

[103] A. Papoulis, *Probability, Random Variables and Stochastic Processes*, McGraw-Hill, 1991.

[104] J. Juillard and E. Colinet, "Initialization of the BIMBO self-test method using binary inputs and outputs," in *Proceedings of the 46th IEEE Conference on Decision and Control*, 2008, pp. 161–166.

[105] J. C. Aguero, B. I. Godoy, G. C. Goodwin, and T. Wigren, "Scenario-based EM identifcation for FIR systems having quantized output data," in *Proceedings of the 15th IFAC Symposium on System Identification*, 2009, pp. 66–71.

[106] T. Wigren, "ODE analysis and redesign in blind adaptation," *IEEE Transactions on Automatic Control*, vol. 42, no. 12, pp. 1742–1747, 1997.

[107] T. Wigren, "Adaptive filtering using quantized output measurements," *IEEE Transactions on Signal Processing*, vol. 46, no. 12, pp. 3423–3426, 1998.

[108] W. Greblicki, "Nonparametric identification of Wiener systems," *IEEE Transactions on Information Theory*, vol. 38, pp. 1487–1493, 1992.

[109] D. Westwick and M. Verhaegen, "Identifying MIMO Wiener systems using subspace model identification method," *Signal Processing*, vol. 52, pp. 235–258, 1996.

[110] X. Hu and H. F. Chen, "Strong consistence of recursive identification for Wiener systems," *Automatica*, vol. 41, pp. 1905–1916, 2005.

[111] E. W. Bai, "A blind approach to the HammersteinWiener model identification," *Automatica*, vol. 38, pp. 967–979, 2002.

[112] E. W. Bai and J. Reyland, "Towards identification of Wiener systems with the least amount of a priori information on the nonlinearity," *Automatica*, vol. 44, no. 4, pp. 910–919, 2008.

[113] L. Ljung, "Analysis of recursive stochastic algorithms," *IEEE Transactions on Automatic Control*, vol. 22, pp. 551–575, 1977.

[114] L. Ljung and T. Soderstrom, *Theory and practice of recursive identification*, M.I.T. Press, Cambridge MA, 1983.

[115] C. Le Blanc, E. Colinet, and J. Juillard, "Digital implementation of a BIST method based on binary observations," in *Proceedings of the* 11^{th} *Euromicro Conference on Digital System Design; Architectures, Methods and Tools*, 2008, pp. 709–713.

[116] E. Rafajlowicz, "Linear systems identification from random threshold binary data," *IEEE Transactions on Signal Processing*, vol. 44, no. 8, pp. 2064–2070, 1996.

[117] J. Nocedal and S.J. Wright, *Numerical optimization*, Springer, 2000.

[118] A. Papoulis and U. Pillai, *Probability, random variables and stochastic processes.*, New York: McGraw-Hill, 2002.

[119] M. Rosenblatt, *Markov Processes. Structure and Asymptotic Behavior*, Springer-Verlag, Berlin, 1971.

[120] S. Bandyopadhyay, *A note on strong mixing* , Iowa State University, 2006.

[121] M. Rosenblatt, "A central limit theorem and a strong mixing condition," *Proceedings of the National Academy of Sciences of the USA*, vol. 42, pp. 43–47, 1956.

[122] S. Haykin, *Adaptive Filter Theory*, Prentice-Hall, NY, 2001.

[123] S. Haykin, *Neural Networks. A comprehensive foundation*, Prentice-Hall, NY, 1999.

[124] B. Farhang-Boroujeny, *Adaptive filters: theory and applications*, John Wiley, NY, 1998.

[125] R.J. Van de Plassche, *CMOS integrated analog-to-digital and digital-to-analog converters*, Springer-Verlag, New York, 2005.

[126] M. Ozisik, *Boundary Value Problems of Heat Conduction*, Dover Pubns, 1989.

[127] O. Legendre, H. Mathias, E. Martincic, M. Zhang, J. Juillard, and F. Mailly, "High resolution micro-Pirani gauge with transient response processing," in *Proceedings of IEEE Sensors Conference*, 2010, pp. 1478–1482.

[128] I. Kovacic and M.J. Brennan, *The Duffing Equation: Nonlinear Oscillators and their Behaviour*, Wiley, 2011.

[129] H. Aeidel, "Silicon as a mechanical material," *Proceedings of the IEEE*, vol. 70, no. 5, pp. 420–457, 1982.

[130] S. D. Sentura, M. Mehregany, P. Nagarkar, and J. H. Lang, "Operation of microfabricated harmonic and ordinary side-drive motors," in *Proceedings of IEEE MEMS*, 1990, pp. 1–8.

[131] H. L. John, *Flip chip technology*, McGraw-Hill, 1995.

[132] K. F. Harsh, B. Su, W. Zhang, V. M. Bright, and Y. C. Lee, "The realization and design considerations of a flip-chip integrated mems tunable capacitor," *Journal of Sensors and Actuators*, vol. 80, no. 2, pp. 108–118, 2000.

[133] T. Yi, L. Li, and C. J. Kim, "Microscale material testing of single crystalline silicon: process effects on surface morphology and tensile strength," *Journal of Sensors and Actuators*, vol. 83, pp. 172–178, 2000.

[134] T. Tsuchiya, A. Inoue, J. Sakata, and M. Hashimoto, "Fatigue test of single crystal silicon resonator," in *Tech. Digest of the 16th Sensor Symposium*, 1998, pp. 277–280.

[135] C. L. Muhlstein, S. B. Brown, and R. O. Ritchie, "High-Cycle Fatigue of Single-Crystal Silicon Thin Films," *Journal of Microelectromechanical systems,*, vol. 10, no. 4, pp. 593–600, 2001.

[136] T. Wigren, "Convergence analysis of recursive identification algorithms based on the nonlinear Wiener model," *IEEE Transactions on Automatic Control*, vol. 39, no. 11, pp. 2191–2206, 1994.

[137] T. Wigren, "Recursive prediction error identification using the nonlinear Wiener model," *Automatica*, vol. 29, pp. 1011–1025, 1993.

[138] L. Ljung, "On positive real transfer functions and the convergence of some recursive schemes," *IEEE Transactions on Automatic Control*, vol. 22, pp. 539–551, 1977.

[139] S. A. Billings and S. Y. Fakhouri, "Identification of nonlinear systems using the Wiener model," *Electronics letters*, vol. 13, pp. 502–504, 1978.

[140] S. A. Billings and S. Y. Fakhouri, "Identification of systems containing linear dynamic and static nonlinear elements," *Automatica*, vol. 18, pp. 15–26, 1982.

[141] Q. Zhang, A. Iuditsky, and L. Ljung, "Identification of Wiener system with monotonous nonlinearity," in *Proceedings of the 14th IFAC Symposium on System Identification*, 2006, pp. 166–171.

[142] S. A. Billings and S. Y. Fakhouri, "Identification of a class of nonlinear systems using correlation analysis," *Proceedings of IEEE*, vol. 125, no. 7, pp. 691–697, 1978.

[143] J. Voros, "Parameter identification of Wiener systems with discontinuous nonlinearities," *Systems and Control Letters*, vol. 44, no. 5, pp. 363–372, 2001.

[144] C. Robert and G. Casella, *Monte carlo statistical methods*, Springer, 2004.

[145] F. Bannon, J. Clark, and T. Nguyen, "High-Q HF microelectromechanical filters," *IEEE Journal of Solid-State Circuits*, vol. 35, no. 4, pp. 512–526, 2000.

[146] C. Barthod, Y. Teisseyre, C. Géhin, and G. Gautier, "Resonant force sensor using a PLL electronic," *Journal of Sensors and Actuators A*, vol. 104, no. 2, pp. 143–150, 2003.

[147] S. Sung, J.G. Lee, B. Lee, and T. Kang, "Design and performance test of an oscillation loop for a MEMS resonant accelerometer," *Journal of Micromechanics and Microengineering*, vol. 13, pp. 246–253, 2003.

[148] S. Haueis, J. Dual, C. Cavalloni, M. Gnielka, and R. Buser, "A fully packaged single crystalline resonant force sensor," *Journal of Micromechanics and Microengineering*, vol. 11, pp. 514–521, 2001.

[149] K.E. Wojciechowski, B.E. Boser, and A.P. Pisano, "A MEMS resonant strain sensor with 33 nano-strain resolution in a 10 kHz bandwidth," in *Proceedings of IEEE Sensors Conference*, 2005, pp. 947–950.

[150] K. Ekinci, X. Huang, and M. Roukes, "Ultrasensitive nanoelectro-mechanical mass detection," *Applied Physics Letters*, vol. 84, no. 22, pp. 4469–4471, 2004.

[151] H. Sone, Y. Fujinuma, and S. Hosaka, "Picogram mass sensor using resonance frequency shift of cantilever," *Japanese Journal of Applied Physics*, vol. 43, pp. 3648–3651, 2004.

[152] M. et al. Villaroya, "System on chip mass sensor based on polysilicon cantilevers arrays for multiple detection," *Journal of Sensors and Actuators A*, vol. 132, pp. 154–164, 2006.

[153] L. Nicu, *Etudes théoriques et expérimentales du comportement mécanique de microstructure de type levier ou pont. Applications á la mesure de la viscosité de liquides et á la caractérisation électrique de nanostructures*, Ph.D. thesis, Université Paul Sabatier Toulouse III, 2000.

[154] F. et al. Battiston, "A chemical sensor based on a microfabricated cantilever array with simultaneous resonance frequency and bending readout," *Journal of Sensors and Actuators B*, vol. 77, pp. 122–131, 2001.

[155] M.N. Horenstein, J.A. Perreault, and T.G. Bifano, "Differential capacitive position sensor for planar MEMS structures with vertical motion," *Journal of Sensors and Actuators A*, vol. 80, pp. 53–61, 2000.

[156] S.H. Lim, D. Raorane, Satyanarayana S., and A. Majumdar, "Nano-chemomechanical sensor array platform for high-throughput chemical analysis," *Journal of Sensors and Actuators B*, vol. 119, pp. 466–474, 2006.

[157] L. Spangler and C.J. Kemp, "A smart automotive accelerometer with on-chip airbag deployment circuits," in *Proceedings of Technical Digest of Solid-State Sensor and Actuator Workshop*, 1996, pp. 211–214.

[158] S. Cass, "MEMS in Space," *IEEE Spectrum*, vol. 38, pp. 56–61, 2001.

[159] C.S. Smith, "Piezoresistance effect in Germanium and Silicon," *Physics Review*, vol. 94, no. 1, pp. 42–49, 1954.

[160] L. Rolindez, *A BIST technique for Sigma-Delta ADCs*, Ph.D. thesis, Institut National Polytechnique (INP) de Grenoble, 2007.

[161] C.K. Ong and K.T. Cheng, "Self-testing second-order Delta-Sigma modulators using digital stimulus," in *Proceedings of IEEE VLSI Test Symposium*, 2002, pp. 123–128.

[162] C.K. Ong, J.L. Huang, and K.T. Cheng, "Delta-sigma based mixed-signal BIST architecture for SoC," in *Proceedings of IEEE International Mixed-Signal Testing Workshop*, 2003, pp. 47–52.

[163] C.K. Ong, K.T. Cheng, and L.C. Wang, "A new Sigma-Delta modulator architecture for testing using digital stimulus," *IEEE Transactions on Circuits and Systems-I*, vol. 51, no. 1, pp. 206–2013, 2004.